POLITECNICO DI MILANO

SCHOOL OF ENGINEERING

POLO REGIONALE DI LECCO

FACOLTÀ DI INGEGNERIA CIVILE, AMBIENTALE E TERRITORIALE

MASTER OF SCIENCE IN CIVIL ENGINEERING

On the Influence of Pore Pressure
on the Apparent Tensile Strength of Concrete

M.Sc. THESIS

Advisor: Prof. Roberto FELICETTI

Co-advisor: Francesco LO MONTE

AUTHORS

Mehmet Baran ULAK (750397)

Murat HACIOGLU (749388)

2011/2012

Abstract

This thesis deals with the effects of pore vapor pressure on concrete exposed to elevated temperatures. In order to comprehend these effects, experiments and numerical analysis were conducted. The main purpose was to evaluate tensile strength alteration caused by pore vapor pressure. However, evaluation of tensile strength alteration of concrete exposed to high temperature is a complex process, since it depends on many factors. In this work, these factors and their effects were tried to be distinguished and determined separately. It is a fact that magnitude of temperature, heating rate and pore pressure are main factors which affect the tensile strength of concrete. However, these factors are also correlated each other, which make them difficult to be evaluated separately. Despite of this difficulty, it was tried to reveal an evident relationship in between pore vapor pressure and tensile strength of concrete.

In chapter 1, general view of the problem is presented. Concrete response to high temperature such as change in chemical properties, thermal properties, mechanical properties are presented in this chapter. Moreover, well known high temperature induced failures of concrete are identified.

In chapter 2, review of literature is made. Researches, thesis and other works related with this topic, are tried to be summarized and introduced. Comments and criticism of these papers are made.

In chapter 3, the experimental set-up, numerical analysis and preliminary experiments are explained. Preparation of samples, test procedures, choices of heating rates etc. are presented in this chapter.

In chapter 4, the results of main tests are presented. It was tried to show effects of pore pressure, heating rate and temperature on tensile strength of concrete. The revealed differences in between plain concrete and poly-propylene fiber reinforced concrete are indicated.

In chapter 5, analytical models that states the relation between pore pressure and tensile strength, are investigated.

In chapter 6, brief conclusions about the results are made.

In summary deeper insight has been developed on a fundamental aspect of fracture behavior of concrete at high temperature. This is still one of the "hottest" open issues in the fire safety of structures.

Contents

List of Figures

1. INTRODUCTION

1.1. Introduction

Concrete has been considered to perform well under fire condition as a historical view due to its non-combustible nature and ability to behave as a thermal barrier, preventing heat and fire spread. The results of tests in which concrete were exposed to "standard fire" have formed the basis of design criteria. On the other hand, the argument about the general applicability and usefulness of this approach might come out considering the possible difference of the heating regime between real world and the experiments. Especially, more rapid initial heating rates might be the case and "cooling phase" differs in all real fires; in both conditions, additional thermal stresses are induced on in-situ structures leading to high restraining effect on them. Hence there are still obvious gap to understand the true behavior of concrete subjected to fire. The temperature dependent material properties are used to identify the fire behavior of concrete in fundamental terms. The low thermal diffusivity of concrete compared to steel usually leads to the generation of high temperature gradients within the concrete members subjected to fire, *i.e.* it might take long time to heat up the core due to the high thermal inertia. Therefore, while there occurs a rapid decrease in the compressive strength of concrete beyond a critical temperature, similar to the equivalent temperature for loss of steel strength, the structural member might stand until the whole body of the material exceeds the critical temperature. It is required to analyze the thermal response of the entire structural element. There is another problem called spalling which happens when concrete is subjected to high temperature. This phenomenon includes explosive ejection of chunks of concrete from the surface, because of the decrease in surface tensile strength. The reason for this is the mechanical forces formed inside the element as a result of strong heating or cooling. This means that thermal stresses and the rapid expansion of moisture in a concrete causing an increase in the pore pressure within the structure might be the possible mechanism of the generation of mechanical forces in concrete. When strong temperature gradients are imposed on concrete in the case of heating or cooling, spalling

may occur. The composition and the type of concrete (normal-strength, high-performance (HPC) or ultra-high-performance (UHPC)) affect the performance of concrete under fire conditions.

The starting point of evaluation of the recoverability of a structure subjected to fire involves   event data collection and the assessment of damage. The classification of a damage considering materials rather than structures is proposed and repair criteria and repair methods are summarized. When assessing the damage, it is important to investigate and evaluate the building or the load-bearing structure in a careful way. In order to achieve this, information is required along with a standard on how to perform such an investigation in a given case. Standard procedures may be proposed for the assessment and repair of the structures exposed to fire, as a future goal. The awareness of both thermal and mechanical properties of main types of engineering materials such as concrete, wood and steel allows structural engineers to perform fire damage assessments. Providing the information, which is necessary to perform evaluations of the residual bearing capacity and durability of the structure and to design any strengthening or repair intervention is the main purpose of fire damage assessment in concrete. A general view can be obtained about the possible approach to overcome this problem in a couple of recognized technical publications on the assessment and repair of fire damaged structures.

As mentioned above, thermal induced stresses and pore pressure affect tensile strength. The failure mechanism under fire conditions is of complex nature. The purpose of this research is to evaluate the tensile strength reduction due to the pore pressure within the concrete. The tests, which were planned to be performed, concentrated mainly on the effect of pore pressure. In order to provide better understanding of the failure mechanism, the results of some numerical thermal analysis will be introduced in chapter 3.

Before this research, there were conducted several researches on the measurements of pore pressures at elevated temperatures. However, so far there was no intention to see the direct influence of pore pressure on the tensile strength of concrete. In this thesis Pore pressure measurements and the Brazilian tests were used to find a correlation between

pore pressure and tensile strength reduction. The details of this work were given in latter Chapters.

The relevant thermal and mechanical properties of concrete at elevated temperatures were briefly mentioned in the following section. These properties are thermal conductivity, specific heat, thermal expansion and mass loss. The thermal properties are introduced in equation forms that express the values of these properties as a function of temperature, ranging between 20°C and 1000°C. As for the mechanical properties, stress-strain relationships are given for the concretes at elevated temperatures. The effect on mechanical properties compared to the thermal properties is greater and is expected to be beneficial to the fire resistance of structural elements constructed of reinforced concrete. As stated before, the fire resistance of concrete structures id quite good. On the other hand, various effects may be observed under prolonged fire conditions. There are obvious indications of distress, which are cracking and spalling of the surfaces, which is the result of differential expansion of successive layers of the concrete as it is heated and by internal pressure as moisture in the concrete is turned to super-heated steam.

Even though concrete is a poor conductor of heat, it can be considerably damaged when subjected to fire. It is important to unravel the history heating for further researches and also is important to identify whether the concrete structure exposed to fire is damaged or not. Visual observation of color change, cracking and spalling are the starting point of the assessment of concrete structures subjected to fire. Imposing heating may lead to color change (pink discoloration is usually the case). The observation of the color change is important because it coincides with the onset of strength loss of concrete. Generally speaking, concrete looses all of its strength at the temperature above 500°C has lost all its strength. When temperature exceeds this value, in many cases the pink/red discoloration indicates the damage limit of concrete. On the other hand, the color change may not be present for all types of aggregates. In any case, it is required to carry out a physical assessment of the concrete strength.

Concrete is subjected to several degradation process under fire conditions because of the fact that multi-chemo-physical mechanisms are generated in the porous concrete media resulting in thermal softening as well as thermal expansion, drying shrinkage and

internal pore pressure build-up (Figure 1).Conduction and convection of heat take place through the material when subjected to fire. This give rise to variations in the chemical composition, physical structure and fluid (water, gas and vapor) contents in the porous material influencing the overall mechanical (strength, stiffness, fracture, etc) and other physical properties (thermal conductivity, permeability, porosity, etc). For the safety assessment of tunnels and high rise buildings, the degradation process have become important and the need for the comprehensive understanding of concrete under fire conditions has been aroused. Spalling is one of the failure mechanism when concrete is exposed to fire. As a result of the generation of additional stresses caused by severe temperature gradients and internal pore pressure which is built up by the formation of moisture clog due to multi physics transport of mass and energy.
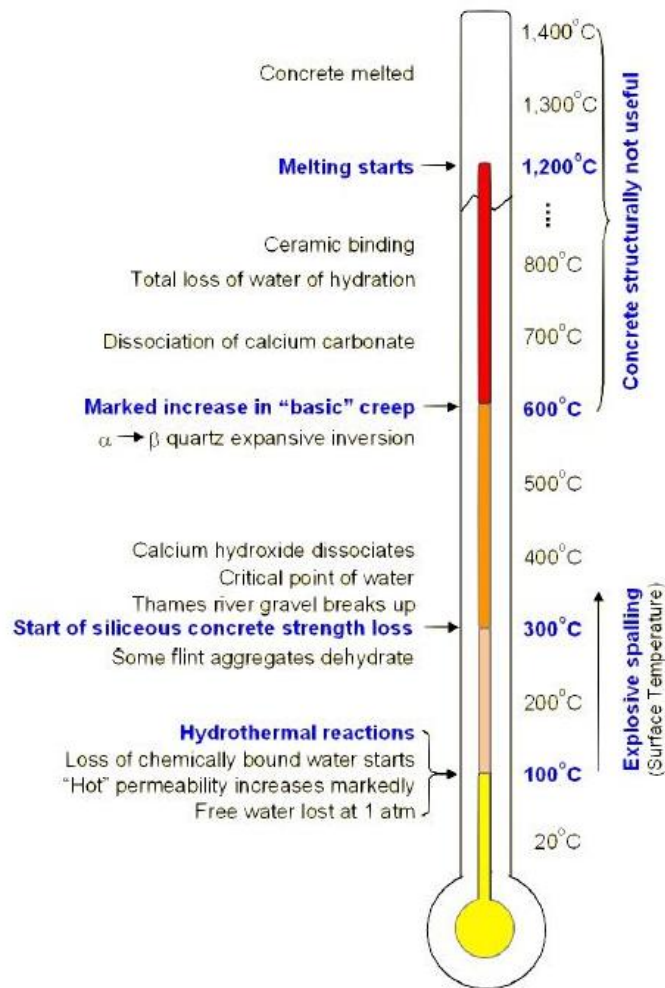
Figure 1 Kboury Thermometer

Concrete structures are considered to perform well under fire conditions. A considerably large amount of reinforced concrete buildings, subjected to severe fires has been fixed and brought back into use. An endothermic reaction, which is one of the factors leading to reduction in the temperature rise in fire- exposed concrete structures takes place in the cement paste within concrete when heated up.

In order to determine the behavior of concrete structures under fire conditions, load exerted on the structures, elevated temperatures in the concrete and reinforcement bar, and mechanical properties of concrete at those temperatures should be known.

1.2. Thermal properties of concrete

Concrete is a construction material used worldwide, *i.e.* it is used in all different climatic regions for all kinds of structures. It is essential to provide knowledge of thermal expansion in structural elements exposed to high temperature changes such as fire, subsequent cooling, resulting in cracks, loss of serviceability and durability.

The type of aggregate, the original moisture content of the concrete and the age of concrete are the factors on which the required thermal parameters depends. The type of coarse aggregate used in concrete mix is the main factor affecting the change in concrete properties due to high temperature. The aggregate types can be sorted out into three types: carbonate, siliceous and lightweight. Carbonate aggregates involve limestone and dolomite. Siliceous aggregate involves silica and include granite and sandstone. Lightweight aggregates are usually produced by heating shale, slate or clay.

The thermal parameters which are important to identify the behavior of concrete are:

- Density
- Thermal conductivity
- Thermal diffusivity
- Specific heat
- Coefficient of thermal expansion

1.2.1. Density

The mix design of concrete is the main factor influencing density of concrete. The density of a typical concrete is about 2300 kg/m^3. The presence of lightweight aggregates or air entrainment used to cast lightweight concrete decrease the density by half or 1/3 of this value. The temperature rise has a slight effect on the density of concrete. The main density loss, which is about 100°C, due to the rise in temperature occurs at 100 ºC where free water evaporates. The evaporation of free water has no significant effect on thermal response. While the moisture content decreases with temperature, the density change of concrete isn´t much at elevated temperature, except for limestone aggregate concrete which decomposes above 800°C with a corresponding decrease in density.

The density change of concrete with temperature is given by the equation 1 below (EN1992-1-2 section 3.3.2-(3));

Equation 1:

$$\rho(t) = \rho(20°C) \; for \; 20°C < t < 115°C$$

$$\rho(t) = \rho(20°C).(1 - 0.02 \, (t - 115) \, / \, 85) \; for \; 115°C < t < 200°C$$

$$\rho(t) = \rho(20°C).(0.98 - 0.03 \, (t - 200) \, / \, 200) \; for \; 200°C < t < 400°C$$

$$\rho(t) = \rho(20°C).(0.95 - 0.07 \, (t - 400) \, / \, 800) \; for \; 400°C < t < 1200°C$$

The weight loss is related to:

- Vaporization of free water
- Loss of bound water
- Decomposition of hydrates and aggregate (e.g. $CaCO_3 >> CaO + CO_2$)
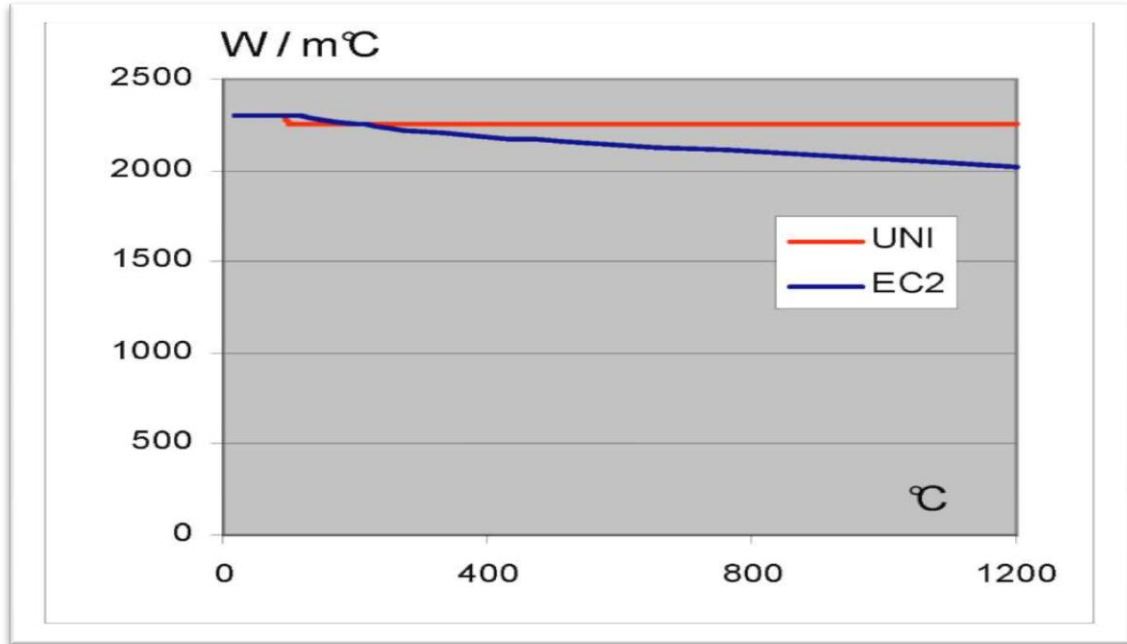
Figure 2 Density of concrete vs. temperature

1.2.2. Thermal Conductivity

Thermal conductivity represents the ability of a material to conduct heat and expressed as the ratio of the flux of heat to temperature gradient. The unit of thermal conductivity is joules per second per square meter of area of body in the case of 1°C temperature deference per meter thickness of the body. Type of aggregate, moisture content, density, and temperature of concrete are three factors which influences the thermal conductivity of concrete. The range of conductivity varies generally between about 1.4 and 3.4 j/m2s °C/m at the point of saturation of concrete. As can be seen in the figure below, the thermal conductivity depends on temperature and the type of aggregate influences it. The design values are given in the figure 4.
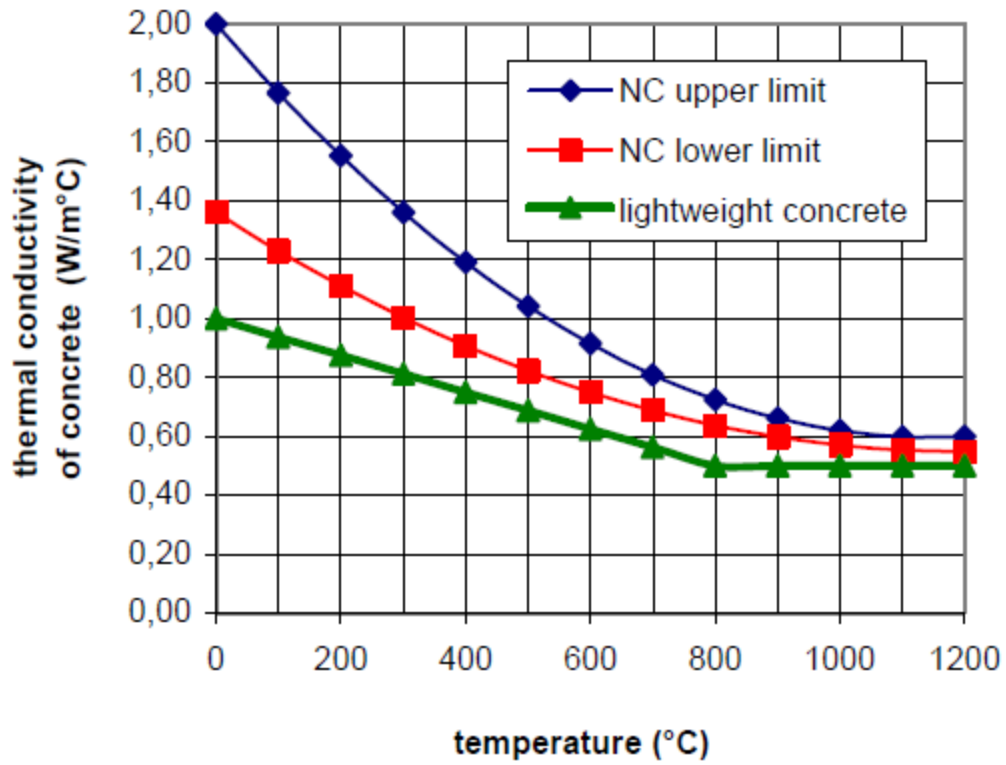
Figure 3 Thermal conductivity of normal and ligthweight concrete
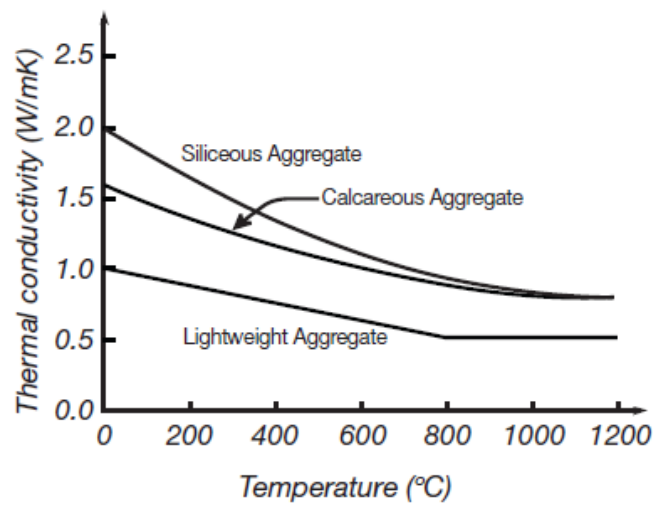
Figure 4 Thermal Conductivity

1.2.3. Thermal Diffusibility

Diffusivity is a measure representing the rate at which temperature changes within the concrete mass. Diffusivity is defined by the formula given in Equation 2 below. The conductivity, density, and heat capacity is used to calculate diffusivity. Temperature gradient is identified during transient heating problem.

Equation 2:

$$Diffusivity = \frac{Conductivity}{C\rho}$$

Where;

- C is the specific heat, and
- ρ is the density of concrete.

The diffusivity of concrete varies between 0.002 and 0.006 m^2/h.

1.2.4. Specific Heat

Specific heat measures the amount of heat which is needed to increase the temperature of a unit mass of a material by 1°C.It usually varies between 840 and 1170 j/kg per °C. The moisture content also affects the specific heat of concrete varying in board range. As can be observed in figure 5, the peak occurs in between 100°C and 200°C due to the need of energy to make water be driven off during heating process. The figure shown below represents the variation in the specific heat $c_p(\theta)$ of light concrete as a function of temperature and the effect of moisture content can be easily observed in the graph:
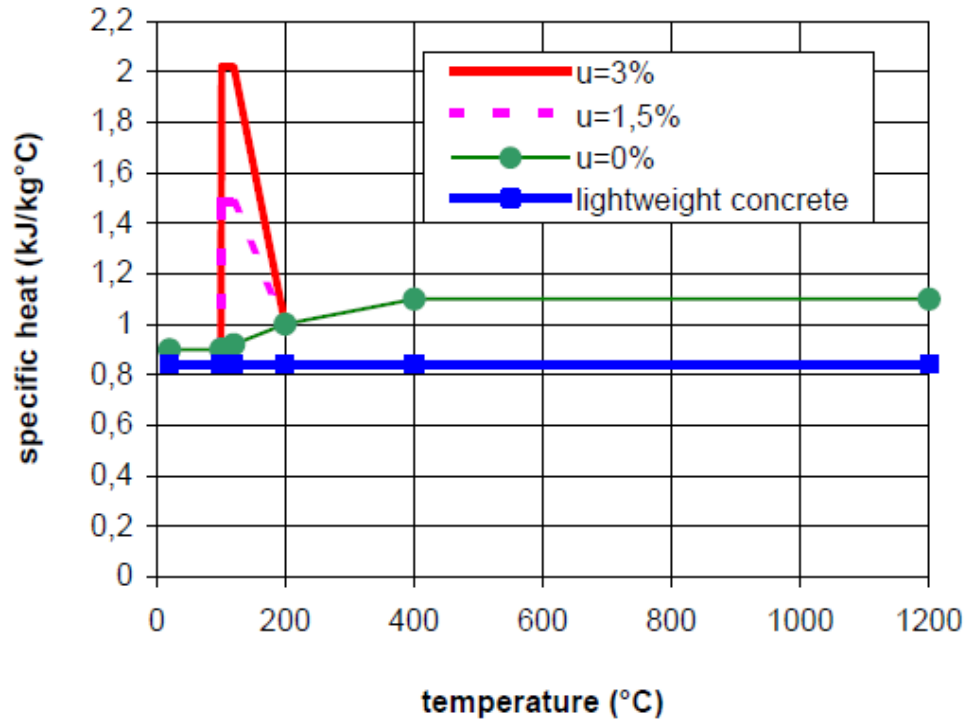
Figure 5 Specific Heat

Eurocode [6] introduces approximate values for design purposes as follows (EN1992-1-2).

Equation 3:

$$cp(t) = 900 \ (J/kg \ K) \ for \ 20°C < t < 100°C$$
$$cp(t) = 900 + (t - 100) \ (J/kg \ K) \ for \ 100°C < t < 200°C$$
$$cp(t) = 1000 + (t - 200)/2 \ (J/kg \ K) \ for \ 200°C < t < 400°C$$
$$cp(t) = 1100 \ (J/kg \ K) \ for \ 400°C < t < 1200°C$$

1.2.5. Coefficient of Thermal Expansion

Coefficient of thermal expansion is a measure of the change in unit length per degree change of temperature. Coefficient of thermal expansion of concrete is dependent on the mix proportions. Coefficient of thermal expansion of hydrated cement paste ranges between 11×10^{-6} and 20×10^{-6} per °C. Coefficient of thermal expansion of aggregates ranges between 5×10^{-6} and 12×10^{-6} per °C. Whilst the values of coefficient of thermal

expansion for Limestone and Gabbros are low, Gravel and Quartzite have high values of coefficient of thermal expansion. Hence it may be concluded that the kind and content of aggregate have obvious influences on the coefficient of thermal expansion of concrete.

Differential expansion and contraction may occur as a result of excessive thermal incompatibility between aggregate and paste. This causes the rupture of bond at the interface of paste and aggregate.

1.3. Mechanical Properties of Concrete at Elevated Temperature

As mentioned before, the rise in temperature has a great influence on the mechanical properties of concrete, such as strength, elastic modulus and volume deformation, causing a remarkable decrease in these properties. This results in the decrease in the structural quality of concrete. Moreover, for the concrete structures, Durability is remarkably affected by high temperature due to the physical deterioration process which may lead to undesirable structural failures. Thus, in order to reduce the harmful effects of high temperature on concrete, some preventative measures such as choosing the right materials should be introduced. As already known, the behavior of concrete subjected to fire are strongly dependent on material properties, such as the properties of the aggregate, the cement paste and the aggregate- cement paste bond, as well as the thermal compatibility between the aggregate and cement paste. Considerable variations may be observed on the chemical composition and physical structure of the concrete at elevated temperatures. Significant dehydration, involving the release of chemically bound water from calcium silicate hydrate, occurs at above $110\,^0C$.

1.3.1. Compressive Strength

Mix proportions, the maximum temperature and conditions of loading during heating have the most significant effect on the residual strength for the dense concrete after cooling. Concrete is able to resist temperatures up to 300°C without significant loss of its strength, *i.e.* the residual strength reduction is not severe up to this point. Age of concrete is another factor affecting the residual strength. At the temperatures greater than 500°C,

the compressive strength of structural concrete is decreased to small fraction of its original strength. In addition to this, the concrete containing a considerable amount of calcium oxide (CaO) possibly have a greater decrease in its strength which may not be enough to resist forces acting on the concrete members due to the expansion of calcium oxide under moisture attack. Free water is driven off above 100°C. This doesn´t affect the strength, but reduces the modulus of elasticity by about 10-20%. The decomposition of silicate hydrates starts at above 300°C while the dehydration of the portlandite starts at above 500°C. As can be seen clearly in the graph which shows the coefficient for reduction of characteristic strength changing with temperature below, slow decrease in compressive strength can be observed up to 450-500°C, while a relatively rapid decrease is the case above 500°C. Some aggregates start to convert or decompose such as SiO_2 and lime stone at 600°C.

Curve 1 : Normal weight concrete with siliceous aggregates

Curve 2 : Normal weight concrete with calcareous aggregates
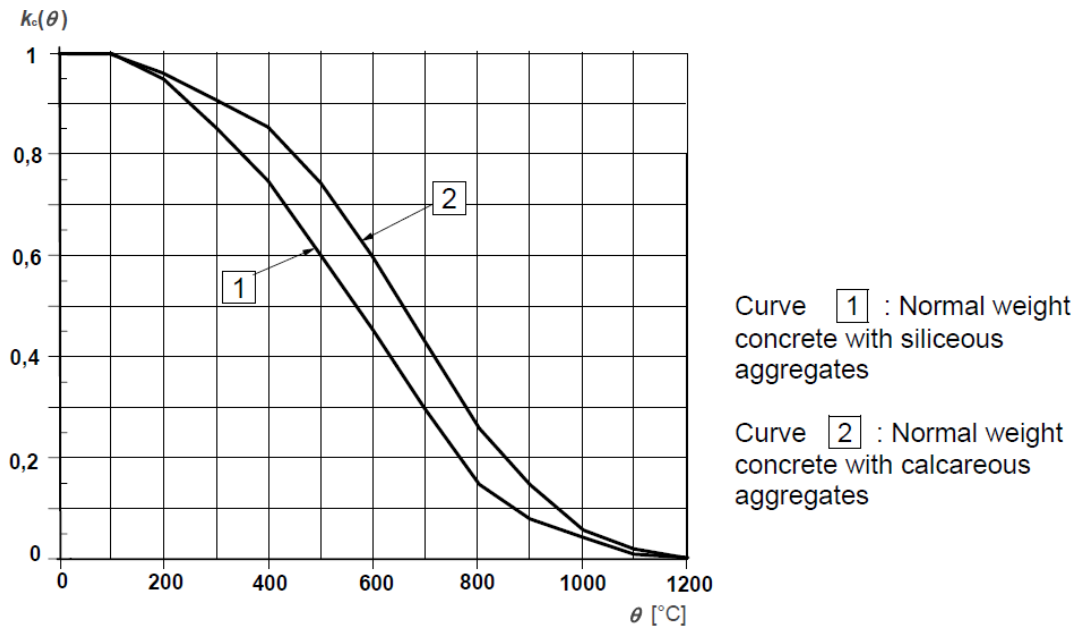
Figure 6 Coefficient $k_c(\theta)$ for reduction of characteristic strength (f_{ck}) of concrete

1.3.2. Tensile Strength

As already known, concrete has a limited capacity to carry tensile forces. Tensile strength of concrete can be expressed by $f_{ct} = \left(\frac{1}{10}\right) - \left(\frac{1}{15}\right) f_c$. Concrete is in-homogeneous at the micro-structural level (aggregates, cement paste, sand pockets, pores, voids) & pre-damaged (shrinkage-induced micro-cracking). Concrete has limited toughness (steep softening). Due to the limited capacity to release energy through inelastic deformations, concrete fracture can hardly be controlled. After cooling, the tensile behavior is even worse than in the virgin conditions as a result of thermal micro-cracking ($f^T_{ct}/f^T_c = 1/20$-$1/25$). Concrete tensile behavior requires the formulation of two different constitutive laws, one for loading branch (stress-strain law) and one for softening branch (stress-crack opening law), the latter requiring the evaluation of the fracture energy of the material.

kc,t(θ) values is given as:

kc,t(θ) = 1,0 for 20 °C $\leq \theta \leq$ 100 °C

kc,t(θ) = 1,0 - 1,0 (θ -100)/500 for 100 °C $< \theta \leq$ 600 °C
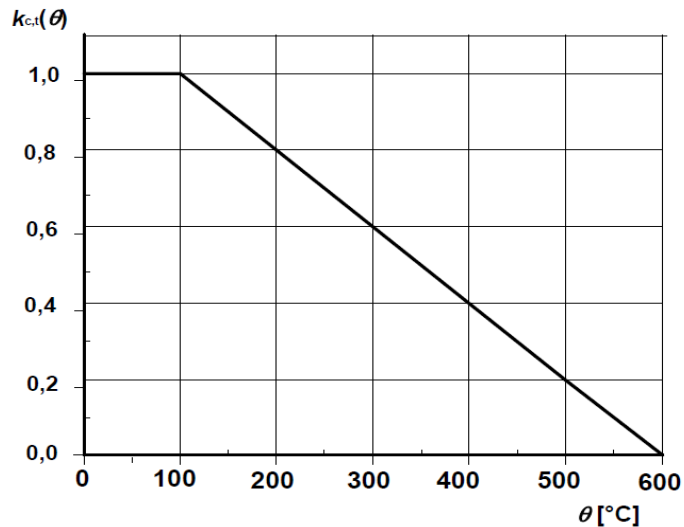
Figure 7 Coefficient $k_{c,t}(\theta)$ for reduction of tensile strength at elevated temperature

1.3.3. Modulus of Elasticity

The modulus of elastic of concrete which is taken as the tangent to the stress-strain curve at the origin is strongly dependent on the temperature changes under fire conditions. The elastic modulus is reduced to 80%−90% of the modulus of elasticity at room temperature, as the temperature increases to 100℃. Increasing the temperature reduces the modulus of elasticity. The dehydration process between.100℃ and 400℃ give rise to gradual loss in the bond between materials. This lead to a reduction of modulus of elasticity by about 20%−35% of the value at room temperature.

As can be seen in the table below, considerable reduction in modulus of elasticity is generated. After fire exposure, the amount of elastic modulus is reduced by 50%. When the temperature exceeds 600℃, the loss of elastic modulus reaches to 90% of its initial value. On the other hand, the elastic deformation of concrete member may not have significant influence compared to other effects. Table 1 shows the change in elastic modulus and strength of concrete including quartzitic aggregate at high temperatures.

	Temperature(^0C)						
	200	300	400	500	600	800	100
Strength (%)	80	70	60	40	20	5	0
Elastic-Modulus (%)	60	50	40	30	10	5	0

Table 1 Material properties of structural concrete after fire exposure

1.4. Failure of Concrete at Elevated Temperature

1.4.1. Spalling

Spalling is a phenomenon leading to the separation of layers or pieces from the surface of structural concrete. In normal strength concrete, rapid temperature changes typically at a rate of 20℃/min (Khoury 2000) lead to spalling. The permeability affects the spalling

behavior. That is why the tendency of high strength concrete (HSC), which possess low permeability to explosive spalling is higher than the tendency of normal strength concrete. Even in the case of relatively low heating rate (less than 5°C/min), explosive spalling of HSC may occur (Phan, L.T. et al. 2001). On the other hand, this phenomenon takes place on the surface of concrete.   So far there has been no clear model explaining why it occurs on the surface but not inside the concrete. The spalling may vary due to the structure size, strength, temperature history, etc. In order to understand the main reason for explosive spalling leading to considerable loss of section and load-bearing capacity, many researches has been conducted. As an example of the event leading to explosive spalling of concrete members, the 1996 Channel Tunnel fire causing almost 100% loss of the segment of the concrete due to spalling can be given. The concrete types used in these tunnels are high performance concrete having the compressive strength greater than 100 MPa. Considering the origin of spalling, it can be sorted out into three types which are aggregate spalling (splitting of aggregates), corner spalling, and surface spalling.

The spalling can also be classified into two types named progressive and explosive spalling according to physical mechanisms .Whilst concrete surface layers sloughs off gradually in progressive spalling , concrete pieces are burst out violently due to the sudden release of energy in explosive spalling.

Even though there have been performed many experimental and theoretical studies for several years, there are still some gaps in full understanding of this phenomenon. In the light of results of the studies fulfilled so far, it can be inferred that there are two factors driving the spalling. The thermal induced stresses led by high strains as a result of high temperature gradients and the generation of pore pressure on the heated surface due to the vaporization of water are two possible reasons for spalling. The combined effects of pore pressure and thermal induced stresses may cause explosive spalling under fire conditions. When the generated stresses in the concrete surpass the tensile strength, cracks are formed parallel to surfaces. Sudden energy dissipation results in uncontrollable failure of the heated surface. The contemporary results of the researches indicate that several factors have more influence on the spalling performance of HSC than normal strength concrete due to the permeability effects. Initial moisture content, porosity and permeability of concrete, type of aggregates, shape and dimension of structures appear

to have   significant effects on these phenomena, as well as concrete strength (both compressive and tensile) and the rate of temperature increase.

It appears that explosive spalling occurs in concrete columns, beams and girders within a limited range of stresses and moisture content. The time range of the occurrence of explosive spalling is generally 30 minutes under fire conditions and proceeds with a series of disruptions, each locally removing layers of shallow depth. The second type of spalling named sloughing off is of non-violent nature compared to explosive spalling. Falling off the concrete pieces occurs at the edges of columns and beams in a gradual way. As mentioned before the type of aggregates can be used to classify the spalling types. The concrete involving limestone spills off in thin layers ,having fracture planes passing through the coarse aggregate, while the concrete including gravel leaves an "exposed aggregate" surface after spalling. The loss of concrete layers due to spalling make the inner layers exposed to high temperature increasing the transmission rates through the deeper layers where the reinforcement may be present.

1.4.2. Cracking

The cracking is driven by the similar factors as those which lead to spalling. The fissures may be generated by thermal expansion and dehydration of the concrete at elevated temperatures. The formation of fissures may allow heat to reach up to reinforced bar in a direct way, imposing more thermal stresses, which result in further cracking. Cracks may cause fire spread between adjacent compartments under certain circumstances. Geogali and Tsakiridis [1] have conducted a case study on cracking in a concrete building exposed to fire, emphasizing on the penetration depth of cracks in concrete. It was observed that the temperature of the fire has an influence on the penetration depth. In other words, the higher the temperature concrete has experienced, the deeper the cracks penetrate. Major damage occurred on the surface near to the fire origin. The temperature that concrete has been subjected to can be determined by the proper evaluation of discoloration of concrete and the cracking pattern. It was identified that the temperature reached up to 700°C at around the reinforcement bars by this method. The cracks penetrating more than 30mm into concrete are related to a short

heating/cooling cycle. I should be stated that the stress conditions in the concrete are of great importance. Compressive loads resulted from thermal expansion contributes to the compaction of the material and prevention of the generation of cracks. This leads to much smaller reduction in compressive strength and modulus of elasticity. [1].

Thermal expansion of steel reinforcement is much greater than that of concrete at high temperatures. This gives rise to high thermal stresses and cracks around the steel bars in reinforced members. Such cracks usually take places at positions where the incipient cracks have already been formed due to shrinkage, flexural loading, etc. Moreover, the additional stresses may be generated by the thermal incompatibility of aggregate and cement paste causing the surface cracks. The following marks give detailed information about the cracking pattern of concrete after subjected to fire.

(1) The difference between thermal elongation of the cement matrix and aggregates gives rise to generation of additional stresses. Micro cracks can be observed at about 100ºC and this kind of cracks becomes larger with increasing temperature because of the fact that the coefficients of thermal elongation diverge with temperature. Those cracks directly affect strength of concrete.

(2) The difference between thermal elongation of the cement the concrete and the reinforcing steel causes additional stresses. At above 400°C, the effect of this stresses becomes significant for normal dense concrete. The cracks occur near the reinforcements.

(3) Additional stresses may be generated due to different temperature gradients when the size and shape of a cross-section changes along the length. Corners and edges of cross-sections are susceptible to such cracks.

(4) The non-linearity of the temperature gradient within the cross-section produces stresses. This type of cracks is generated in the inner part of a cross-section. On the other hand, stresses imposed by mechanical loading have great influence on the position and occurrence of cracks.

(5) During cooling down, some stresses are formed during if the free re-contraction is prevented. Under extreme conditions cracks caused by this reason, may extend through the total cross-section, but it is also possible that they are confined to the inner part.

(6) The effect of sudden cooling down by a fire extinguishing hose stream should be considered. Re-contraction may be generated in the cross-section due to the water leads. As a consequence some cracks occur near the surface. The abovementioned cracks except for (5) and (6) are reduced by the cooling and re-deformation process of the structure. Nonetheless, it is not possible to close the cracks. In monolithic structures, internal stresses are generated due to thermal deformation of structural members subjected to a fire in the surrounding assembly which is not directly affected and remains cool. Hence, cracks may be resulted from the strong exposure in these regions. This fact should be taken into account, if there is an indication of a strong fire attack by the damage of the heated part of the structure. The hidden cracks must be determined and some preventive measures should be taken because unrepaired cracks may lead to long term deformations of the concrete structure.

1.4.3. Color

The temperature that a concrete member has experienced and the duration of a fire can be determined by examining the color change which alters with the temperature increase. When temperature reaches 300°C, a pink discoloration may readily be observed. The detection of the onset of pink discoloration is of importance because it coincides with the onset of considerable strength loss as a result of heating. Therefore, any pink discolored concrete should be regarded as being suspect (discoloration may also be due to carbonation). The presence of ferrous salts in aggregates or in the sand is responsible for pink discoloration. However, in some cases, ferrous salts may not be present. This means that a concrete structure may be damaged even if there is no pink discoloration. The pink discoloration is of more importance for the concrete involving siliceous aggregates. The

susceptibility of concrete including calcareous and igneous crushed rock or lightweight aggregates to this discoloration effect is less. During fire fighting And cooling process, further color variations may be observed [1].

1.4.4. Conclusion

Briefly, the behavior of concrete subjected to fire is of complex nature. The degradation of physical properties is strongly dependent on the mix proportions of concrete, moisture content and relevant environmental parameters, such as the maximum temperature that the concrete has experienced and fire duration. These variations usually cause the irreversible loss of the physical properties of concrete. It is required to conduct systematic researches on the effects of different heating conditions on concrete. In order to provide a better understanding of the behavior of concrete, missing parts must be enlightened. As mentioned at the very beginning of this chapter, this work mainly focuses on the effect of pore pressure on the tensile strength of concrete under fire conditions. In the latter chapters, the works related to pore pressure measurements inside the concrete, what has been done in this work and the results of the experiments are presented.

2. **Literature Review**

2.1. Temperature, pore pressure and mass variation of concrete subjected to high temperature – Experimental and numerical discussion on spalling risk (Mindeguia J.C., Pimienta P., Noumowe A., Kanema M., 2009)

Pore vapor pressure has an essential role in the mechanism of thermal instability of concrete (i.e. spalling), but determining pore vapor pressure is not easy via experiments and validation of results is needed by numerical analysis. In this work, a device to measure temperature, pore vapor pressure and mass loss of concrete specimens was used in order to better understand the thermo-hydral behavior of concrete exposed to high temperature.

Since having different matrix compactness was important, five concrete mixes were designed, by varying the W/C ratio, and the compressive strength was measured at 28 days on water stored cylindrical samples. The experimental device developed by Kalifa et al. was used.

A radiant heater was placed 3 cm above a prismatic sample ($30x30x12$ cm^3) and the thermal load was applied to the square faces while porous ceramic blocks were used as insulation on lateral faces, therefore heating flux could be assumed to be quasi-unidirectional; the sample was on top of a balance which measures the mass loss continuously during heating (Figure 8).

The main reason of mass loss was the escape of fluid from concrete (water, vapor and dry air). Fluid was able to escape from all sides of the sample due to the reason that it was unsealed.

Six measuring gauges were placed inside the samples during casting, in order to measure pore pressure and temperature simultaneously. The gauges were made of a sintered metal round plate (ϕ 12x1 mm). A thin metal tube (inner diameter 1,6 mm) was welded to these gauges and metal tubes came out of the unheated face of the sample. The tube is then connected to a piezo-electrical transducer thanks to a flexible tube filled with

silicon oil. Afterwards, thermocouples (ϕ 1.5 mm) are inserted into metal tubes until they reach to sintered metal plates.

One of the gauges was single plain tube which was located to just near 2 mm to heated face, to measure the temperature only. The other five tubes were placed at 10, 20, 30, 40, 50 mm of the heated face, in order to measure internal temperature and pressure. In this measurement zone, heating flow and fluid movement were assumed to be unidirectional.
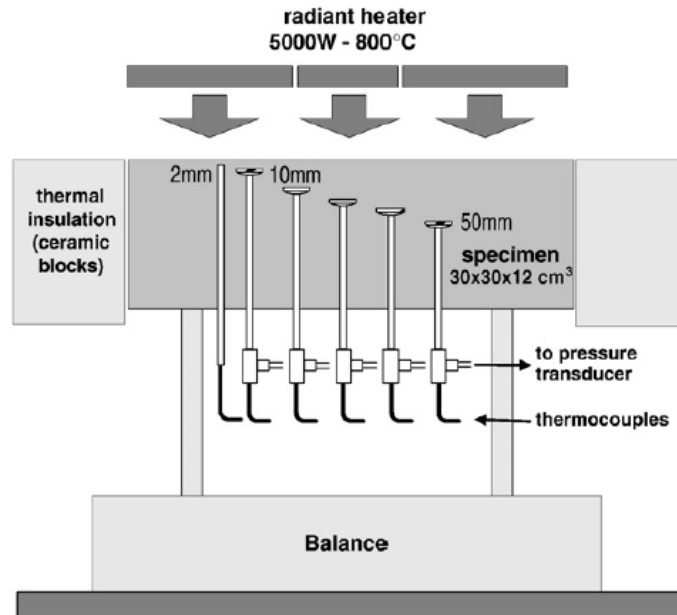
Figure 8 Scheme of experimental setup

It is a fact that concrete is a porous material, partially saturated by liquid water. Three phases fill the porous media: liquid water (free and absorbed water), vapor and dry air. The interface between the liquid water and the gas phase (vapor and dry air) is characterized by a surface tension that induces a discontinuity between the fluids pressures, particularly, the difference between liquid water pressure and gas pressure (defined as the sum of vapor pressure and dry air pressure) is called capillary pressure.

The capillarity pressure mainly depends on the relative humidity of concrete pores and can reach high negative values (for instance, at 20 °C and for a relative humidity of 50%, the capillary pressure equals to −95MPa). One important result is that drying of concrete involves a decrease of capillary pressure, and can explain the delayed strains of concrete (such as drying shrinkage and creep). A simple temperature-volume phase diagram of

water shows that the volume increase of vaporization process is quite more important than the thermal expansion of liquid water. Through neglecting the thermal expansion of dry air, it could be assumed that theoretically measurement system is only able to measure pore vapor pressure.

For each concrete mix, two tests were conducted. The radiant heater was controlled in such a way that its temperature rapidly reached 600 $^{\circ}$C (after 5 minutes) and the power was maintained constant during 6 hr. Such a heating rate was chosen to be fast enough to produce pore vapor pressure and slow enough to avoid too much thermal damage to the concrete sample.

Throughout the test, water drops and vapor flow escaping from the samples were observed. This important damage (i.e. cracking and aggregate spalling) can be explained by the instable behavior at high temperature of the flint aggregates used in the concrete mixtures. Complementary high temperature tests were carried out on flint aggregates (without cement paste); they confirmed the fact that the flint aggregates used in the concrete mixtures are thermally unstable from 120 °C to 200 °C.

Figure 9 presents the temperatures measured into the B350 concrete sample. For several tests, some gauges were unintentionally clogged with cement paste during casting. As a consequence, temperature measurements for some depths may not appear in the graph. For each measuring point, a slight plateau is observed, i.e. a perturbation, in the increase of temperature. This plateau is due to the water phase change (vaporization) which is an endothermic transformation that consumes a great part of the energy that is brought by heating. As a consequence, the heat transfer into concrete sample was slowed down.

It is aimed to emphasize that by this way, the water vaporization can induce additional temperature gradients. These gradients could modify the stresses in a concrete structure during fire.
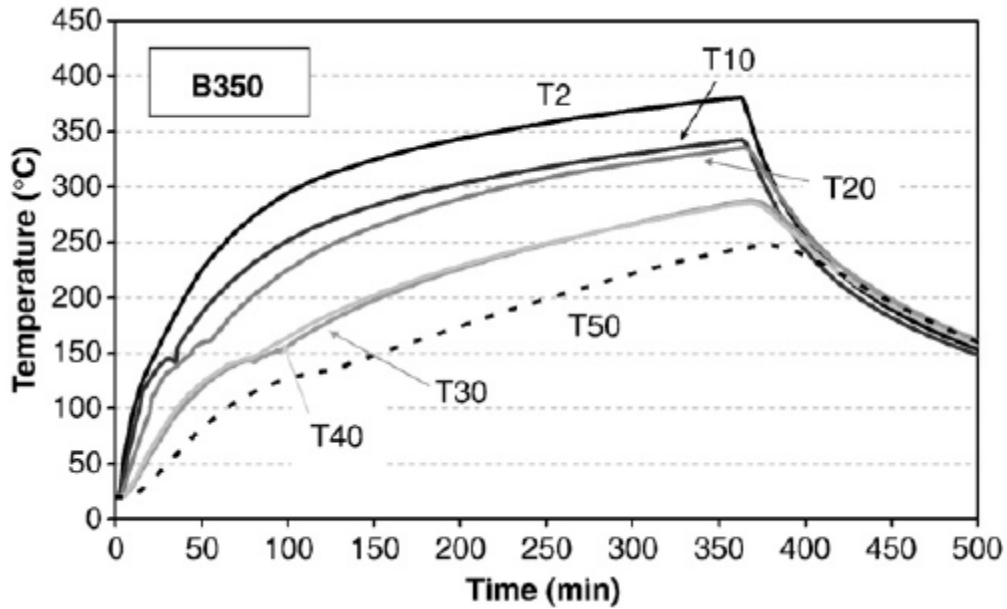
Figure 9 Temperature as a function of time (B350)

It was also observed that the temperature plateau depends on the concrete compactness. This dependence can be explained by the capillary forces that exist in a pore at the interface between liquid water, gas phase (vapor and dry air) and solid (concrete matrix). These capillary forces influence the vaporization process: under a pressure of 0.1MPa, and for an infinite flat surface of water, vaporization takes place at 100 °C. At the opposite, for very small pores, capillary forces reaches high values and higher temperature is needed to extract vapor molecules from liquid water.

The Figure 10 presents the pore pressure measured in the sample B350. If two similar tests are compared, it can be seen that the pressure measurement is scattered. It is a local measurement and the pressure value depends on the tube location (into cement paste, close to an aggregate or in an air void).
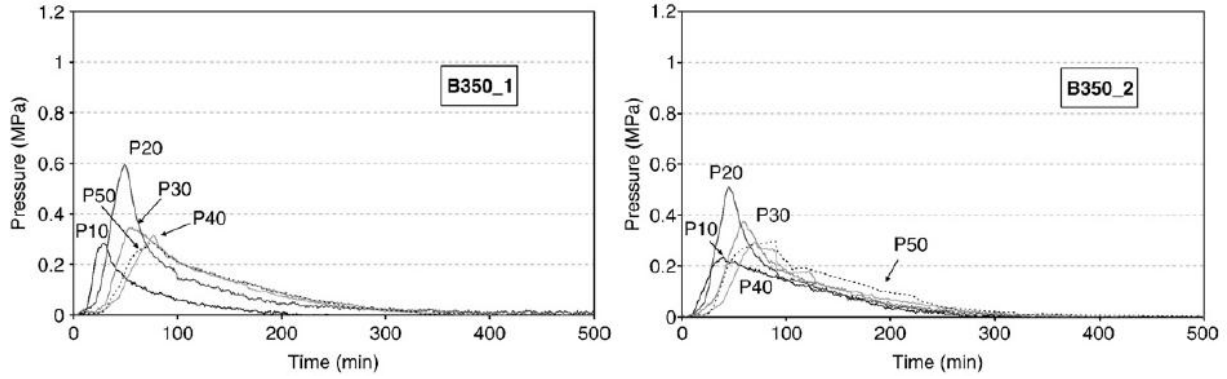
Figure 10 Pressure vs. Time (B350)

It is presented in the Figure 11 that the evolution of temperature and pressure as a function of time that have been measured at 40mm of the exposed surface for one of the five concretes (the same behavior has been observed for all the concretes). It can be seen that the peak of the measured pore pressure was reached during the temperature range of vaporization (slight plateau on the temperature curve). This result indicates that water vaporization into concrete is well assumed to be responsible for the build-up of the pore pressure that is measured by abovementioned experimental device.
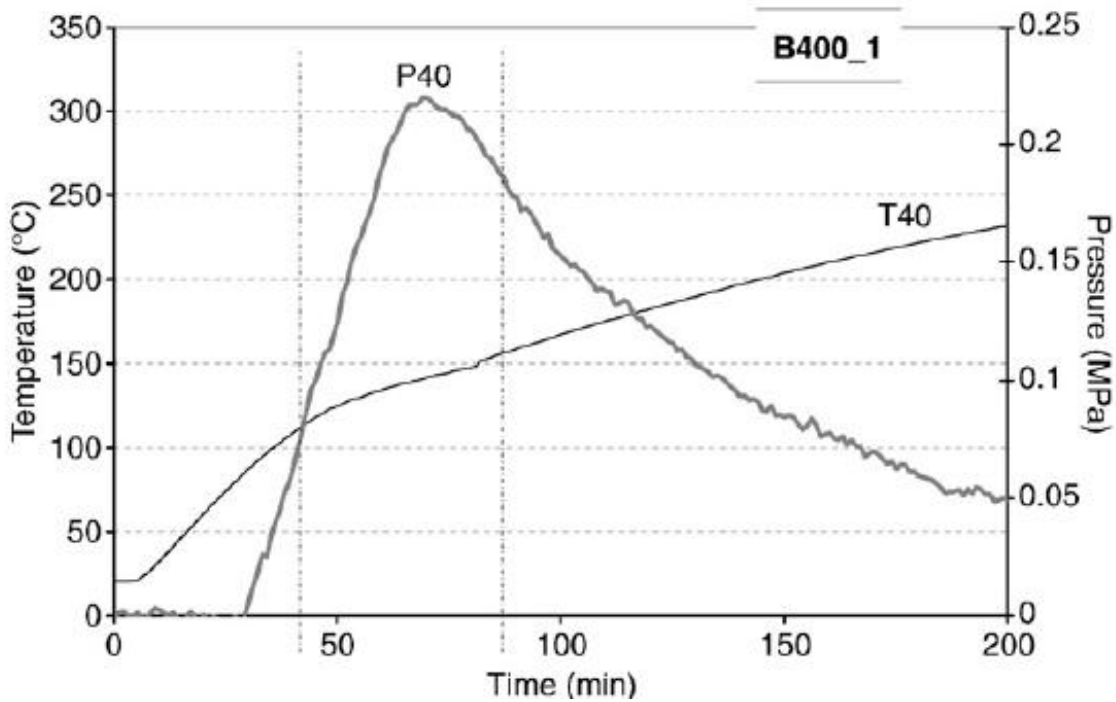
Figure 11 Temperature & pressure evolution

In the Figure 12, the evolution of the pore pressure as a function of temperature can be seen. The measured pressures (P) obtained from experiments are compared with the saturating vapor pressure curve (P_{vs}). In most cases, it can be seen that the measured pressures follow the P_{vs} curve during the ascending branch.

The results seem to demonstrate that the measured pore pressures obtained from the experiments correspond to vapor pressure. On the other hand, some of the measured results exceed the P_{vs}. Because of the fact that it is theoretically impossible, vapor pressure is not responsible for the overpressure. This overpressure is often related to the partial pressure of the dry air which is enclosed in the porous media. The partial pressure of air in a pore strongly depends on its liquid water saturation: the higher the water saturation, the lower the free volume available to the air to expand during heating. As a result, the effect of thermal expansion of dry air on the total pressure will be important for the pores with high liquid water content. However, since it is assumed that water moves into the inner part of the sample during heating, it can be the reason for that the overpressure is more important in the deepest zone from the heated surface of the sample (Figure 12).

It is observed a decrease of the pressure at around 175°C. The reason for this phenomenon can be the important amount of the energy consumption by the phase transformation of water. It is assumed that this consummation is responsible for the cooling of a concrete zone close to the sensor.

Figure 12 Pressure as a function of time (B350) along with the saturating vapor pressure curve P_{vs}

These pressures can be considered as low values compared to those of previous studies carried out on concrete with similar compactness. This may be explained by the important damage (i.e. cracking) of the sample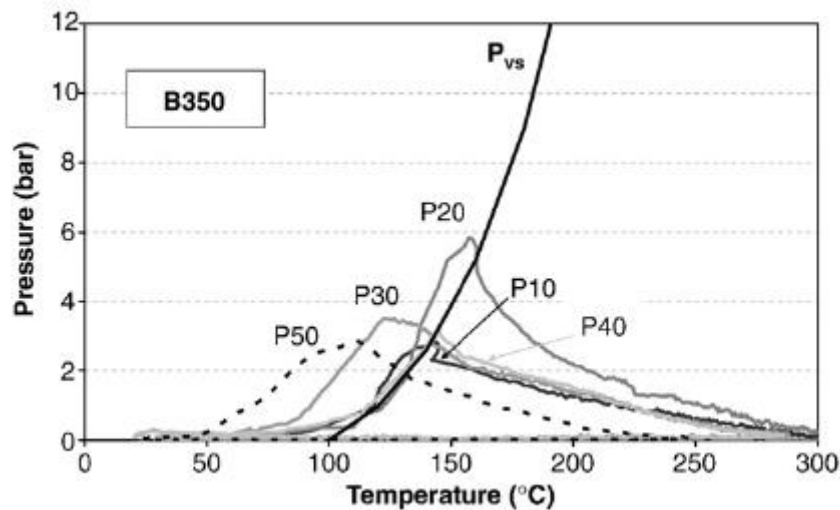s due to the unstable behavior of the flint aggregates used in the concrete mixtures. Indeed, there is an important link between the permeability and the damage of concrete. In particular, high damage strongly modifies the transport properties of concrete, making easier by this way the movement of fluids. As a first conclusion, cracking must be considered in the case of high temperature in order to properly deal with thermo-hygral behavior of concrete. Especially, for rapid heating, pore vapor pressure should be significantly reduced due to possible severe damage in concrete.

The maximal pressure strongly depends on the concrete compactness. In particular, high pore pressure takes place due to the low permeability.

2.2. High Temperature behavior of HPC with polypropylene fibers from spalling to microstructure (Pierre Kalifa, Gregoire Chene., Christophe Galle, 2001)

The usage of polypropylene (PP fibers) for the high performance concrete (HPC) is a way to decrease the risk of concrete spalling at high temperatures. This work focuses mainly on the way the fibers behave and the optimization of the fiber dosage. Standard thermal curves (ISO 834) were used for the tests performed on columns, loaded or not loaded, on small beams, on cylinders and on small-size mortar plates .The degree of efficiency of the fiber considering the spalling was qualitatively estimated by means of visual assessment of the degree of spalling.

The concrete type used in the experiments was studied in the French National Project BHP2000 under the name of M100. The concrete is characterized by calcareous aggregates involving silica fumes (%10 cement), water to binder ratio 0.3.

In the experiments, PP fibers having the length of 19 mm and a cross-section of 50×150 μm^2 were used. The fibers are stored in a bunch and they are scattered when mixing the concrete. The melting point of PP fibers is 171 °C and the fibers vaporize at

341 °C. The PP amounts (α_f) for the tests differs from 0 to 3 kg/m^3.Because of the fact that the addition of fibers reduces the workability, increasing the amount of cement and addition of the super plasticizer seem to be necessary.

The radiant heaters were used to impose the thermal load to the upper part of the specimen (30x30x120 cm^3) while the other four lateral faces are insulated. The balance is placed at the bottom (Figure 13).

Figure 13 The experimental setup
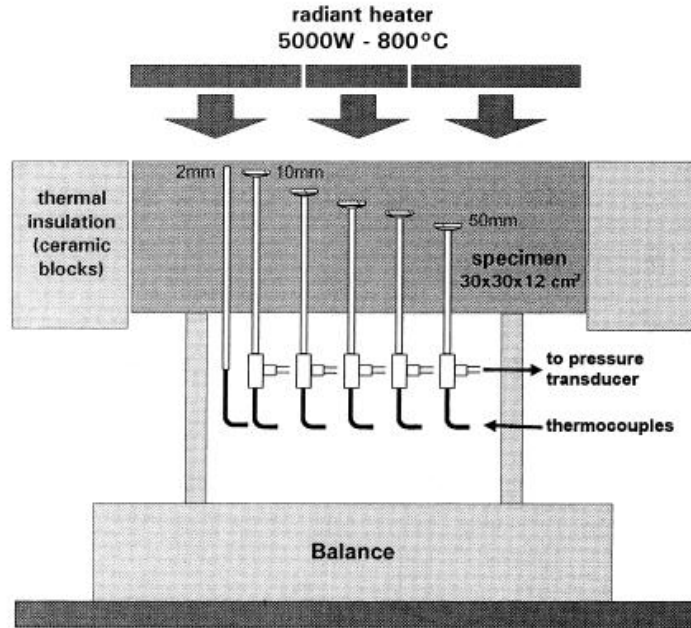
The specimens are equipped with the gauges which enables the pressure and temperature measurements at the same location. As for the gauges, they are composed of a disk of porous sintered metal (ϕ 13 mm) encapsulated into a metal cup which is connected to a metal tube. Piezoelectric pressure transducer and the thermocouple are introduced by means of the connector (Figure 14).
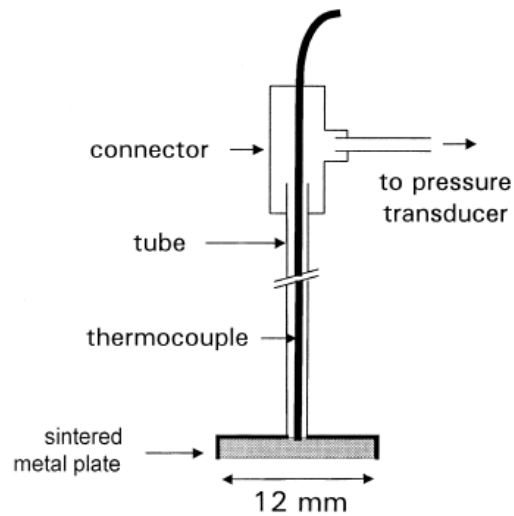
Figure 14 Gauges & metal pipe with thermocouple

Five gauges are placed in the $10 \times 10 \ cm^2$ control zone at 10, 20, 30, 40 and 50 mm from the heated face. In addition to these 5 gauges, a thermocouple in the plain tube is introduced. It is placed 2 mm inward from the heated face.

The tests were performed by heating the concrete up to 600 °C target temperature during 6h. The time required for the heater to reach the target temperature is very short. Two tests were performed for each mix.

The specimens were stored in bags for 3 months after casting in order to have a homogeneous moisture state. The latter was measured on smaller specimens stored in the same conditions by drying at 105 °C until a steady mass state was accomplished (0,02%, 24 h). The initial moisture state ranged between 3.0% and 3.2% by mass.

Temperature field, pore pressure field and mass loss which were measured during the test establish the major indicators of thermo-hydral process.

The temperature field inside the concrete is developed as a function of the thermal properties of the material which changes during heating due to microstructure changes as well as to physical-chemical changes that occurs during heating. Water vaporization is the most energy-consuming transformation in the temperature range.

As a result of the increase in temperature, the mass loss is mainly related to water loss, transferred outwards in vapor state. The fibers inside the specimens do not have any significant effects on mass loss.

All specimens have a similar thermal behavior (Figure 15) at each depth; this implies that fiber dosage does not affect the global temperature rise. On the other hand, the temperature rise in a way that plateau-like disturbance occurs starting from 100 °C till 160 °C and 200 °C ,which is very close to the melting point. In plane concrete, this disturbance ends around 250 °C.

The plateau-like disturbance is related to the consumption of energy due to the vaporization of water in the porous network and the ending point is correlated to the pressure peak. The pressure curves reveal that the post peak pressure drop is higher in fiber concrete and this shows the role of fibers in the creation of the network.
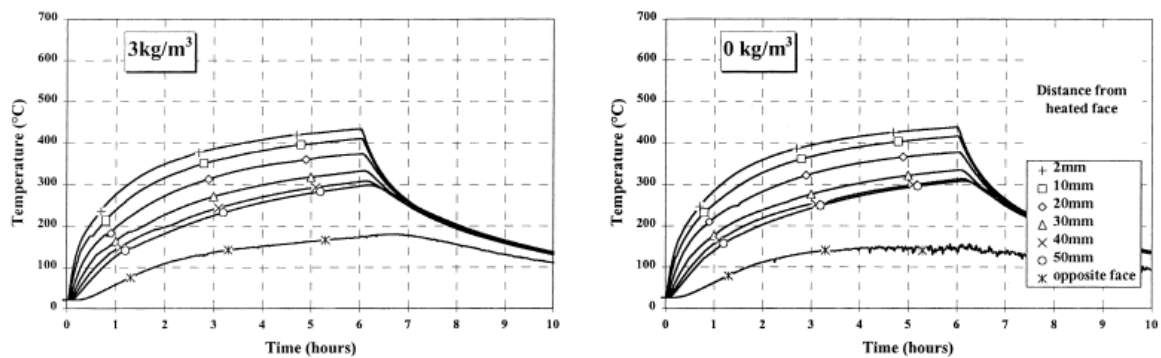
Figure 15 Evolution of temperature with time at various depths

On Figure 16, the effect of fibers can be seen. Pressure versus time curves have similar shape for all dosages. On the other hand, the height of peaks drastically decreases with increasing fiber dosage. Therefore, fibers directly contribute to the reduction of the stress fields in the skeleton due to pore pressure.

Pressure (MPa)

3 kg/m³

3 kg/m³

Distance from heated face

- □ 10mm
- ◇ 20mm
- △ 30mm
- × 40mm
- ○ 50mm

2.4 kg/m³

2.4 kg/m³

1.75 kg/m³

1.75 kg/m³

1.1 kg/m³

1.1 kg/m³
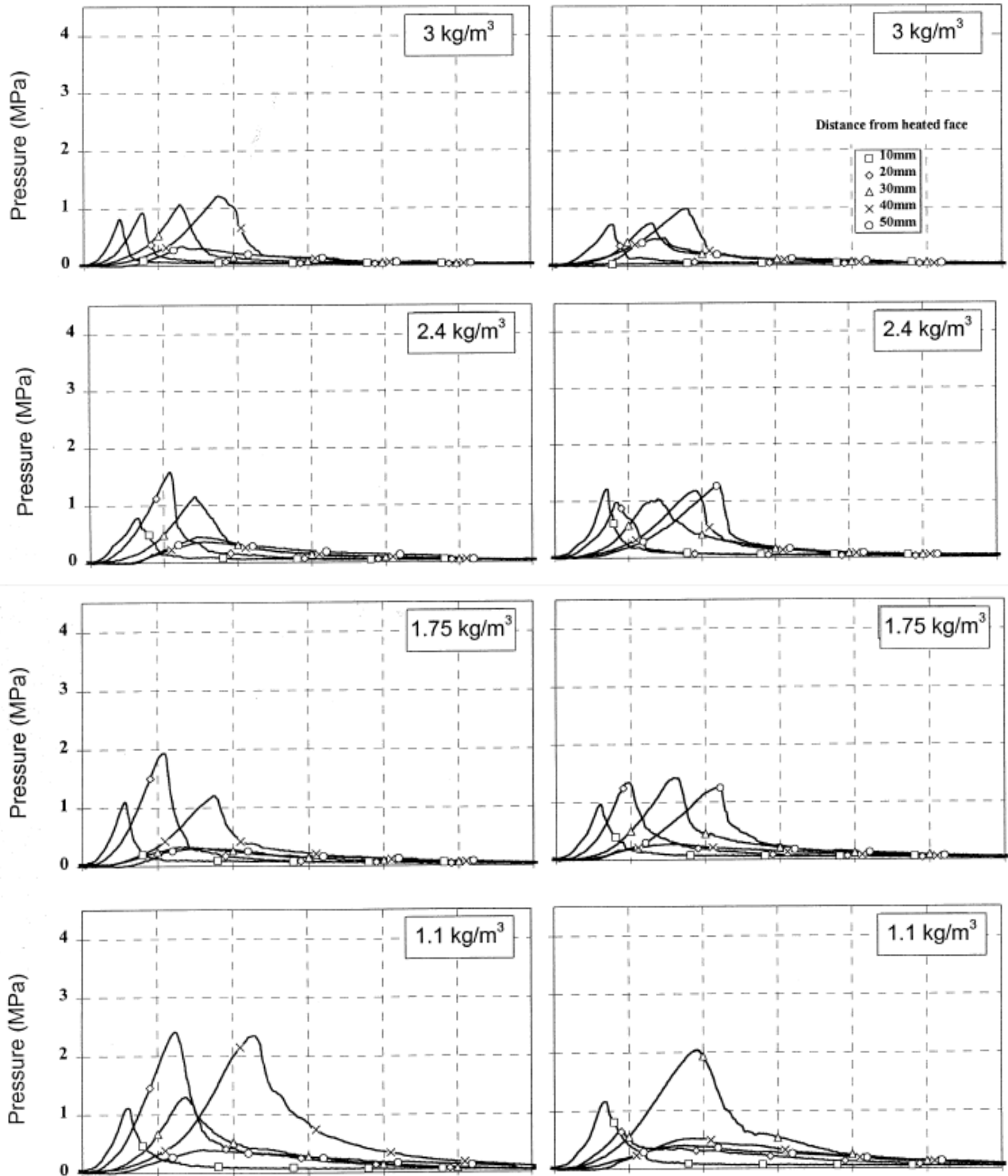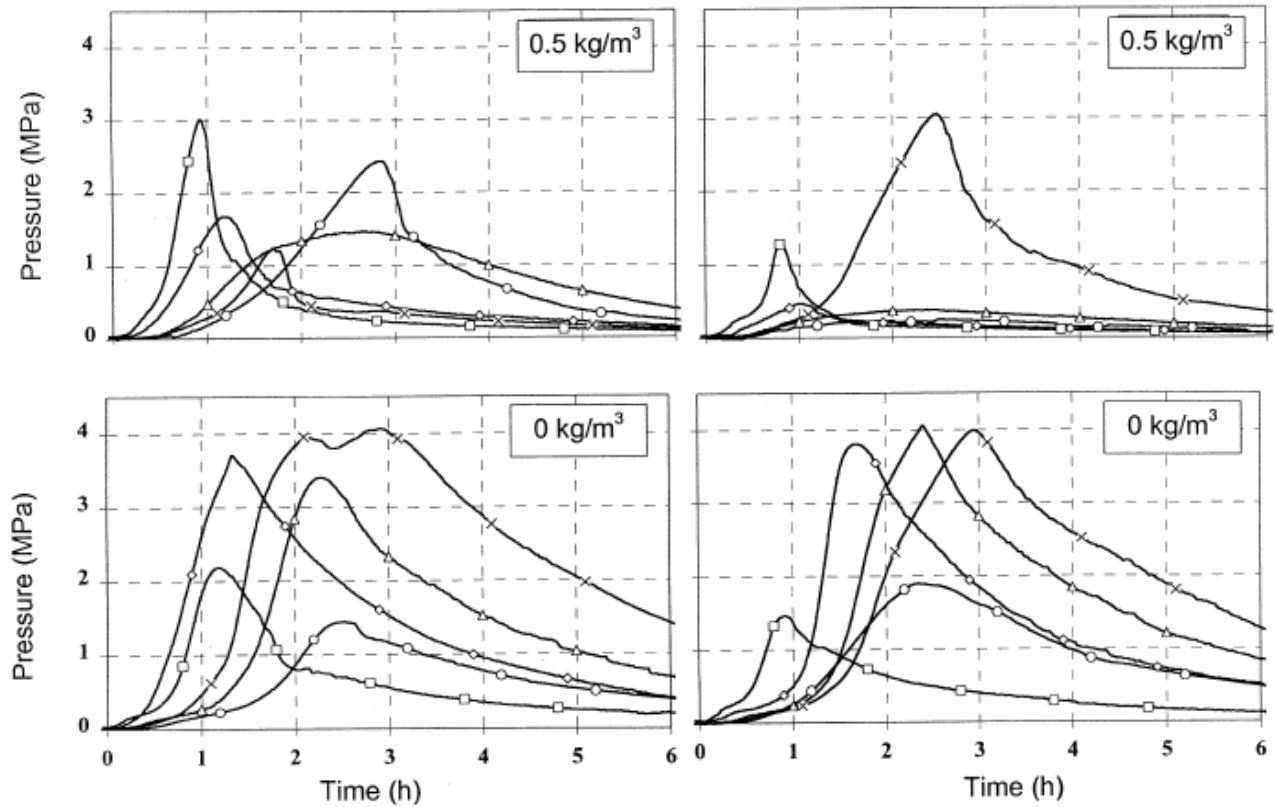
Figure 16 The measured pressure vs. time graphs

2.3. Effect of fire on concrete and concrete structures (Khoury G. A., 2000)

The behavior of concrete in fire depends on its mix proportions and constituents and is determined by complex physicochemical transformations during heating. Normal-strength concretes and high-performance concretes, micro structurally follow similar trends when heated, but ultra-high-performance concrete behaves differently. A key property of concrete, that is unique amongst structural materials, is transient creep. Any structural analysis of heated concrete that ignores transient creep will yield erroneous results, particularly for columns exposed to fire. Failure could occur due to: a) loss of bending or tensile strength, b) loss of bond strength, c) loss of shear or torsional strength, d) loss of compressive strength and e) spalling of concrete.

The risk of explosive spalling in fire increases with decrease in concrete permeability and could be dramatically reduced by the appropriate inclusion of polypropylene fibers in the mix and/or by protecting the exposed concrete surface with a thermal barrier.

There are two problems of concrete in fire:

- deterioration in mechanical properties as temperature rises, due to physicochemical changes in the material during heating (Figure 17);
- explosive spalling, which results in loss of material, reduction in section size and exposure of the reinforcing steel to excessive temperatures.

Figure 17 Physicochemical process

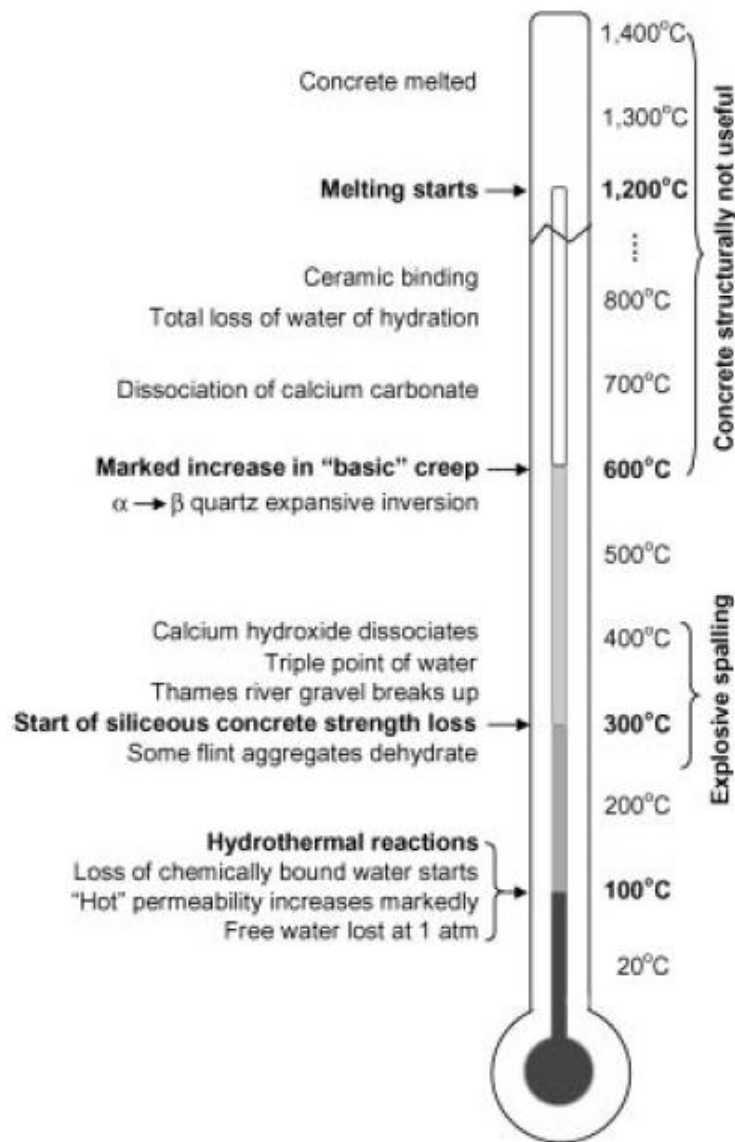Deterioration in mechanical properties of concrete upon heating may be attributed to three 'material' factors:

- physicochemical changes in the cement paste;

- physicochemical changes in the aggregate;

- thermal incompatibility between the aggregate and the cement paste;

and are influenced by 'environmental' factors, such as:

- max temperature;

- heating rate;

- applied loading;

- external sealing influencing moisture loss from the surface.

Up to the 1970s, scientists were puzzled as to why concrete does not break up when heated above 100 ^{o}C, because the differential strain resulting from the expansion of the aggregate and shrinkage of the cement paste is far too large to be accommodated by elastic strains; the discovery of the phenomenon of 'transient creep' provided the answer.

Transient creep (strictly, it should be called load-induced thermal strain, LITS) develops during first heating (and not during cooling) under load. Above 100 ^{o}C it is essentially a function of temperature and not of time and is, therefore, relatively easy to model mathematically in a short-term heating scenario such as fire. LITS is much larger than the elastic strain, and contributes to a significant relaxation and redistribution of thermal stresses in heated concrete structures. Until very recently, all measurements of tensile strength at high temperatures were performed by indirect means. However, there is sufficient evidence to show that the tensile constitutive behavior of concrete at high temperature cannot be adequately determined from indirect 'tension' tests (i.e. splitting and bending). For this reason, stress–strain tests in *direct tension* were performed *at high temperatures* for the first time last year at Imperial College in collaboration with Politecnico di Milano. The direct tensile hot strength declines with increase in temperature.

2.4. An experimental relationship between complete liquid saturation and violent damage in concrete submitted to high temperature (S. Dal Pont, H. Colins, A. Dupas, A. Ehrlacher, 2005)

The work focuses on a damage mechanism for high performance concrete at high temperature in order to offer a low-cost method to demonstrate the damage mechanism and warn against spalling risk.

The goal is reached by measuring gas pressure and the temperature in a concrete cylinder specimen (150 mm diameter and 50 mm thickness) heated on one face up to 280 °C. The heating process is performed by imposing a convective and radiative flux. Especially, the concrete surface reaches 280 °C within 8 minutes under ISO-fire loading.

The analysis results along with the saturating vapor pressure curves made the establishment of a singular and original relationship between them possible, leading to a possible explanation of concrete hygra-thermal damaging and spalling. This experimental correlation emphasizes on the significant role of gas and liquid and provides a deeper understanding of concrete at high temperatures.

The lateral surface of the specimens has been insulated in order to assure a unilateral flux and prevent the thermal dispersions. A pressure sensor and J type thermocouple were inserted to each specimen. The gauges are made of a steel tube, stuck into concrete by means of high-resistance glue, at 20–25 mm from the heated face. Finally, a pressure gauge (able to measure pressures up to about 1.5 MPa) has been also stuck on the free tube end (Figure 18). The use of high thermal resistance glue allowed a perfect seal, and no leak was observed during the tests.
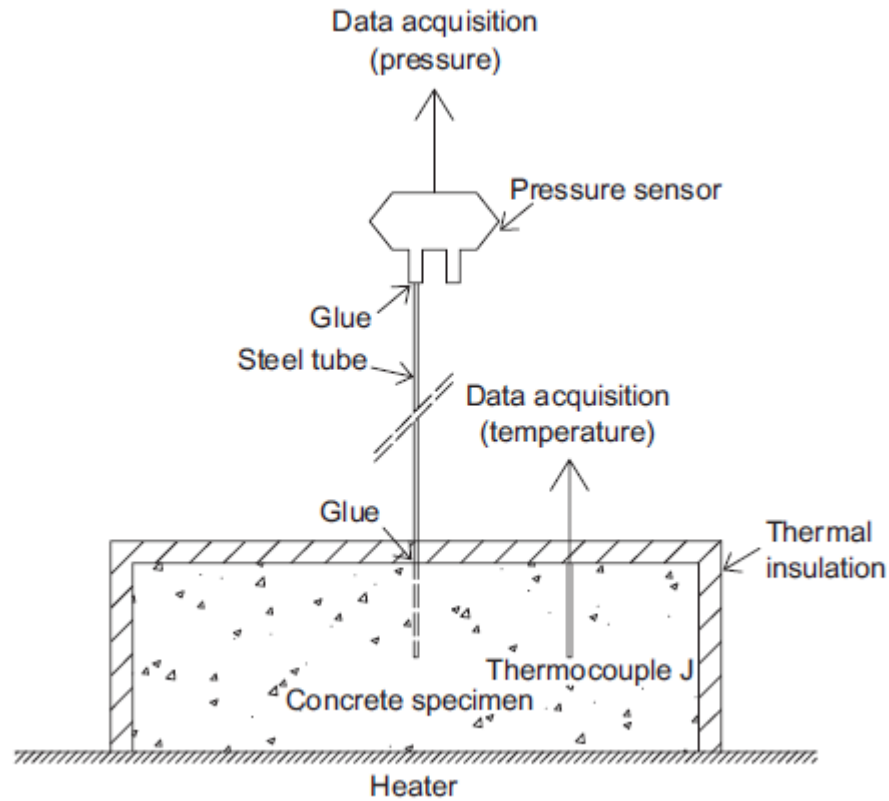
Tests were performed by filling the tube with oil (two different types were used, demolding oil, which is used on moulds for demolding concrete, and silicone oil) or leaving the set empty. At first, oil was used as it is a nearly incompressible fluid; the purpose was to transmit the gas pressure inside concrete at the other side of the tube. Further analysis was carried out leaving the tube empty. Moreover, two different types of steel tubes were used (external diameter $\varphi=2$ mm, internal diameters $\varphi= 0.5$ mm and $\varphi= 0.8$ mm).

The tests were performed on a high-performance concrete, the M100 which has been used in previous studies and during the national French project BHP2000 (Table 2 for characteristics). The concrete was heated to about 280°C at the surface (which corresponds to 220–250°C in the zone where the pressure sensor had been placed) at an

initial heating rate of about 1.5°C/min. No visible cracks were observed on the surface after the tests.

At least three tests were performed for each condition (empty tube, tube filled with silicone oil, tube filled with demolding oil). Some tests failed owing to the high pressures measured by the gauge that is, as the measured pressure approached or exceeded the limit value of 1.5 MPa, the pressure gauge collapsed (Figure 19, Figure 20, Figure 21, Figure 22, Figure 23 & Figure 24).

Table 1. M100 concrete formulation

Constituent	kg/m^3
Water	124
Cement CEM I	377
Seine sand (Silico-calcareous, 0–4 mm)	432
Boulonnais sand (calcareous, 0–5 mm)	439
Boulonnais aggregate (calcareous, 5–12·5 mm)	488
Boulonnais aggregate (calcareous, 12·5–20 mm)	561
Silica fume	37·8
Water-reducing admixture (Resine GT)	12·5
Retarder	2·6
Water/cement	0·33

Table 2

Figure 19 to Figure 24 present the results of the laboratory tests. The heater used during the analysis allowed an initial heat rate of about 1.5 °C/min up to the temperature of about 280°C. It should be emphasized that the heater that was used during the analysis did not allow a perfect reproducibility of the results; that is, the heating rate and final temperatures changed after nearly every test probably owing to different external conditions.

Starting from the temperature of about 50°C, a small augmentation of registered gas pressure has been recorded, namely fickian flows and air thermal dilation are not negligible. The phenomenon is present up to about 100–105 °C. As we could expect, at about 100 °C a small temperature plateau has been observed; that is, during water

vaporization, latent heat is of importance. When the concrete temperature surpasses the temperature of about 105 °C, gas augmentation rate becomes more important.

If we compare experimental measures with the saturating total pressure it is possible to observe that when the pressure approaches the peak value, the pressure curve and the p_g^{max} curve are tangent; this fact is evident in Figure 20, Figure 21, Figure 22, Figure 23 and Figure 24.

The observations showed that the cracking mechanism can basically occur in two ways, which are particularly evident in Figure 20 and Figure 22. In Figure 22 small peaks, nearly tangent to the maximal possible gas pressure curve are present. These small peaks can be interpreted as the consequence of the formation of micro cracks in concrete paste, which are not large enough to let free moisture escape in a sudden way. On the other hand, Figure 20 shows a sudden cracking that increases concrete permeability and leads to a rapid decrease of gas pressure, which means that moisture can rapidly escape the concrete.

In the remaining cases (Figure 23 and Figure 24) the concrete cracked in an intermediate way; that is, neither as soft as the first one (Figure 22), nor as violent as in the second case (Figure 20).

As expected, no spalling was observed at the end of the test. The mechanical performance of the concrete was dramatically reduced when high temperatures occurred.
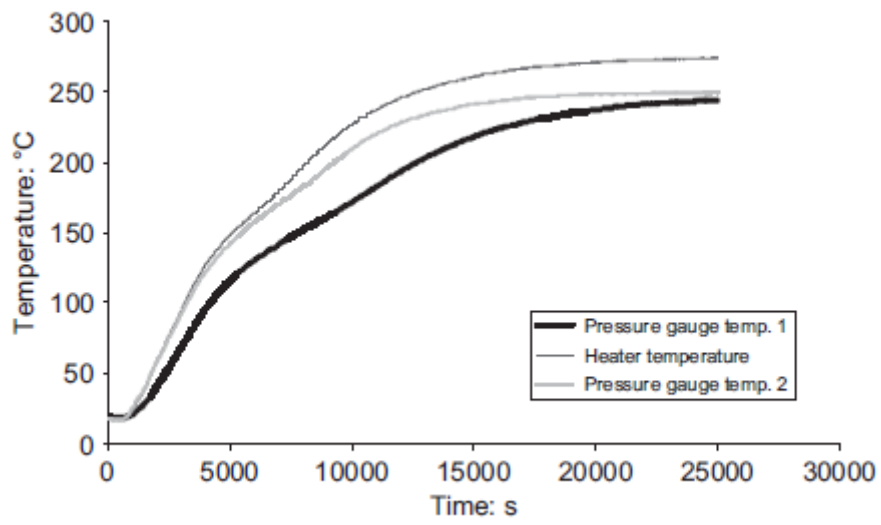
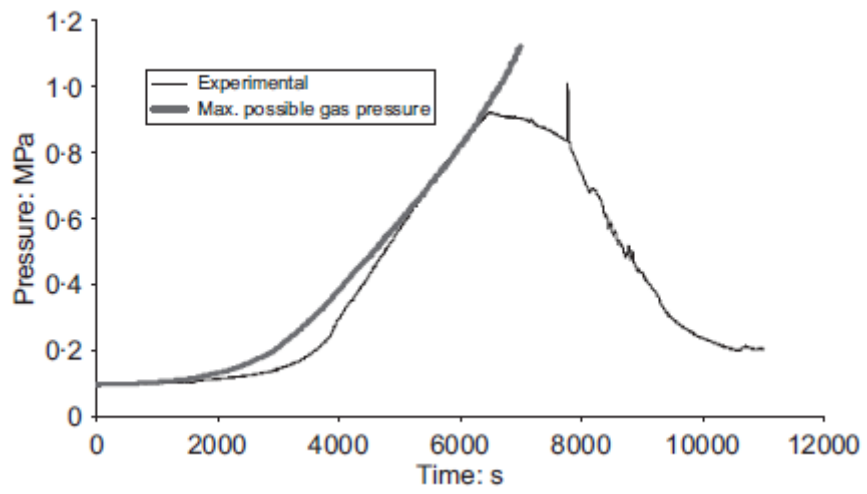**Figure 19 Heater and two internal temperatures**

Figure 20 Measured and maximal gas pressure vs. time
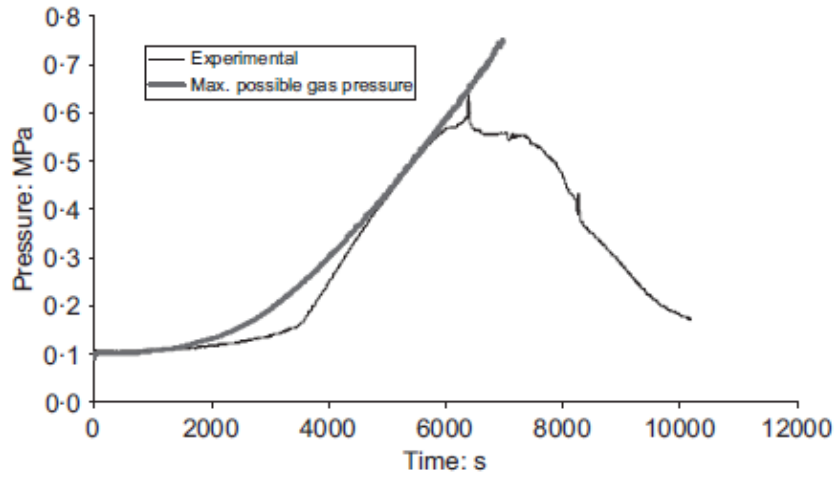
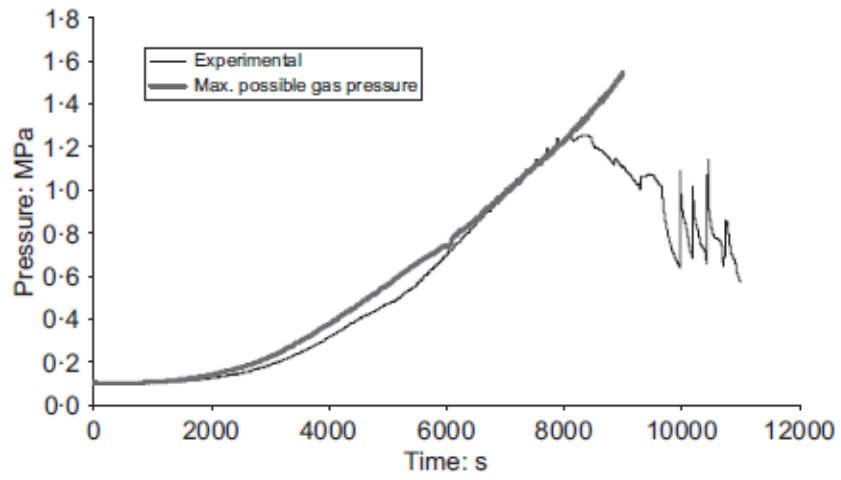**Figure 21 Measured and maximal gas pressure vs. time**

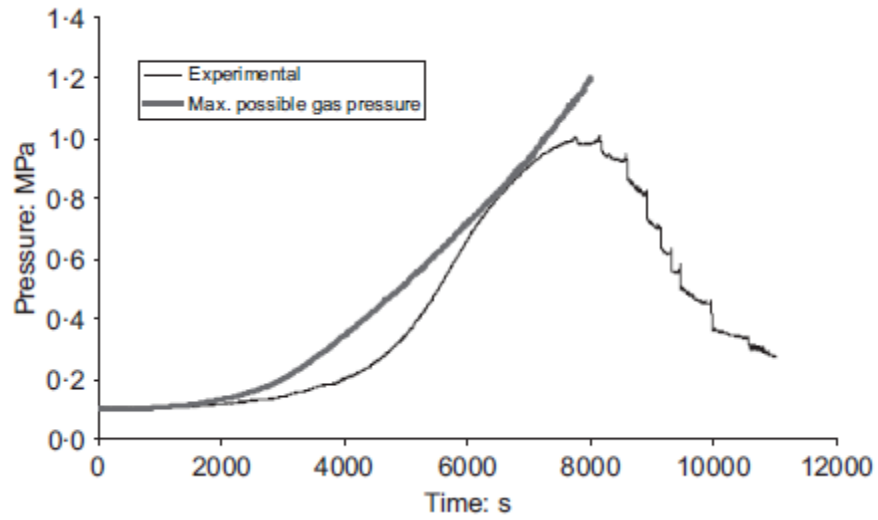**Figure 22 Measured and maximal gas pressure vs. time**

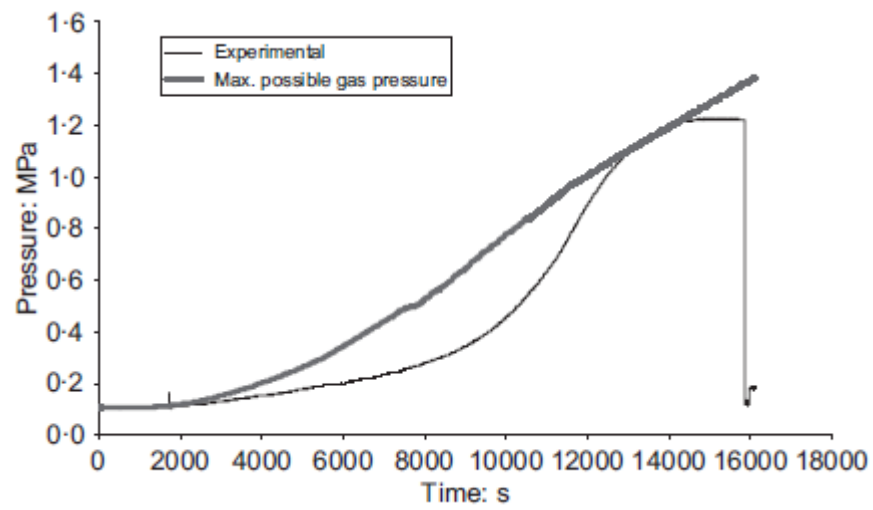**Figure 23 Measured and maximal gas pressure vs. time**

Figure 24 Measured and maximal gas pressure vs. time

2.5. Comments

In the work of Mindeguia J.C., Pimienta P., Noumowe A., Kanema M., (2009), "Temperature, pore pressure and mass variation of concrete subjected to high temperature – Experimental and numerical discussion on spalling risk" , the relationship between pore pressure and spalling at high temperatures was argued. The experimental setup which was developed by Kalifa et al. was used for the pore pressure measurements. Permeability and porosity properties of concrete were given a particular importance by the authors because of the fact that transportation of moisture is crucial for the pore pressure formation. Therefore, five different concrete mixes were developed, even if, only B350 concrete mix's experimental results were presented in the work. This mix has similar properties with the one will be used for the experiments conducted in this work of thesis.

As mentioned above, the setup developed by Kalifa et al. was used for pore pressure measurements. The gauges used for pore pressure measurements are made of sintered metal round plates (ϕ12x1mm) and may create some problems:
- moisture escape from surface of plates due to reduced bond between concrete and smooth plate;
- perturbation linked to the size of these gauges.

This type of gauges could cause considerably big discontinuity inside the concrete matrix which may result with an alteration in mechanical properties of concrete. Using quasi-aggregate gauges would possibly give better results in this manner.

Another problem is linked to the fact that, in the experiments, unsealed specimens were used and this leads moisture escape from all sides of concrete. Moisture escape may cause reduced pore pressure measurements. Sealing the sample by a proper moisture-proof sealing system would improve the accuracy of the measurements.

For heating up the specimens, a very fast heating rate was used. Radiant heaters were controlled to reach 600 $^{\circ}$C in 5 minutes which corresponds to 2 $^{\circ}$C/sec. This kind of very rapid heating is beneficial to involve pore vapor pressure. High thermal stresses, however, could be induced by very rapid heating, which may create cracks, causing the

escape of water vapor, and, moreover, altering the mechanical properties of concrete such as strength. Therefore special care should be given to thermal stresses.

A numerical analysis might be run to comprehend the thermal stresses induced due to rapid heating. Indeed, results of the experiments showed that obtained pore pressure values are lower than the values acquired in previous studies. The unstable behavior of flint aggregates in concrete mix, together with cracks induced by thermal stresses, can cause this lower pressure values.

In the work of Pierre Kalifa, Gregoire Chene, Christophe Galle, (2001), "High Temperature behavior of HPC with polypropylene fibers from spalling to microstructure" The heat was applied to the specimens by placing the heater at the top. The lateral faces of specimens were heat-insulated. In order to acquire the pressure and temperature, five probes were installed inside the specimens. Differently from Kalifa et al., in this work of thesis, heat was intended to be imposed on two opposite faces of the specimen in order to obtain the so-called "moisture clog" in the center of the specimen.

The probes used in the experiments consist of a head made of sintered metal, a tube and a connector. The head is connected to the tube and at the free end of the tube, the connector is mounted in order to allow pressure and temperature measurements. The size of probes used in Kalifa et al. may lead to some problems regarding to the bonding with the concrete. That is why semi spherical sintered metal was chosen to be used in the thesis.

The concrete specimens were casted by introducing PP (propylene) fibers whose dosage varies from 0 to 3 kg/m^3 to identify the effect of fibers and optimize the amount. As for this thesis, B40 type of concrete was chosen to be tested, PP fibers were decided to be added for some of the specimens to make comparison. The strength of this concrete is relatively smaller than the one used in Kalifa et al. The tests were performed by heating the specimens up to 600℃ and then keeping this temperature constant for 6 hours. As already underlined, the fast heating rate of the specimens may lead to high thermal stresses inside the concrete which causes the cracks inside the concrete; reducing the heating rate may results with better understanding of the effect of pore pressure on tensile strength of concrete which is the main purpose of this thesis.

3. Experimental Setup

3.1. Introduction

In this work, the main purpose is to understand how pore pressure, during heating, and tensile strength are related, referring to real problems such as walls or thin web beams heated on two opposite faces, as can be seen in Figure 25a, where a 10 cm thick beam exposed to fire on opposite sides is shown.

This kind of problems is driven by a mono-dimensional behavior in which the heat flux flows from the heated faces towards the center causing moisture and vapor migration; due to the symmetry, in the mid section both the heat and the moisture fluxes must be zero, so that there is a concentration of moisture (and vapor) that can't move from this section (phenomenon called "moisture clog") leading to higher values of pore pressure (Figure 25b).
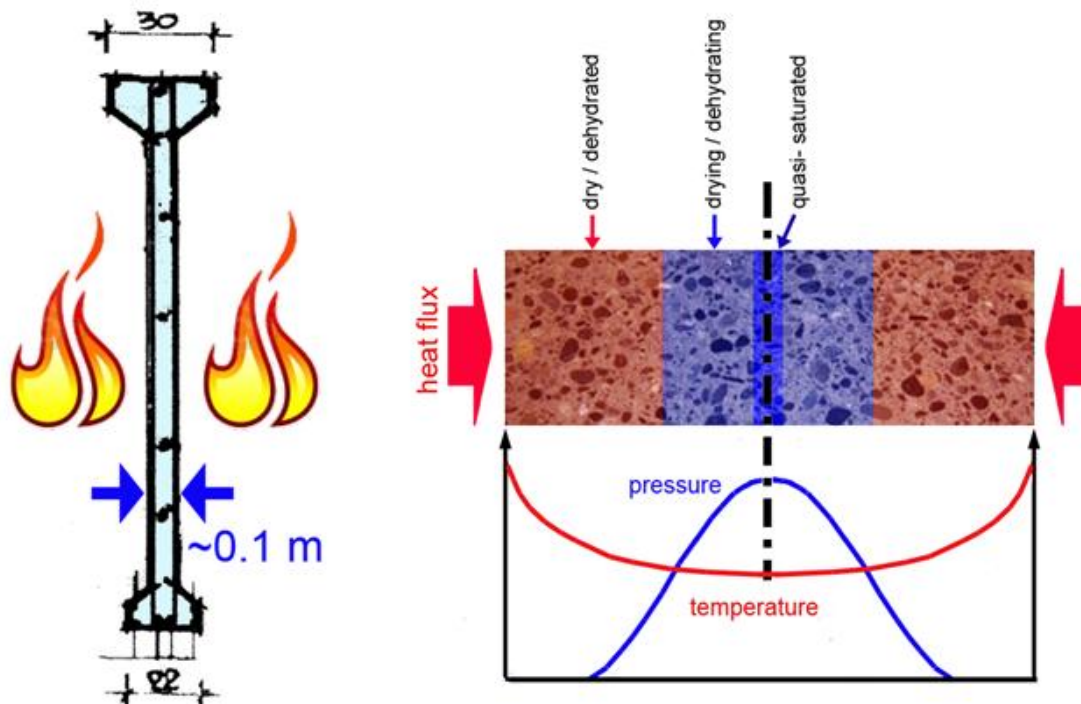

Figure 25a & Figure 25b

3.2. Concrete Mix Design

In order to evaluate the case mentioned above, it was decided to use cube specimens, whose side dimension is 10 cm, and the concrete type B40, whose mix design was one of the concrete types used by Mindegua et al.[2].

This concrete type has a mechanical behavior in between HPC and normal concrete, meaning that spalling will not probably occur. In addition to this, for some of the cube specimens, PP fibers were introduced to see the influence of the fibers. In the Table 3 shown below, the mix design can be shown.

Constituents	Quantity(kg/m^3)
Cement	347
8/12.5 Calcareous	327
12.5/20 Calcareous	714
0/2 Sand	838
Water	186
Additive	1% of the cement

Table 3 Concrete Mix

3.3. Mechanical and Hydro-thermal Boundary Conditions

The specimens will not to be part of a wall or of a thin web beam as stated before, so it is necessary to restore the mechanical and hydro-thermal boundary conditions.

3.3.1. Mechanical Boundary Conditions

In this case we will focus only on the pore pressure – tensile strength relation, disregarding as possible the influence of the thermal stresses caused by the thermal gradient induced by the chosen heating rate. For this reason, the sides of the specimens will not be restrained and they will be free to move.

3.3.2. Hydro-thermal Boundary Conditions

On the other hand is of main interest to restore the hydro-thermal continuity to reproduce the real behavior of a thin wall during a two face – heated fire.

The continuity in moisture and temperature must be satisfied at the time of experiments. For the temperature continuity, the four cold faces were covered with 20-mm thick ceramic fiber insulating material (Figure 26).

The moisture continuity is more complicate to restore due to the high temperature which the sealing is subjected to. It is well explained in the following paragraph.
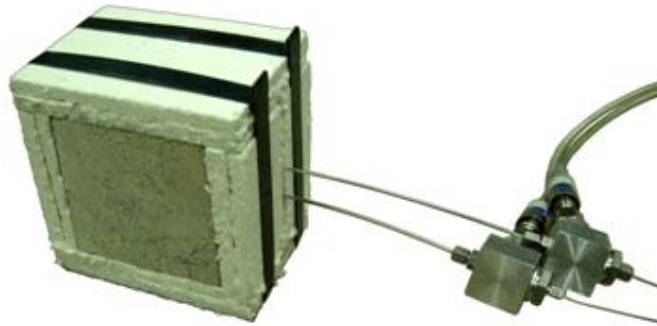

Figure 26 Heat Insulation

3.4. Choice of the Sealing

The choice of sealing type is important in order to satisfy the moisture continuity. In other words, the specimens must keep the moisture inside to obtain accurate pore pressure field representing the real situation. During testing, heat was imposed on two opposite faces to maintain the homogeneous (mono-dimensional) moisture flux through the axis of symmetry. Proper sealing allows the moisture to move towards the mid section without any leakage on the surface.

As for determining the best sealing type, different combinations of materials were tested. These materials were high-temperature resistant silicon, epoxy, carbon-fiber and aluminum foil. A spare concrete specimen was used to identify the bonding between materials and concrete. Three procedures were tested.

3.4.1. Silicon and Carbon Fiber

First combination is made of silicon and carbon fiber. Silicon was smeared on the concrete specimen as thin as possible. After that, a piece of carbon-fiber fabric was placed on the glued surface. The purpose of placing carbon-fiber fabric is to avoid the formation of air bubbles on the surface.

3.4.2. Epoxy and Aluminum Foil

The second one consists of epoxy and aluminum foil. The procedure is the same as mentioned before.

3.4.3. Silicon, Epoxy and Aluminum Foil

The third combination involves three components which are silicon, epoxy and aluminum foil. Firstly, silicon was smeared. Then, epoxy was glued on the silicon layer after drying of silicon. Finally, the aluminum foil was put on the epoxy layer (Figure 27).
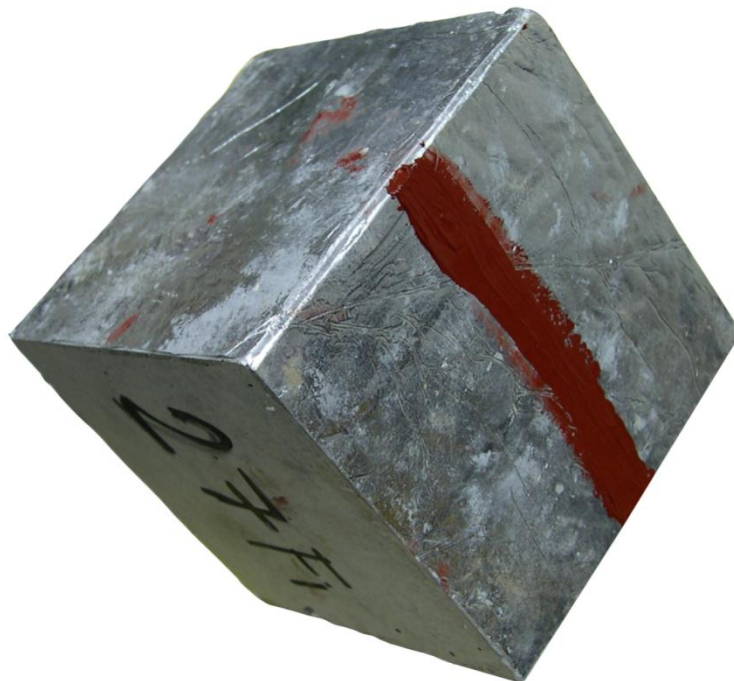

Figure 27 Epoxy-Aluminum sealed cube

3.4.4. Concrete – Sealing Bond Evaluation and Drying Tests

After applying these three combinations, it was observed that the material which formed best bond with concrete was epoxy among the other materials. However, the bond between epoxy and aluminum foil was not what had been expected. The aluminum foil was peeled out when pulling it. For the preliminary drying test, the second combination consisting of epoxy and aluminum foil, and silicon which was smeared without any other material was chosen.

At the very beginning, a small amount of concrete was casted for preliminary tests. The mould used was quite soft. This led to rough concrete surfaces. After this point, for the following casting process, it was decided to use plastic moulds which is harder than the one used for preliminary tests.

For the preliminary drying test, four cubes were chosen. Two of them were sealed with the materials which had been decided to use and other two specimens were not sealed to see the effect of sealing. The temperature was set at 120 ºC and the weight measurements were taken continuously during three days. The graph shows the weight loss of the specimens (Figure 28).
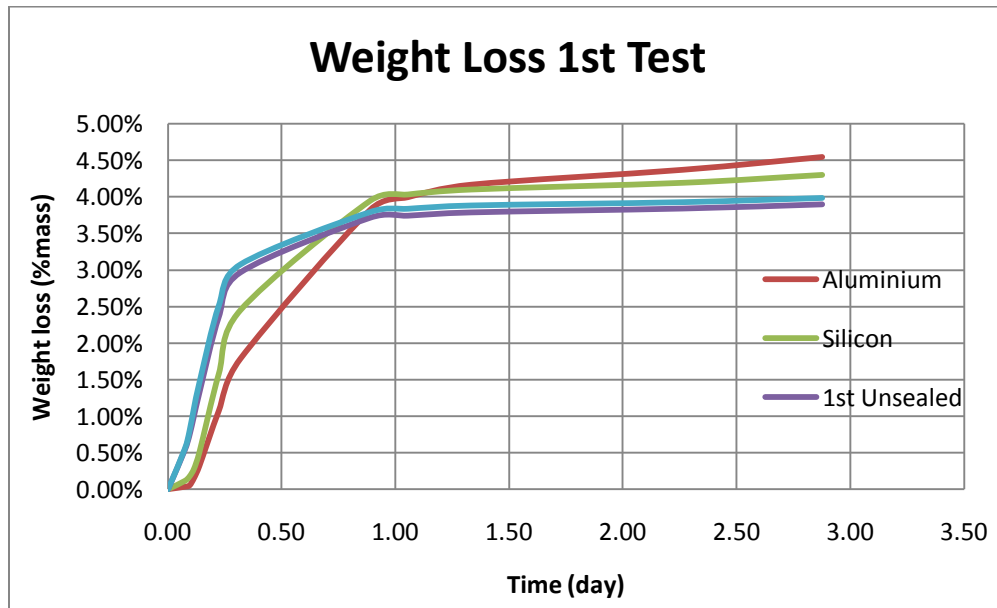

Figure 28 Weight Losses 1st Test

As can be seen in the graph, the weight losses converge to 4-4.5 % which is the average moisture content. The sealing for the preliminary tests seems to be not effective. During the tests, air bubbles were observed on the sealed specimens. The Figure 29 shows the air bubbles on the specimen sealed with silicon. For the main drying test, it was decided to use epoxy and aluminum foil combination. In the preliminary test, the reason for ineffectiveness of the sealing might be the improper way of smearing the epoxy. For the main drying test, the epoxy was smeared both on concrete and on aluminum foil in a way that the pores on the surface was filled with epoxy, in order to prevent air bubbles.
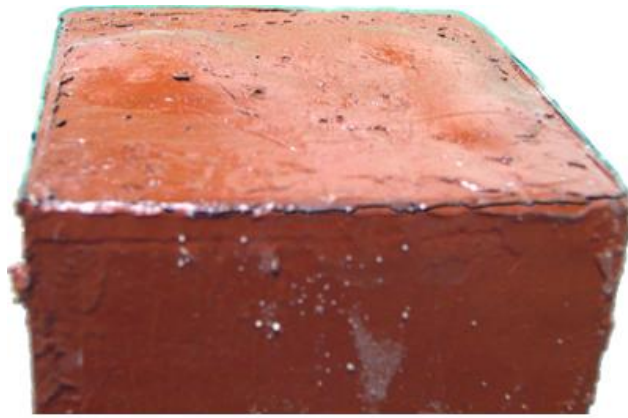

Figure 29 Bubbles after drying test

For the main drying test, six specimens were chosen. Two of them were sealed as mentioned before with aluminum foil (one with PP fiber). By the way, these cubes were cured for about two months. Afterwards, they were sealed. The temperature was set at 120 ºC as it was before. The measurements were taken continuously during two weeks. The percentage of weight loss can be seen in Figure 30.
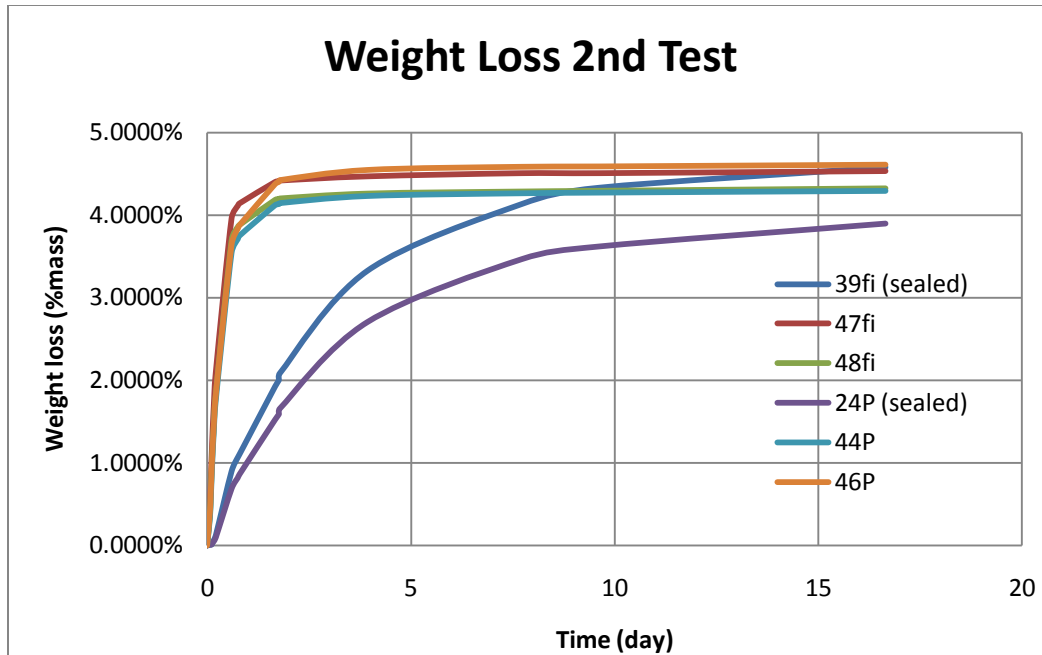
Figure 30 Weight Losses 2nd Test

The results show that the sealing is more effective than before. The moisture content is the same as the previous test. However, the weight loss of sealed specimens stabilized after two weeks. In the previous test, it took three days to stabilize.

3.4.5. Conclusions of Sealing Evaluation

As a result, it was observed that best sealing was achieved by using epoxy and aluminum foil. The procedure of sealing was applied as mentioned before. In the beginning of drying tests, primary samples were prepared by smearing the epoxy on concrete and then covering by aluminum. Afterwards, this procedure was decided to be improved and epoxy was applied both on concrete and aluminum foil. As can be seen by comparing Figure 30 with Figure 31, the improved procedure was much more effective, therefore it was used for sealing the samples.

3.5. Heating Set-up and Heating Rate

The heating set-up was prepared in order to reproduce the real case shown previously. As can be seen in Figure 25a, the opposite sides are exposed to fire. That's why the

radiative heaters were placed on two opposite faces. Figure 31 shows the heating system used in the experiments.
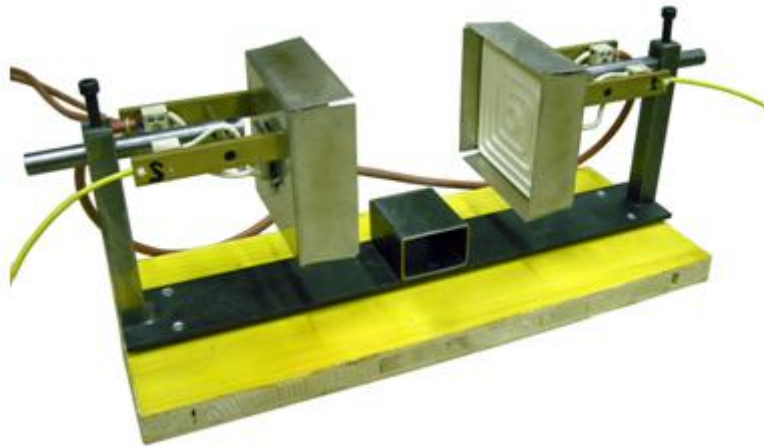
Figure 31 Heating system

The heating system consists of two radiative panels placed on two opposite sides of the concrete cubes, in order to obtain symmetrical heating with respect to the mid-section of the specimen. These radiative panels can be controlled by an electronic control device, which can regulate the power of the heaters. By regulating the power, the temperature of the heaters can be adjusted according to desired value. Hence, the heating rate can be decided and introduced into the control device to heat up the specimen.

The heating rate is one of the most important issues in measuring pore pressure.

To decide the heating rate, it is crucial to know the response of the concrete to the rate of temperature increase. In previous works, usually, very rapid heating or very slow heating was applied to measure pore vapor pressure. It is a fact that rapid heating is better to simulate real fires which may occur in concrete structures. Moreover, rapid heating rate is supposed to be beneficial for development of higher pore pressure. On the other hand rapid heating rate may damage the concrete due to both thermal stresses and thermal incompatibility between cement paste and aggregates, so leading to the formation of cracks which result in escape of vapor and reduction of concrete strength.

In the choice of heating rate the goals are:
- To achieve high pore pressure;
- To do not induced high thermal gradient.

In order to comprehend the effect of heating rate on concrete in regard to pore pressure and thermal stresses, some preliminary experiments and numerical analysis were performed.

3.5.1. Preliminary Tests to Evaluate Pore Pressure

For the preliminary tests, three different heating rates were applied to specimens. These specimens were of two kinds of concrete: standard mix B40 without polypropylene fibers (plane concrete), and with polypropylene fibers (fiber reinforced concrete). Heating rates were decided according to obtain different responses:

- very rapid heating rate (2^oC/sec);
- moderate heating rate (10^oC/min);
- slow heating rate (1^oC/min).

The target temperature was decided to be 600^oC and the controlling device was set to reach 600^oC. The thermo-couples inside the radiative panels measured 600^oC at the end of heating which compromise the predefined target. However external measurements made by the same type thermo-couples from heating face of radiative panels showed lower values of temperature (Figure 32). Each heating rate was applied to both concrete types (except 2^oC/sec) and pore vapor pressure results were obtained (Figure 33, Figure 34, Figure 35, Figure 36, Figure 37 and Figure 38).
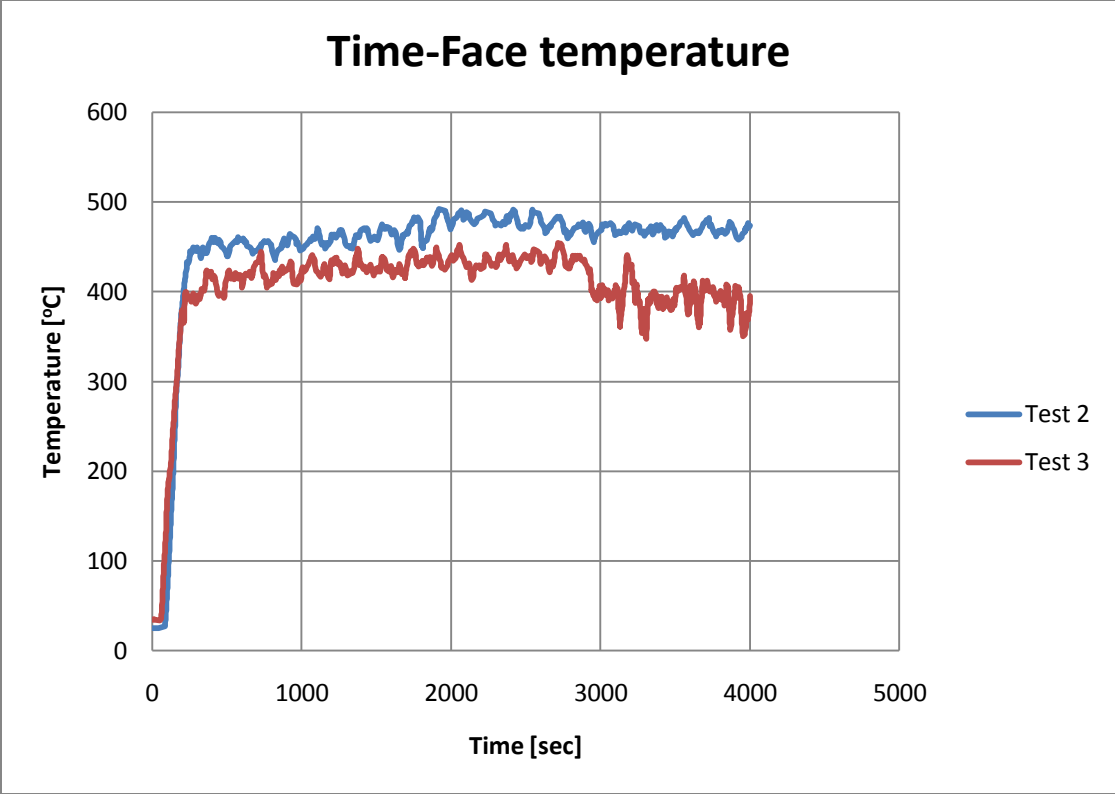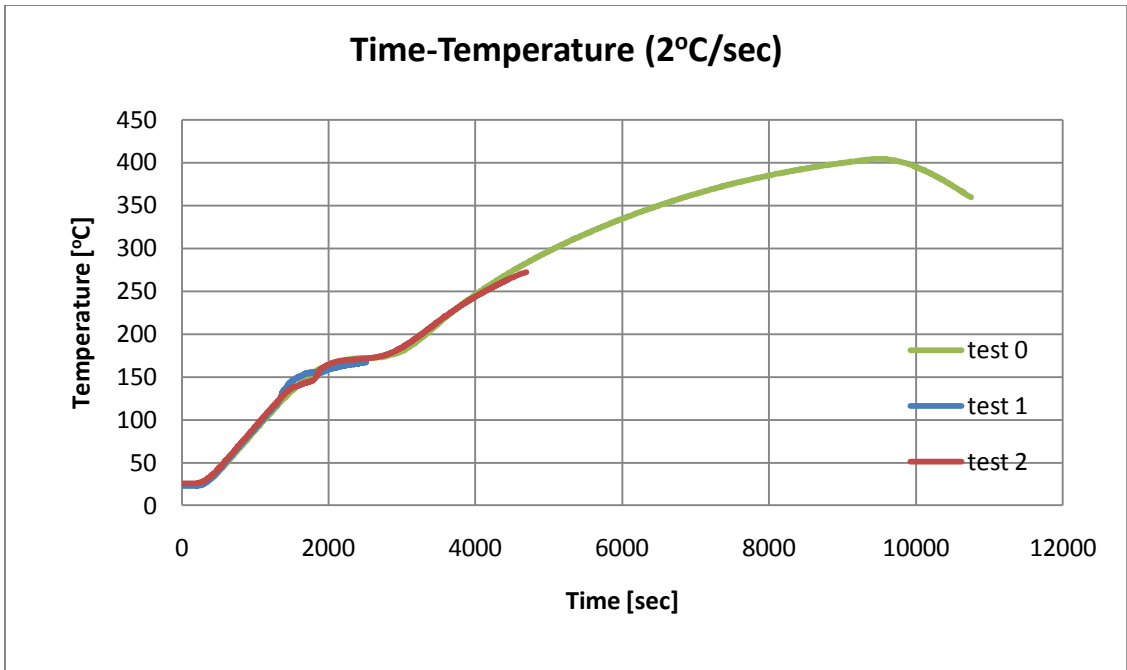
Figure 32 Time-Face temperature
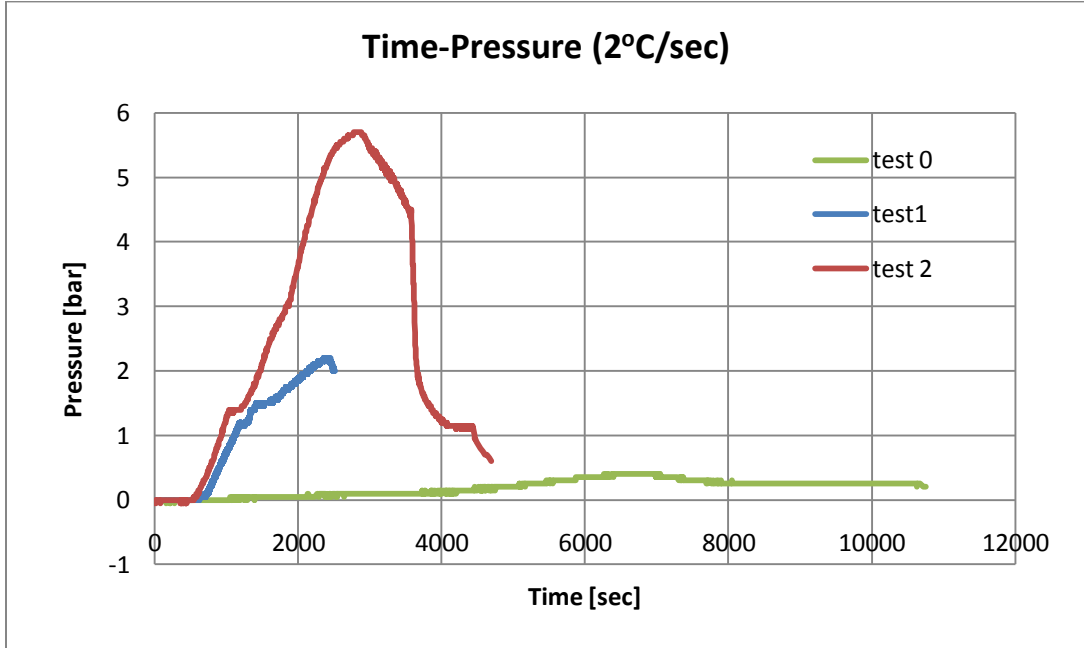
Figure 33 Time-Temperature curve
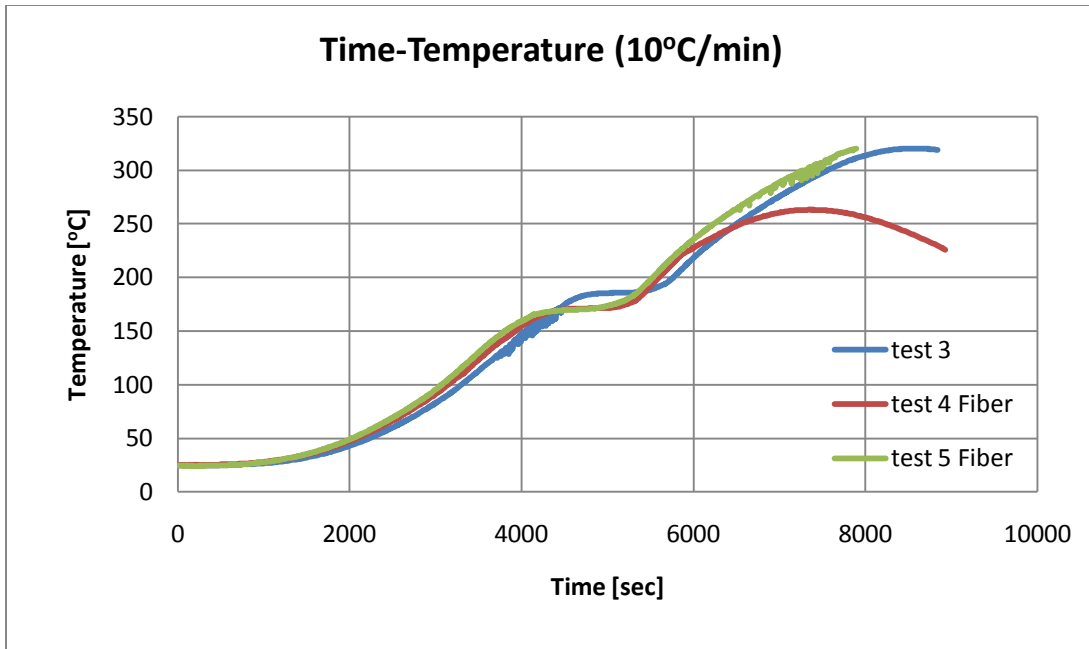

Figure 34 Time-Pressure curve

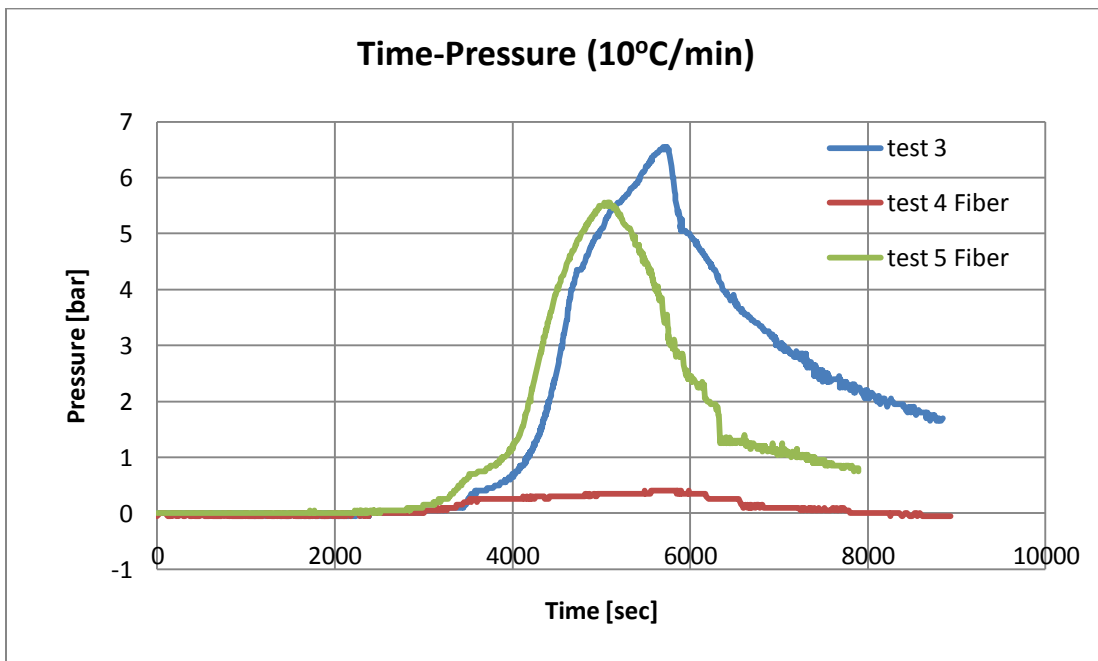**Figure 35 Time-Temperature curve**

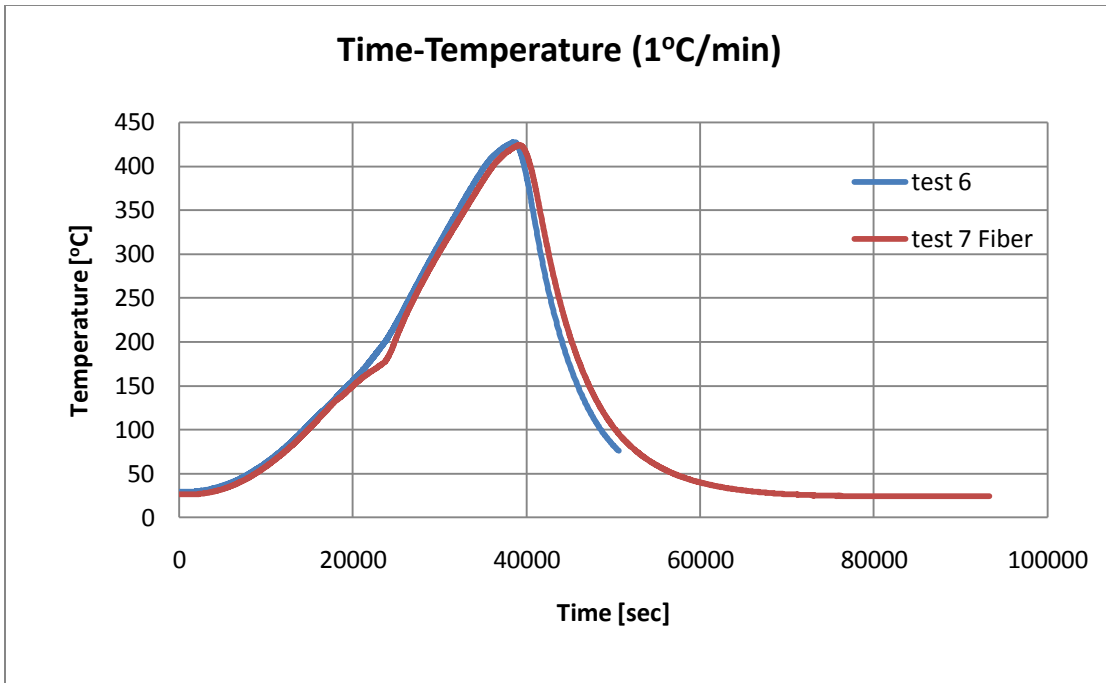**Figure 36 Time-Pressure curve**
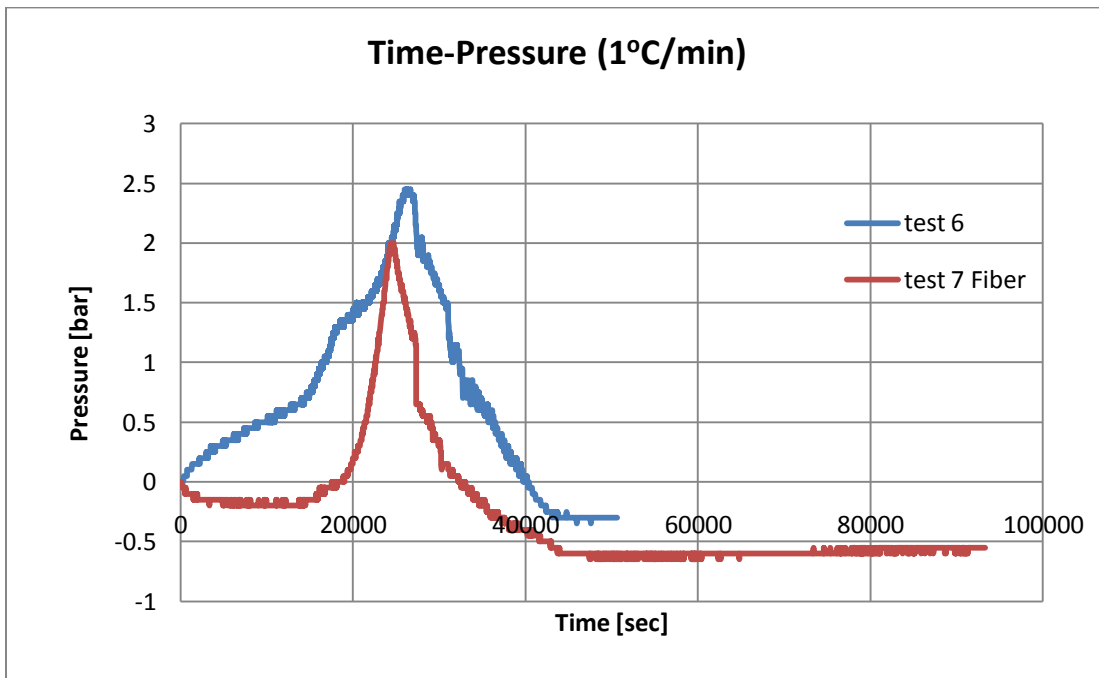
Figure 37 Time-Temperature curve

Figure 38 Time-Pressure curve

Above figures were plotted for three types of heating rates as mentioned before. These figures were an indication on the selection of heating rate that would be applied in future experiments. It is obvious and expected that in rapid and moderate heating rate, higher pore pressure values were achieved with respect to slow heating rate. In the case of slow heating (1°C/min), the pore pressure was measured to be around 2-2.5 bars, whereas in rapid (2°C/sec) and moderate (10°C/min) heating rates, pore vapor pressure was up to 6.5 bars. Rapid heating rate and moderate heating rate were seemed to be alike; in other words, in both cases almost same pore pressure values were measured. It was observed that moderate heating leads to more repeatable measurements of pore vapor pressure, with respect to rapid heating.

3.5.2. Numerical Analysis to Evaluate Thermal Stresses

As mentioned above, there is a scatter of results that were obtained from experiments performed by rapid heating rate. This variation could occur due to thermal cracks that are expected to form when the concrete is heated too fast. Thermal cracks are induced by thermal stresses and thermal incompatibility between cement paste and aggregates. In order to determine the thermal stresses, numerical analyses were performed and for each heating rate, level of stress inside the specimens were tried to be estimated. To estimate the thermal stresses which could be induced due to different heating rates, a numerical model was developed with ABAQUS software. A eighth of the whole cube sample that corresponds to one of the eight corner portions was modeled, in order to better define the mechanical and thermal boundary conditions exploiting the plane symmetries (Figure 39). Initially, the geometric properties of the model were introduced into the software, which are 5x5x5 cm cube with 2 cm isolation on two sides.

For the material properties, temperature dependent properties of materials were needed to be determined. Hence, the provisions of Eurocode 2: Part 1-2 [6] (EN1992-1-2) and results of other works were investigated. Eventually, the material properties which are conductivity, density, specific heat, thermal expansion and modulus of elasticity of concrete and heat insulating material were determined.
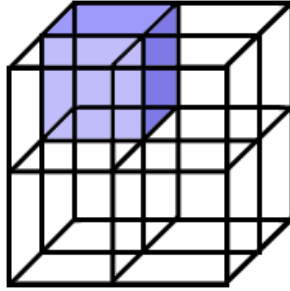
3.5.2.1.Density

Density of concrete dependent to temperature was assessed according to EN1992-1-2 section 3.3.2-(3) [(Equation 4). The variation of density is shown in Figure 40.

Equation 4:

$$\rho(\theta) = \rho(20°C) \qquad\qquad\qquad\qquad\qquad for \quad 20°C \leq \theta \leq 115°C$$

$$\rho(\theta) = \rho(20°C) * (1 - 0.02(\theta - 115)/85) \qquad for \ 115°C < \theta \leq 200°C$$

$$\rho(\theta) = \rho(20°C) * (0.98 - 0.03(\theta - 200)/200) \quad for \ 200°C < \theta \leq 400°C$$

$$\rho(\theta) = \rho(20°C) * (0.95 - 0.07(\theta - 400)/800) \quad for \ 400°C < \theta \leq 1200°C$$
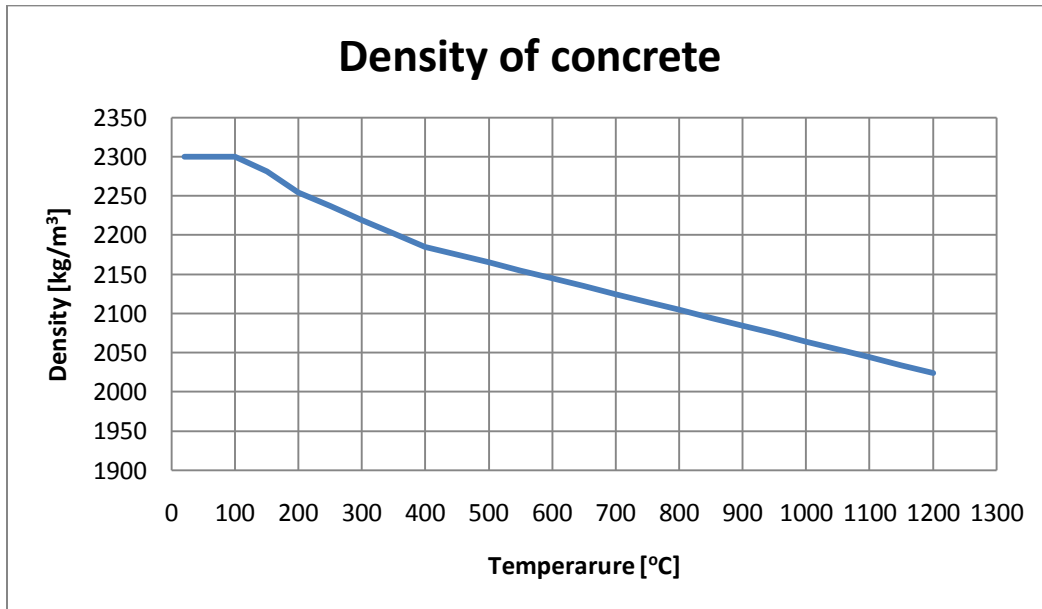

Figure 40 Density of concrete

3.5.2.2. Conductivity

Conductivity of concrete was determined according to EN1992-1-2 section 3.3.3. The upper limit of thermal conductivity was decided to be used (Equation 5). The curve of change by temperature is shown in Figure 41.

Equation 5:

$$\lambda_c = 2 - 0.2451(\theta/100) + 0.0107(\theta/100)^2 \quad W/mK \quad for \ 20°C \leq \theta \leq 1200°C$$
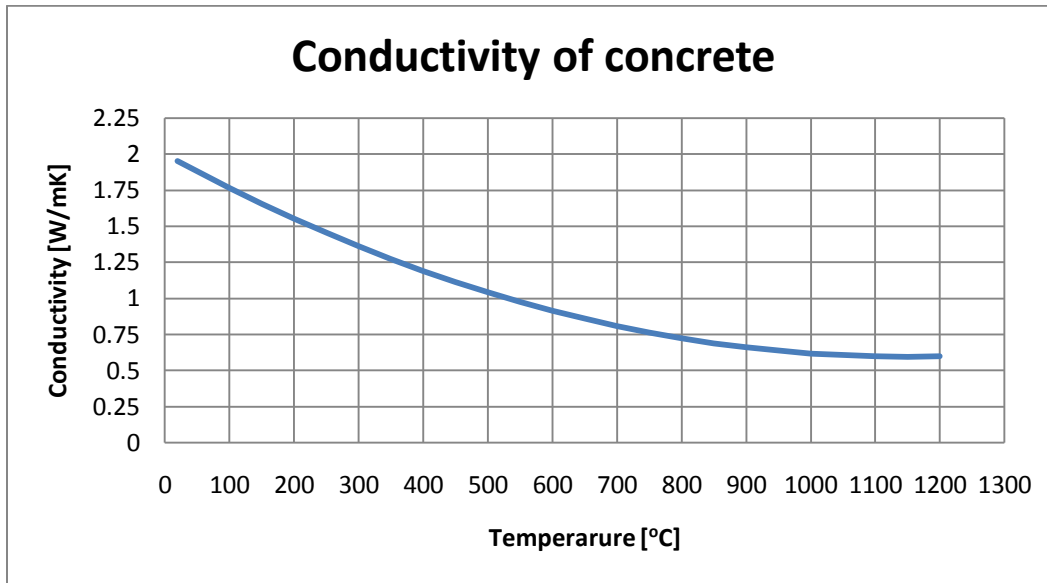
Figure 41 Conductivity of Concrete

3.5.2.3. Specific Heat

Specific Heat of concrete was determined according to EN1992-1-2 section 3.3.2-(1) (Equation 6); it is shown in Figure 42. The peak that is expected to occur in between 100°C and 115°C was calculated by linear interpolation of given 1.5% and 3% moisture content specific heat peaks for 4% moisture content which was the case for the samples of this work.

Equation 6:

$$C_p(\theta) = 900 \ (J/kg \ K) \qquad\qquad for \ 20°C \leq \theta \leq 100°C$$

$$C_p(\theta) = 900 + (\theta - 100) \ (J/kg \ K) \qquad for \ 100°C \leq \theta \leq 200°C$$

$$C_p(\theta) = 900 + (\theta - 200)/2 \ (J/kg \ K) \qquad for \ 200°C \leq \theta \leq 400°C$$

$$C_p(\theta) = 1100 \ (J/kg \ K) \qquad\qquad for \ 400°C \leq \theta \leq 1200°C$$

$$C_{p.peak} = 900 \, J/kg \, K \quad for \ moisture \ content \ of \ 0\% \ of \ concrete \ weigth$$

$$C_{p.peak} = 14700 \, J/kg \, K \quad for \ moisture \ content \ of \ 1.5\% \ of \ concrete \ weigth$$

$$C_{p.peak} = 2020 \, J/kg \, K \quad for \ moisture \ content \ of \ 3\% \ of \ concrete \ weigth$$
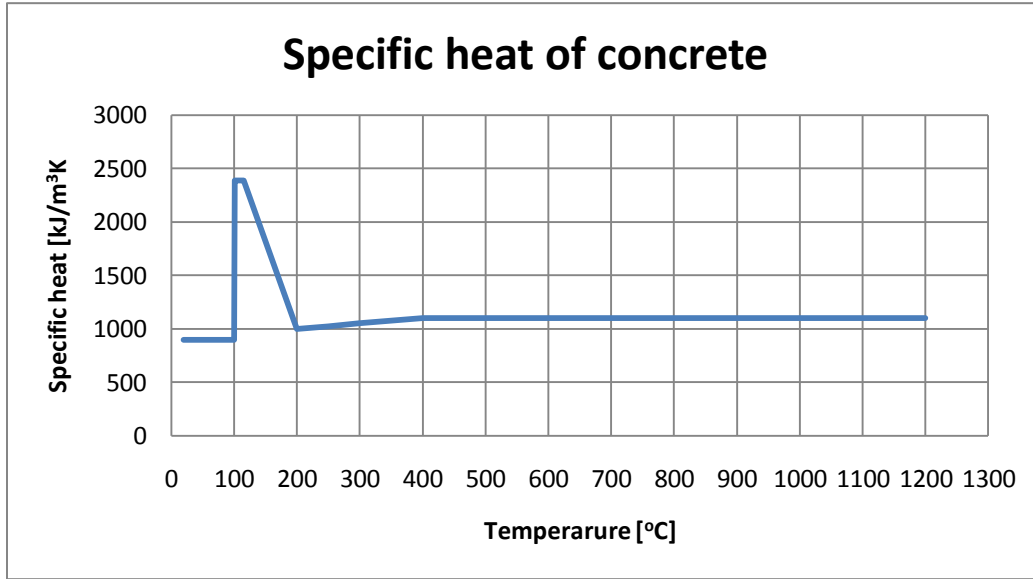
Figure 42 Specific Heat of Concrete

3.5.2.4. *Coefficient of Thermal Expansion*

Coefficient of Thermal Expansion of concrete was determined according to EN1992-1-2 section 3.3.1 (Equation 7). EN1992-1-2 gives thermal elongation, in other words, temperature dependent strain of concrete. But in the model, coefficient of thermal expansion was needed rather than thermal elongation. Therefore the secant approach was used to evaluate the coefficient of thermal expansion starting from the given thermal elongation with respect to temperature. Equation 8 states the operation, above described. Figure 43 shows variation of coefficient of thermal expansion due to temperature.

Equation 7:

$$\varepsilon_c(\theta) = -1.2 * 10^{-4} + 6 * 10^{-6} * \theta + 1.4 * 10^{-11} * \theta^3 \quad for \ 20°C \leq \theta \leq 805°C$$

Equation 8:

$$\alpha_\theta = -1.2 * 10^{-4} * {1}/{(\theta - \theta_{ref})} + 6 * 10^{-6} * {\theta}/{(\theta - \theta_{ref})} + 1.4 * 10^{-11}$$
$$* {\theta^3}/{(\theta - \theta_{ref})}$$

$$where;\ \theta = temperature \quad \theta_{ref} = 20°C$$
$$\alpha_\theta = coefficient\ of\ thermal\ expansion$$
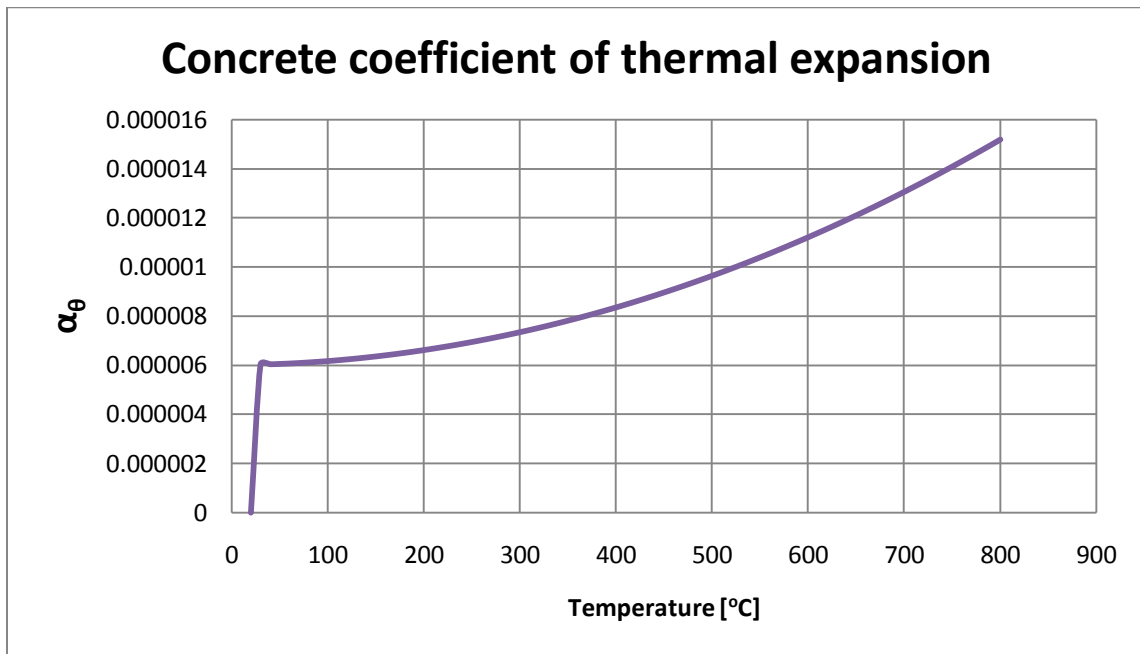
Figure 43 Coefficient of Thermal Expansion

3.5.2.5.*Modulus of Elasticity*

Modulus of Elasticity of concrete was determined by comparison of EN1992-1-2 provisions with the results of work of Mindeguia et al.[2]. EN1992-1-2, section 3.2.2.1 provides a mathematical model for stress-strain relationship of concrete at elevated temperatures which takes into account also creep and transient creep (Equation 9). The derivative of the stress $\sigma_c(\theta)$ with respect the strain $\varepsilon_c(\theta)$ gives the modulus of elasticity at elevated temperatures (Equation 10).

Equation 9:

$$\sigma_\theta = \frac{3 * \varepsilon_c(\theta) * f_c(\theta)}{\varepsilon_{c1}(\theta) * \left[2 + \left(\frac{\varepsilon_c(\theta)}{\varepsilon_{c1}(\theta)}\right)^3\right]}$$

$$\sigma_\theta = \frac{\varepsilon_c(\theta) f_c(\theta)}{\varepsilon_{c1}(\theta)} * \frac{3}{\left[2 + \left(\frac{\varepsilon_c(\theta)}{\varepsilon_{c1}(\theta)}\right)^3\right]}$$

$$\frac{\sigma_\theta}{f_c(\theta)} = \frac{\varepsilon_c(\theta)}{\varepsilon_{c1}(\theta)} * \frac{3}{\left[2 + \left(\frac{\varepsilon_c(\theta)}{\varepsilon_{c1}(\theta)}\right)^3\right]}$$

Equation 10:

$$\frac{d\sigma_\theta}{d\varepsilon_c(\theta)} * \frac{1}{f_c(\theta)} = \frac{1}{\varepsilon_{c1}(\theta)} * \frac{3}{\left[2 + \left(\frac{\varepsilon_c(\theta)}{\varepsilon_{c1}(\theta)}\right)^3\right]} + \frac{\varepsilon_c(\theta)}{\varepsilon_{c1}(\theta)} * \frac{9 * \left(\frac{\varepsilon_c(\theta)}{\varepsilon_{c1}(\theta)}\right)^2 * \frac{1}{\varepsilon_{c1}(\theta)}}{\left[2 + \left(\frac{\varepsilon_c(\theta)}{\varepsilon_{c1}(\theta)}\right)^3\right]^2}$$

$$\left[\frac{d\sigma_\theta}{d\varepsilon_c(\theta)}\right]_{\varepsilon=0} = E_{c,\theta} \quad modulus\ of\ elasticity$$

$$\frac{E_{c,\theta}}{f_c(\theta)} = \left[\frac{3}{2 * \varepsilon_{c1}(\theta) + \frac{[\varepsilon_c(\theta)]^3}{[\varepsilon_{c1}(\theta)]^2}} + \frac{9 * \left(\frac{\varepsilon_c(\theta)}{\varepsilon_{c1}(\theta)}\right)^3}{\varepsilon_{c1}(\theta) * \left[2 + \left(\frac{\varepsilon_c(\theta)}{\varepsilon_{c1}(\theta)}\right)^3\right]^2}\right]_{\varepsilon=0} = \frac{3 * f_c(\theta)}{2 * \varepsilon_{c1}(\theta)}$$

So:

$$E_{c,\theta} = \frac{3 * f_c(\theta)}{2 * \varepsilon_{c1}(\theta)}$$

$$where\ f_c(\theta)\ \&\ \varepsilon_{c1}(\theta)\ are\ given\ in\ EN1992 - 1 - 2\ Table\ 3.1$$

The modulus of elasticity values that depend on temperature are presented on the Table 4 and Table 5. Figure 44 obviously shows that the results of Mindeguia et al.[2] are very close to the results of equation that is provided by EN1992-1-2. In the model, the values obtained from EN1992-1-2 were used for temperature dependant modulus of elasticity of concrete.

	EUROCODE [6]		f_{ck}=40Mpa
temp. (θ)	$\varepsilon_{c1,\theta}$	$f_{c,\theta}/f_{ck}$	$E_{c,\theta}$
20	0.0025	1	24000
100	0.004	1	15000
200	0.0055	0.97	10581.82
300	0.007	0.91	7800
400	0.01	0.85	5100
500	0.015	0.74	2960
600	0.025	0.6	1440
700	0.025	0.43	1032
800	0.025	0.27	648

Table 4 EN1992-1-2

|		MINDEGUIA		
temp. (θ)	$\Sigma(\varepsilon_{c,\theta})$	$\varepsilon_{c\ elastic,\theta}$	reduction	Ec
20	527.7782	527.7782	1	24000
50	722.2228	583.3338	0.8076923	19384.615
100	1166.667	805.5562	0.6904767	16571.441
150	1777.778	833.334	0.4687503	11250.008
200	2222.222	833.334	0.3750003	9000.0065
250	2666.669	805.5562	0.3020833	7250
300	3194.445	944.4452	0.2956524	7095.6573
350	3861.114	1111.112	0.2877698	6906.4748
400	4666.667	1277.7788	0.2738097	6571.4333

Table 5 Mindeguia et al.[2]
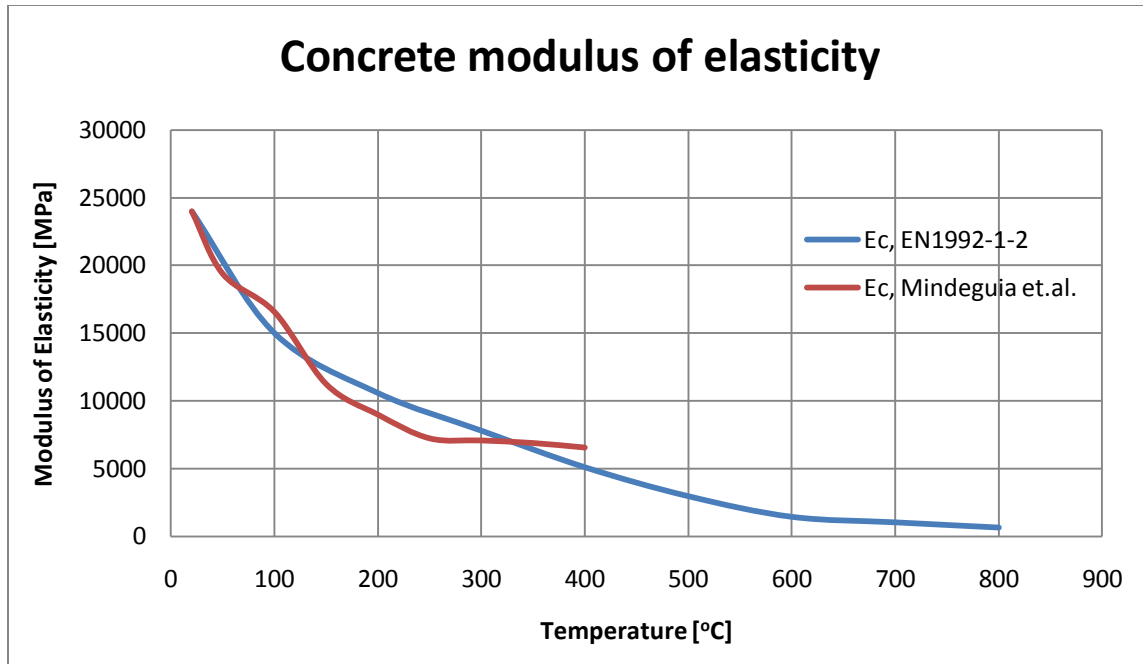
Figure 44 Modulus of Elasticity of Concrete

3.5.2.6. *Numerical Analysis*

Introducing the material properties into the model, thermal load was applied to the faces of the model with different heating rates, while the two faces which of the insulating material were exposed to ambient temperature (20°C). It was desired to observe development of thermal stresses and temperature with respect to time in the mid-section, the section that was wanted to be focused. As a result, time-temperature and time-thermal stress diagrams were obtained for different heating rates with target temperature of 600°C. Figure 45, Figure 46 and Figure 47 show temperature distribution through mid-section in the ultimate case. Figure 48, Figure 49 and Figure 50 shows the thermal stress distribution in the mid-section at the moment of maximum stress formation.
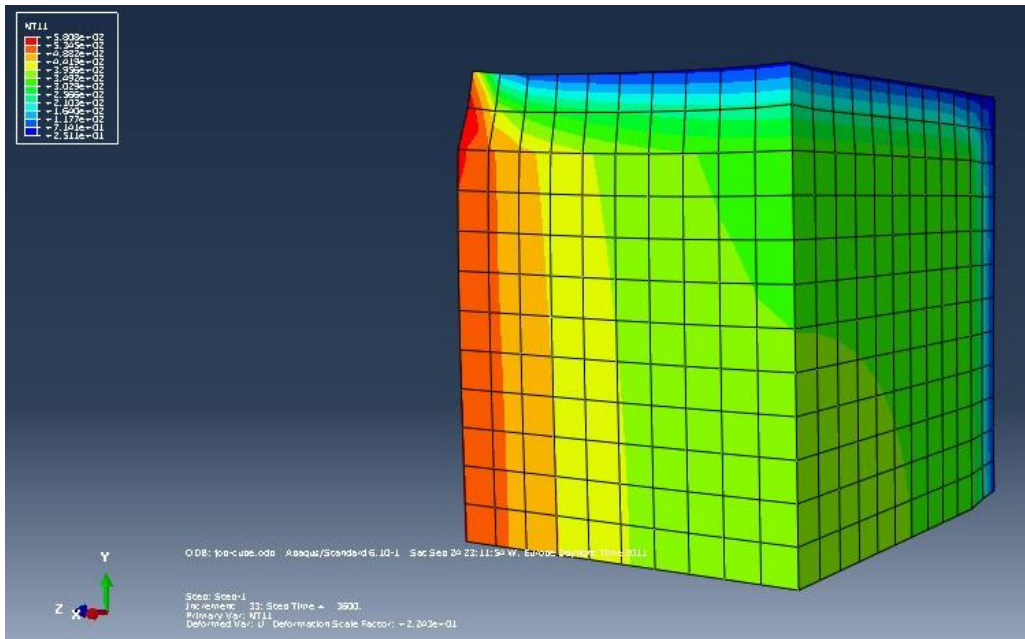
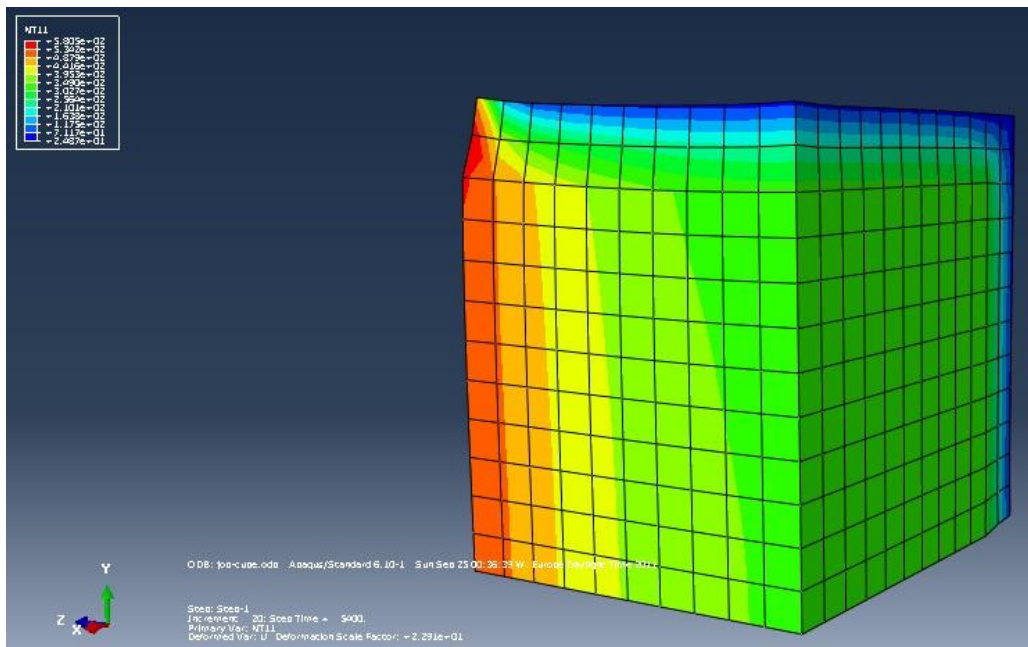**Figure 45 (2°C/sec) ultimate temperature at 1 hour**

Figure 46 (10°C/min) ultimate temperature at 1.5 hours
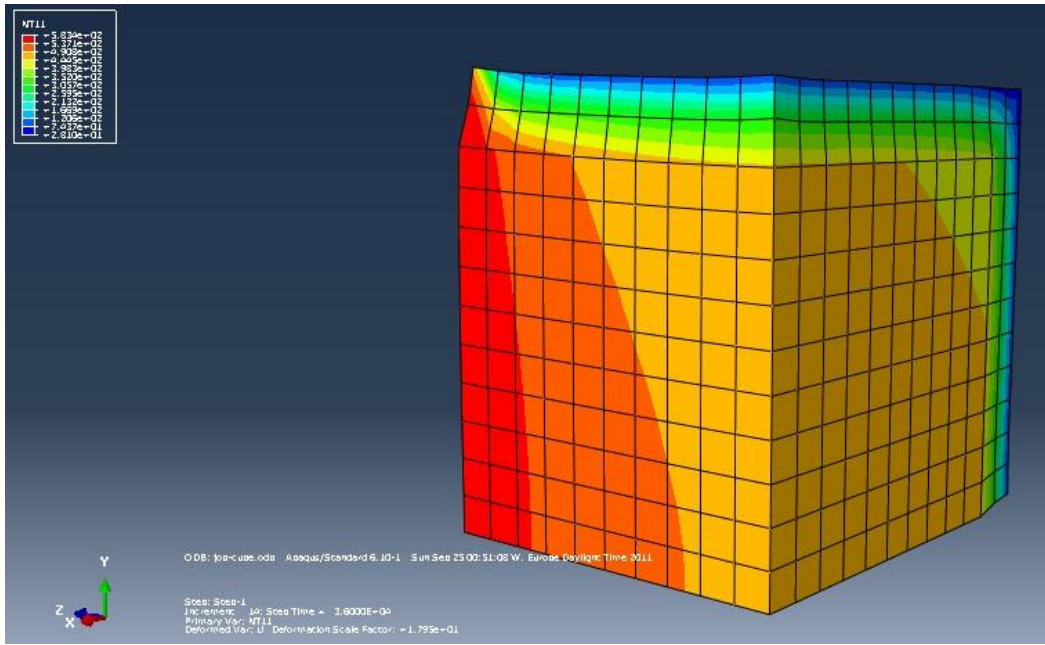
Figure 47 (1°C/min) ultimate temperature at 10 hours
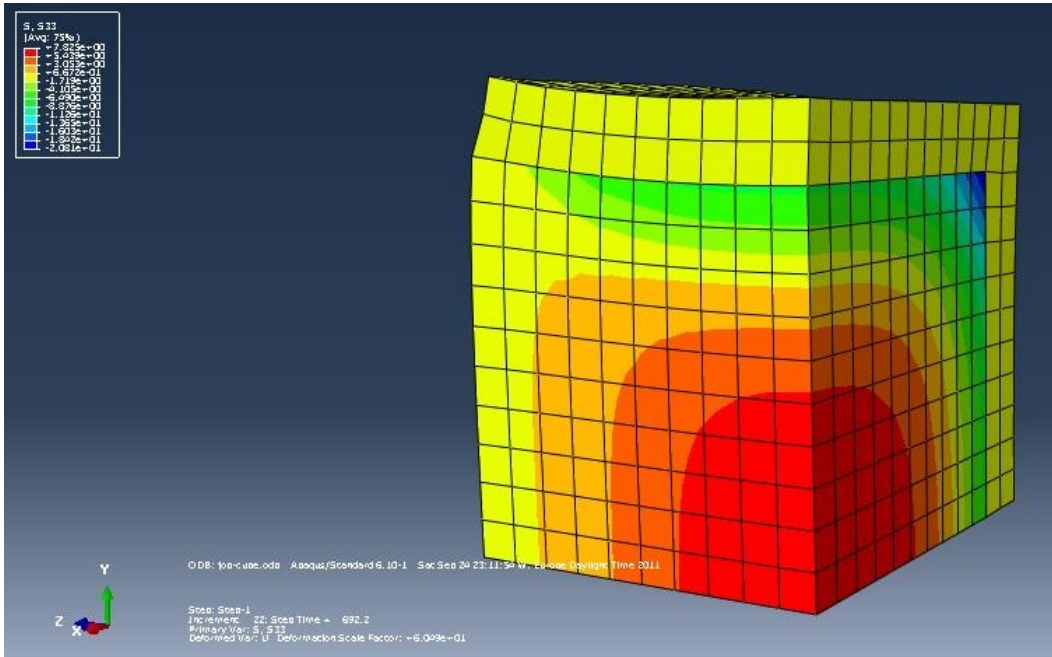

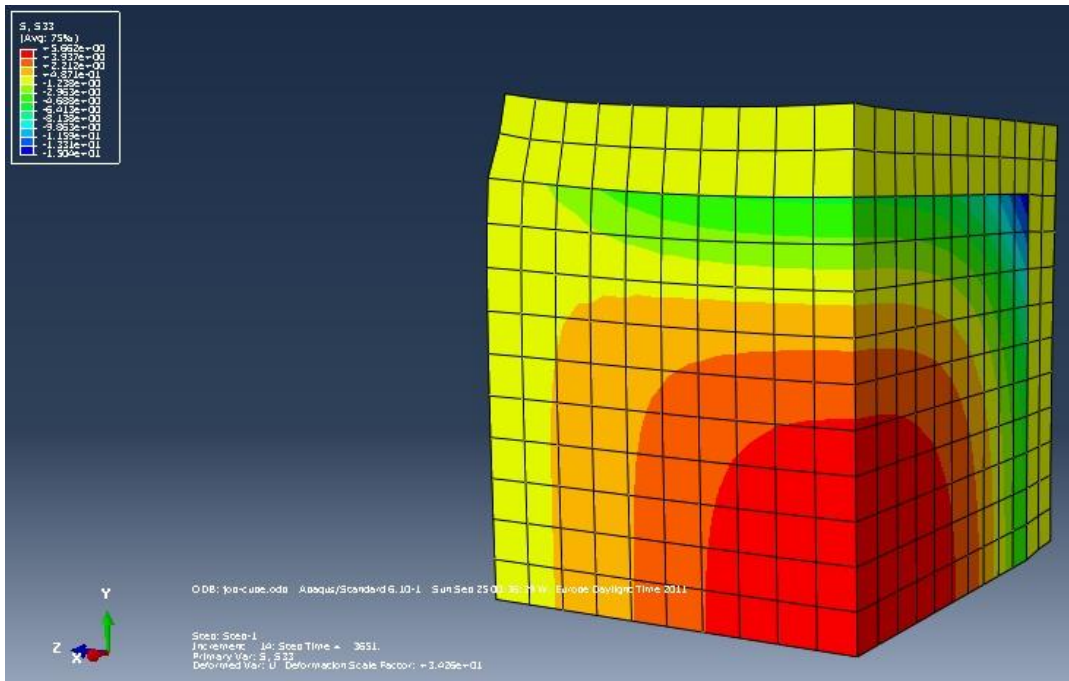**Figure 48 (2°C/sec) maximum stress at the center**

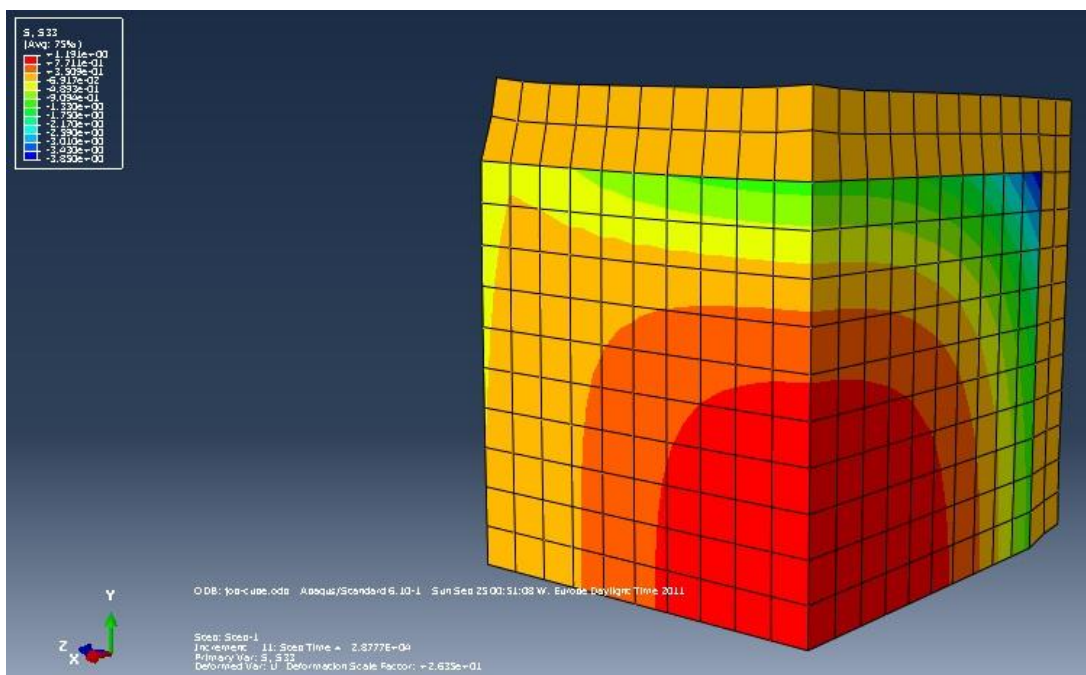**Figure 49 (10°C/min) maximum stress at the center**

Figure 50 (1°C/min) maximum stress at the center

Following, the graphs of temperature and thermal stresses variation were drawn. In other words, these graphs represent the cases for rapid heating and slow heating. Two points in the mid section, namely center point and corner point were considered to be stated for temperature and thermal stress variation through time. The locations of these points on the model are shown in Figure 51. Center point is not at the center of the model but at the corner. It is called center point because it is the center point of the real cube. As mentioned before, one eighth of a real cube was modeled; therefore the center point of real cube corresponds to the corner point in the numerical model.
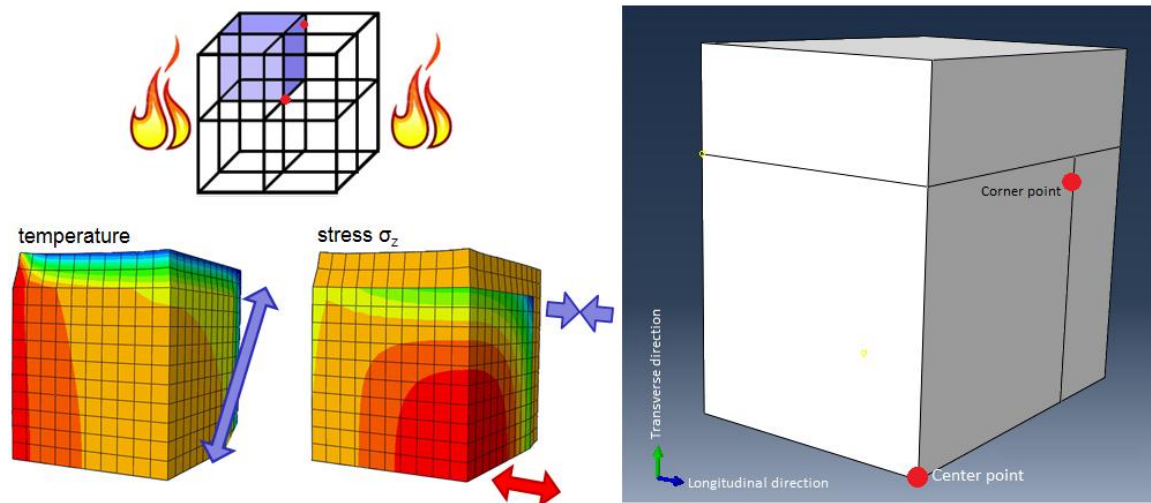
Figure 51 Locations of Points

Figure 52, Figure 53, Figure 54 and Figure 55 show temperature and thermal stress development through time for two heating rates (rapid and slow) at the two abovementioned points. Note that experimental results are also plotted on time-temperature graphs, only referring to the center points due to the unavailability of taking measurement of corner point.

Figure 52 Time-Temperature (2°C/sec)

Figure 53 Time-Temperature (1°C/min)

Figure 54 Time-Stress (2°C/sec)

Figure 55 Time-Stress (1°C/min)

According to the numerical analysis, it is obvious that rapid heating (2°C/sec) of concrete induces much higher thermal stresses than slow heating (1°C/min) (Table 6). In the light of these results, it is not inconvenient to state that faster is the heating, higher are the thermal stresses, and vice versa.

High thermal stresses induce formation of thermal cracks and thus water vapor escapes through these cracks; this leads to reduction in pore vapor p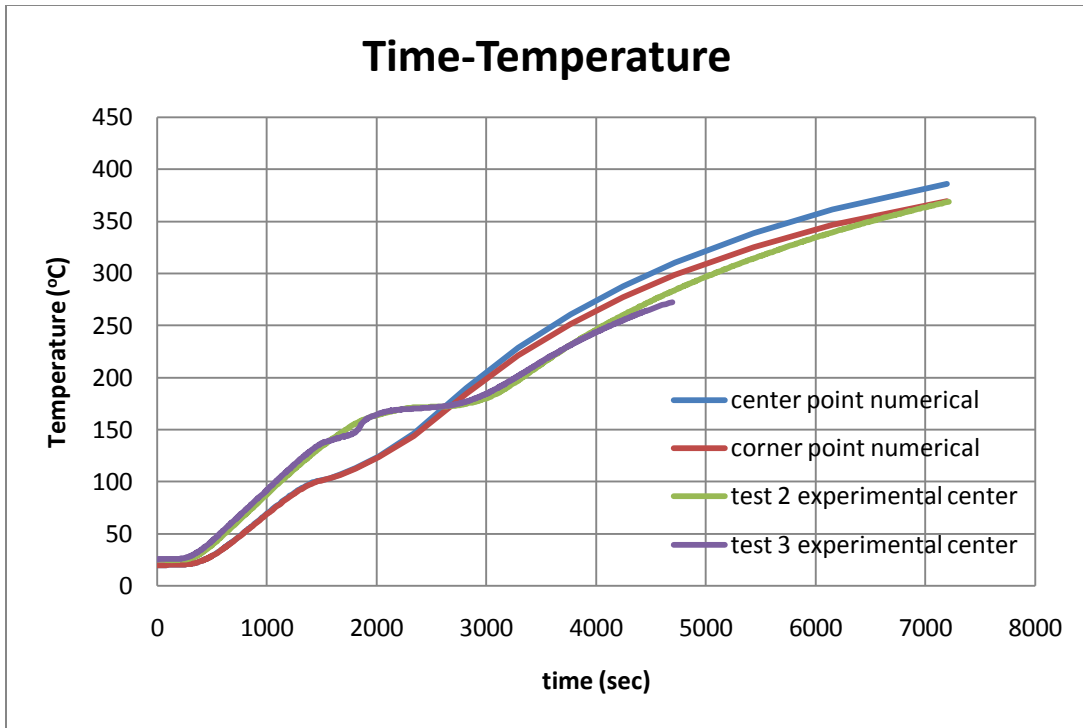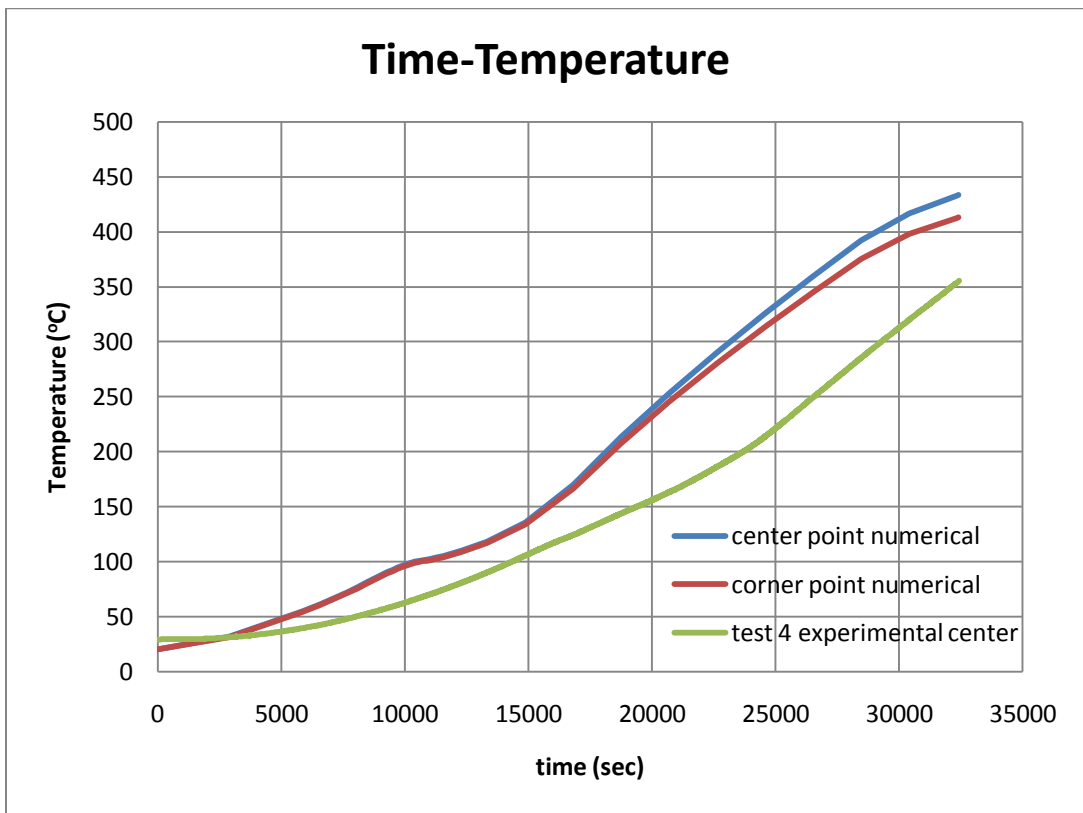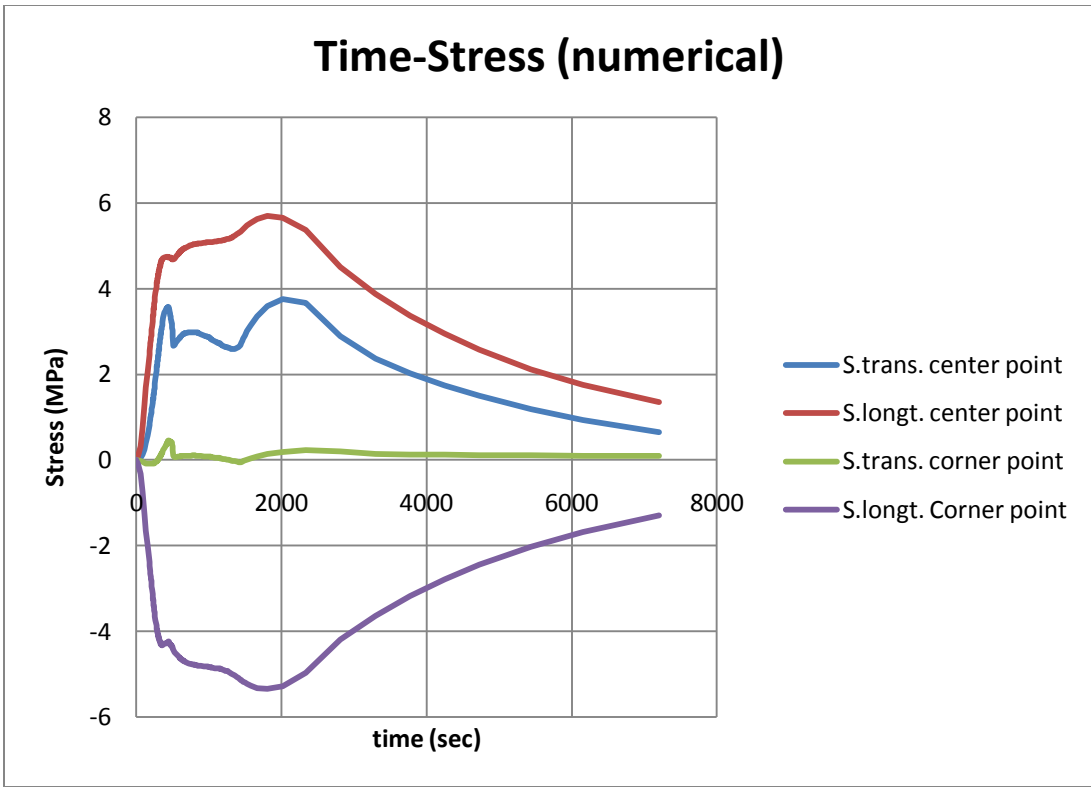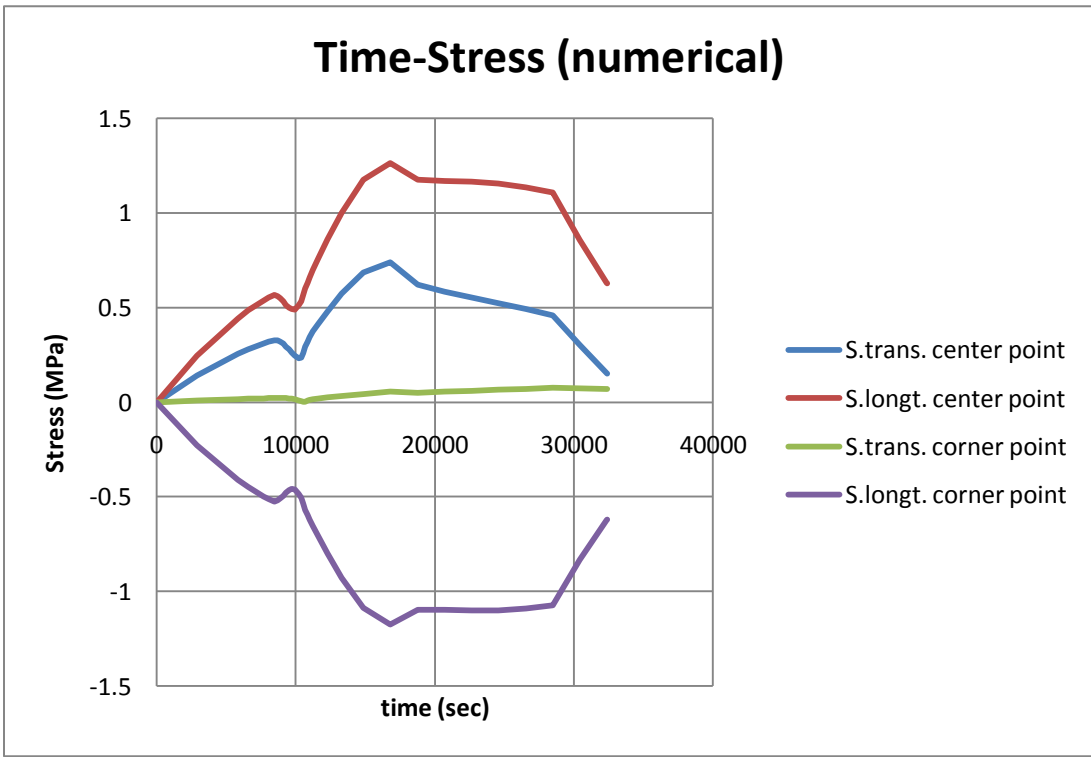ressure. Therefore it can be suggested that the experiments performed by rapid heating would possibly result with measuring lower pore vapor pressure values. Alteration of mechanical properties of concrete such as tensile strength is another issue that can be related to thermal stresses. Indeed, at the center point, thermal stress arises as tensile stress. Therefore, the tensile capacity of concrete may reduce due to this additional self-stress. On the other hand, it should be kept in mind that in some design provisions, self-stresses are not regarded to be affecting the overall capacity.

	2 ^{o}C/sec		1 ^{o}C/min	
	Long. Str. [MPa]	Tras. Str. [MPa]	Long. Str. [MPa]	Tras. Str. [MPa]
center p.	5.7	3.75	1.26	0.74
corner p.	-5.34	0.45	-1.17	0.074

Table 6 Thermal stress comparison (tension is positive).

3.6. Tensile Strength Test

One of the most important issues in this work is to measure tensile strength of concrete subjected to high temperature. In order to understand the relationship between tensile strength and pore pressure, which is formed due to heating the concrete, tensile strength tests were needed to perform.

There are various methods to measure the tensile strength of concrete; in this work, indirect tensile strength test (Splitting test or Brazilian test) was chosen. This kind of test was chosen due to the fact that it is very difficult to perform direct tensile test for high temperature heated samples. Moreover, the specimens were needed to be tested during

heating at the moment that maximum pressure occurs. Therefore, it was much more convenient to conduct indirect tensile strength test.

3.6.1. Splitting Test

In this section (3.6.1.) is cited the work of Rocco C., Guinea G. V., Planas J. and Elices M. "Review of the splitting test standards from a fracture mechanics point of view, 2000".

3.6.1.1.*Description of Splitting test*

In the splitting (or Brazilian) test, a cylindrical or prismatic specimen is compressed along two diametrically opposed generators as shown schematically in Figure 56. To prevent multiple cracking and crushing at the points of loading, the load is distributed through two bearing strips whose width, *b*, differs in the various standards. If the material behavior is linear-elastic, this geometry leads to a nearly uniform tensile stress along the plane of loading, and the expected rupture mode is the splitting of the specimen in two halves across that plane [7]. In the case of concentrated loads, the maximum tensile stress on this plane can be calculated by Equation 11.

Equation 11:

$$\sigma_{max,P} = \frac{2P}{\pi BD}$$
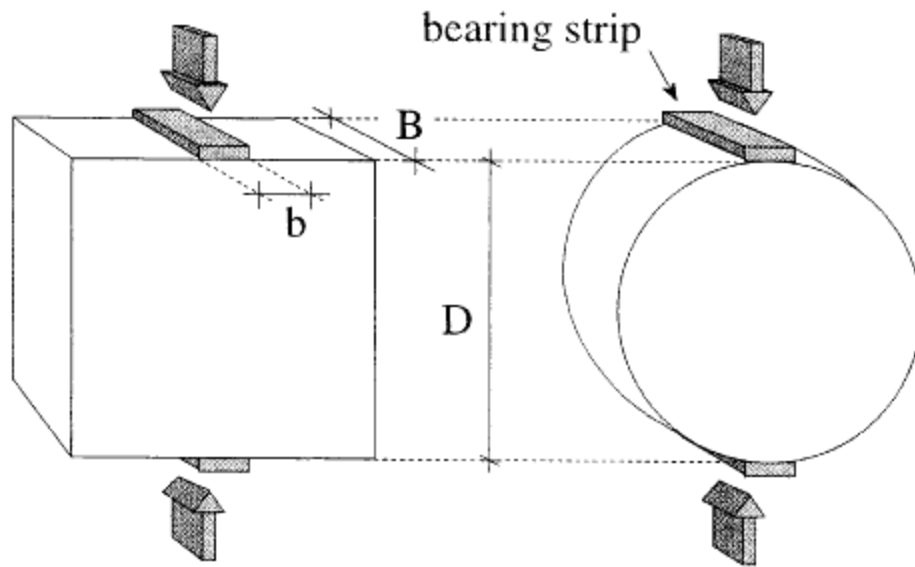
Where $\sigma_{max,P}$ is the maximum tensile stress in the specimen when the applied load is P, while D and B are the specimen depth and thickness, respectively (Figure 56). Following the standards, the maximum tensile stress at failure, calculated from the theory of elasticity, is a material property called splitting tensile strength, f_{st}. If the load-bearing strips are narrow enough to consider the loading concentrated, and the material behavior is linear-elastic-brittle, f_{st} is close to the tensile strength determined by an ideal uniaxial tensile test [7]. From Equation 11, the splitting tensile strength f_{st} is evaluated in the standards by Equation 12.

Equation 12:

$$\sigma_{max,P} = \frac{2P_u}{\pi BD}$$

Where P_u is the maximum load recorded during the test. The splitting tensile strength is then calculated on the assumption of a hypothetical load-bearing strip of zero width (concentrated load).

3.6.1.2.Review of the Linear-Elastic Solution

The standard equation to calculate the splitting tensile strength is derived from elasticity theory assuming that two compressive line loads are applied in two opposite sides of the specimen; i.e. the load is distributed along a line of zero width. However, this assumption is violated in the standards since bearing strips of finite width are prescribed to distribute the load and, consequently, the tensile stress distribution from which Equation 12 was derived is not fulfilled in practice.

As the width of the load-bearing strips increases, the maximum value of the tensile stress along the plane of loading decreases, for any given value of the load. Then, the splitting tensile strength calculated from Equation 12 is overestimated [7]. For cylindrical and cubical specimens, the dependence of the maximum tensile stress at the plane of loading on the width of the load-bearing strips can be calculated from Equation 13 [7].

Equation 13:

$$\sigma_{max,P} = \frac{2P}{\pi BD} * (1 - \beta^2)^{\frac{3}{2}} \qquad for\ cylindrical\ sample$$

$$\sigma_{max,P} = \frac{2P}{\pi BD} * \left[(1 - \beta^2)^{\frac{5}{3}} - 0.0115\right] \quad for\ cubical\ sample$$

Where B and D are the specimen dimensions (Figure 56), P is the load, and $\beta = b/D$ is the relative width of the load bearing strips. Both equations are valid for $\beta \leq 0.20$.

In brittle materials with linear-elastic behavior, it is generally assumed that failure occurs when the maximum tensile stress reaches a critical value. If, for practical purposes, it is assumed that this critical value coincides with the true tensile strength, f_t - obtained from an ideal uniaxial test - the failure criterion can be written from Equation 13[7].

Equation 14:

$$f_t = \frac{2P_u}{\pi BD} * (1 - \beta^2)^{\frac{3}{2}} \qquad for\ cylindrical\ sample$$

$$f_t = \frac{2P_u}{\pi BD} * \left[(1 - \beta^2)^{\frac{5}{3}} - 0.0115\right] \quad for\ cubical\ sample$$

Where P_u is the maximum load recorded during the test (the peak load). Note that by definition f_t coincides with the theoretical value of the splitting tensile strength for a

cylindrical specimen with b/D=0. The splitting tensile strength evaluated from the standard test is given by Equation 12, and by taking into account Equation 14, it can be rewritten as:

Equation 15:

$$f_{st,c} = f_t * (1 - \beta^2)^{-\frac{3}{2}} \qquad for\ cylindrical\ sample$$

$$f_{st,q} = f_t * \left[(1 - \beta^2)^{\frac{5}{3}} - 0.0115\right]^{-1} \quad for\ cubical\ sample$$

Where $f_{st,c}$ and $f_{st,q}$ refer to the splitting tensile strength for cylinders and cubes, respectively. Figure 57 shows the splitting tensile strength in terms of the tensile strength f_t as a function of the relative width of the load-bearing strips b (Equation 15). According to this theoretical prediction, the splitting tensile strength increases with the width of the load-bearing strips. Nevertheless, within the range prescribed by the standards (0.04 ≤ b ≤ 0.16), the differences with f_t are within a 6% deviation, which corresponds to the larger width permitted in the standards (b = 0.16), and when f_{st} is evaluated from cubical specimens [7].
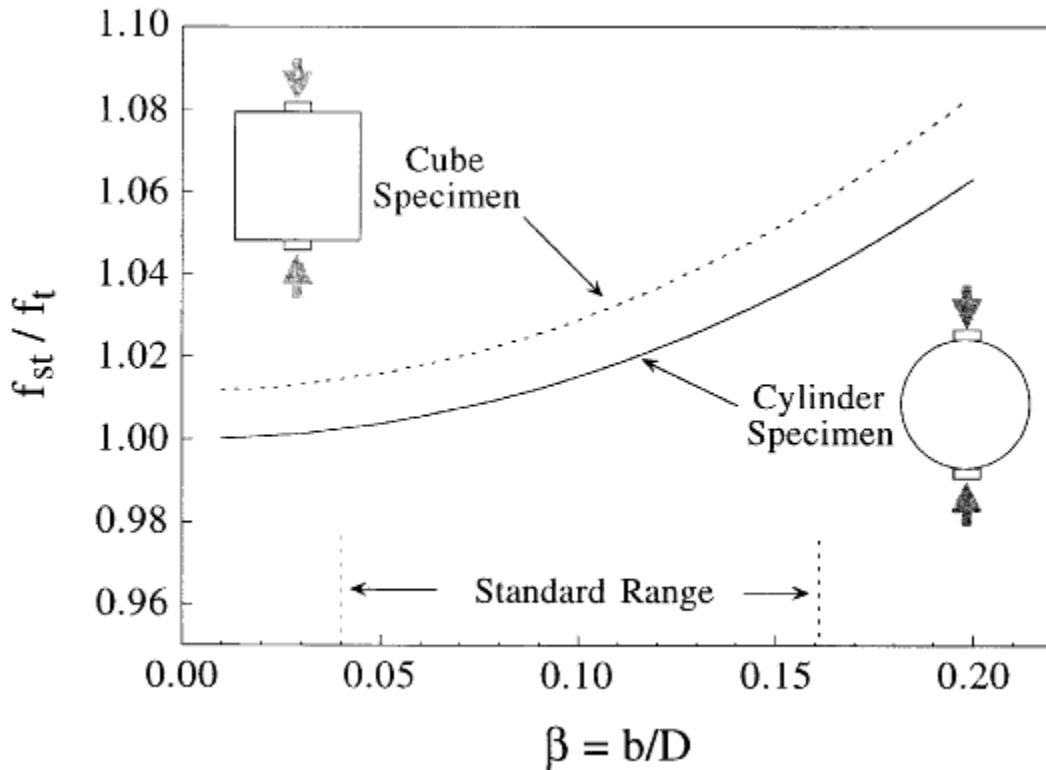

Figure 57 Variation of splitting tensile strength with the relative width of the load bearing strips [7]

These results justify the use in the standards of a very simple equation such as Equation 12 to estimate the splitting tensile strength. Within the framework of the theory of elasticity, and assuming a purely brittle material, the error due to applying this equation, which does not take into account either the specimen geometry or the width of the load-bearing strips, is under 6%.

3.6.2. Preparations for Splitting Test

Provisions of EN12390 part 6 were investigated and indirect tensile tests were performed according to these provisions. For the loading of the specimens, Instron press was used, it has the following properties;

- 100kN load capacity;

- Electro-mechanical actuator;

- Closed loop control (displacement, load and strain).

Initially, packing strips were prepared by using hardboard with specified dimensions (EN12390 part 6 4.3.). Then the loading frame (Figure 58) which is completely made of steel was prepared. The bottom part of the loading frame is fixed and cannot be rotated or shifted while the upper steel loading piece was designed to be independent from the rest of frame, which means it can rotate in all directions and can be shifted upwards. The two pillars which hold the upper piece were adjusted to be short enough not to restrain the loading.

The samples were mounted on the system basically by removing the upper steel loading piece. Then, specimens were prepared for tests with respect to provisions considered in EN12390 part 6 5.3.

Figure 58 Loading Frame

The samples were marked by two lines along which to apply the load. These lines were opposite to each other in an axial plane (EN12390 part6 5.3.). As for positioning, the specimens were placed centrally in the loading frame with regards to the marks. The packing strips had been already stacked by using adhesive tape. Then upper loading piece was carefully positioned. Samples mounted on the loading frame were arranged in a way that the loading direction was perpendicular to the casting direction.

The loading rate was determined to be 0.8 kN/sec by using the formulas given by EN12390 part 6 6.3. which proposes a constant rate of loading within the range of 0.04 MPa/sec to 0.06 MPa/sec. Abovementioned loading rate was found out by applying the Equation 16.

Equation 16:

$$R = \frac{s * L * d * \pi}{2}$$

Where:

L: is the length of specimen in mm

d: is designated dimension of specimen in mm

s: is the increase in rate of stress in MPa/sec

R: is the rate of increase of load in N/sec

As a result, the tensile splitting test strength of specimen was calculated by Equation 17 (EN1992 part 6 7.).

Equation 17:

$$f_{ct} = \frac{2 * s}{L * d * \pi}$$

Where

L: is the length of specimen in mm

d: is designated dimension of specimen in mm

f_{ct}: is tensile splitting strength in MPa

F: is the maximum load in N

3.7. Test Procedures: from Casting to Splitting

3.7.1. Choice of the Mould

In the previous sections, the real situation which was simulated and the choice of the heating rate based upon preliminary experiments and numerical analysis were explained.

What should be done as a next step is to describe each step of experimental set up and things to do when performing tests.

At the very early stages of this work, the decision of concrete type which was planned to use and the type of sintered metal were made. As mentioned before, a concrete type which is in between HPC and normal concrete was chosen. The concrete class is B40. The receipt of this concrete class was taken from Mindegua et al.[2] The concrete mix is given in Table 2.

At first, for the preliminary tests, polystyrene moulds were used to cast concrete. The receipt was used to mix concrete. In order to increase workability, plasticizer was used. However, the amount of plasticizer given in the receipt was too high. The concrete was poured into the polystyrene moulds. One day after casting, the specimens were extracted and were put into bags and they were kept in the moisture room. Some of these

specimens were used in preliminary drying test and the ones including probes (several probes were used) were restored for the pressure and temperature field measurements.

There were some problems with the polystyrene moulds. Because of the softness of the mould, on the surfaces the coarse aggregates caused roughness which could not be removed by grinding it. Due to this problem, plastic moulds, which were considered to have a better performance, were preferred. In the Figure 59, the plastic moulds which were used to cast concrete for the main experiments can be seen.
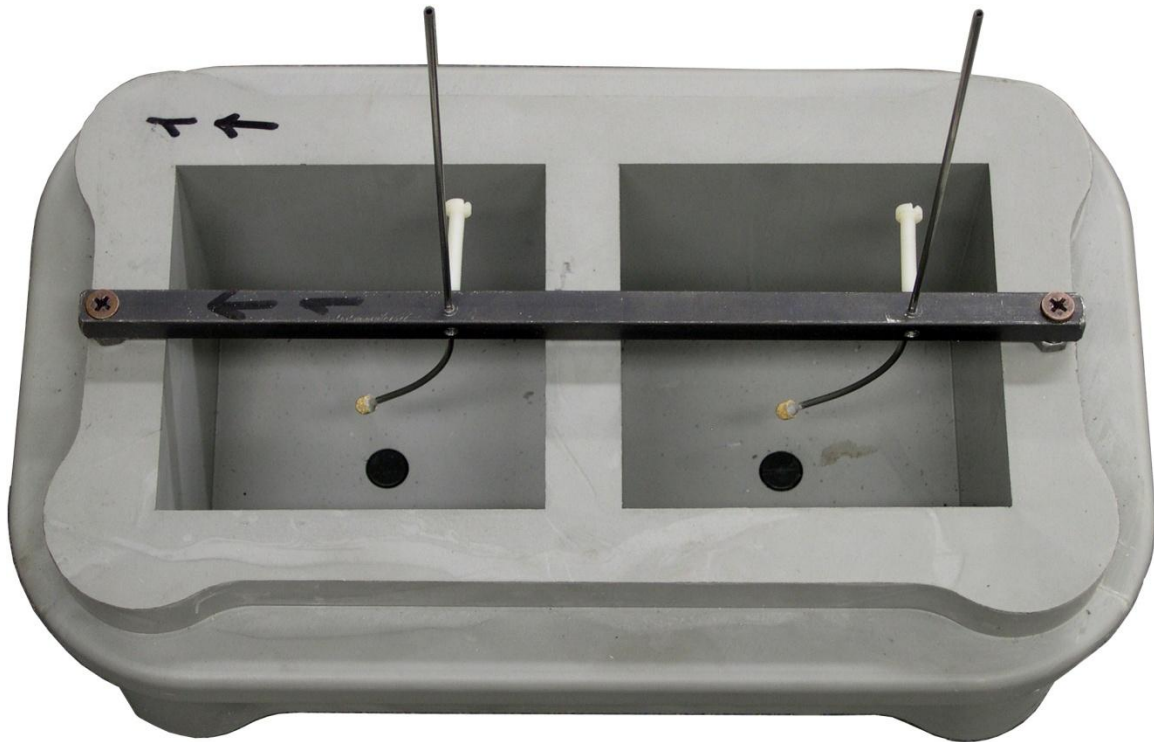

Figure 59 Plastic mould

3.7.2. Disposition of the Probes

As for the pressure heads stuck at the probe, several options were considered. The one used in work of Mindegua et al.[2] was one of them. The material is sintered metal, while the shape of the head is circular and this may lead to some bonding problems with concrete.

Another option was to use the probe without any head. However, in the thesis, the head was improved in order to make it "compatible" with the concrete. In order to

achieve this, the semi-spherical shaped sintered metal (quasi-aggregate) was used. The circular and semi spherical shaped heads can be seen in Figure 60.

Figure 60 Comparison of two pressure heads

After determining the type of pressure head, what kind of material for sticking the head to the probe were decided. Epoxy and the cement used in the concrete mix were two possible options. Even though epoxy was quite good, the cement was decided to be used because the same material used in concrete would be more compatible with concrete.

Now the mould type and the pressure head were already determined. The next thing is how to mount the probes into concrete and the casting procedure.

In this work, differently from previous works Brazilian test was aimed to be performed after heating up until the pore pressure reached its maximum. When performing the splitting test, the probe must not be in the cracking plane. In order to avoid this, the probes were bent as can be seen in Figure 61.

Figure 61 The probes mounted into specimens

After this point, the probes must be installed such that it stays still during casting. As mentioned before, it was decided that the pressure and temperature field measurements would be taken in the mid part of the concrete. In order to keep the pressure head in the desired position, steel rods, which would be mounted in the moulds, were introduced.

The rods and the moulds were drilled at both ends to screw rods to mould. Two holes were bored so that the probes could be placed. Next to these two holes, there were drilled screw holes to hold the probes in a way that the pressure head stayed still in the desired position (i.e. the center point of the cube). The plastic screws were used for probes.

The Figure 62 shows the steel rods.

Figure 62 Steel rods used to keep the probes in position

3.7.3. Realization of the Specimens

As a next step, the plastic plates were prepared. The purpose of this is to make the surface as smooth as possible. As mentioned before, the coarse aggregates lead to roughness on the surface which may lead to improper sealing. In order to avoid this, two plastic plates for each mould were introduced. These were installed to moulds keeping some space between steel rod and mould after pouring the concrete into moulds. The Figure 63 shows the plastic plates.

Figure 63 Plastic Plates

Everything needed to cast concrete were explained so far. The moulds ready to be used can be seen in Figure 64 and the procedure of casting is as follows:

1. Wet the mixer;
2. Mix the solid ingredients (cement, aggregates, sand) for 1 minute;
3. Add water and admixture in 30 seconds (water and additive should be mixed before adding it);
4. Mix for 1.5 minutes;

5. In the following 2 minutes check workability and add some extra admixture only if needed;

6. After mixing, the specimen casting procedure into 2 steps for small specimens:

- get your mould half filled with concrete, then use a vibrating table;
- get your mould half filled with concrete, then use a vibrating table.

7. The specimens must be taken out from the mould 24h after casting;

8. Then they will be kept in airproof bags.

Figure 64 the moulds ready to use

The concrete specimens were kept in airproof bags during approximately 2 months. Some of them were used for drying tests and, some other specimens were reserved for determining reference strength. Before performing the experiments, the sealing was applied to the specimens. By the way, the surface had to be grinded before sealing in order to have better bonding between materials used in sealing and the concrete surface.

As for the surface where the probes get out, epoxy was smeared to avoid the escape of vapor. For the split test, the cracking line was cut and covered with silicon (Figure 65).

3.7.4. Heating and Splitting Test

Some pore pressure tests were performed as mentioned in the previous section as preliminary tests. Considering the thermal stresses and the results of pore pressure, heating rates applied to the specimens were decided.
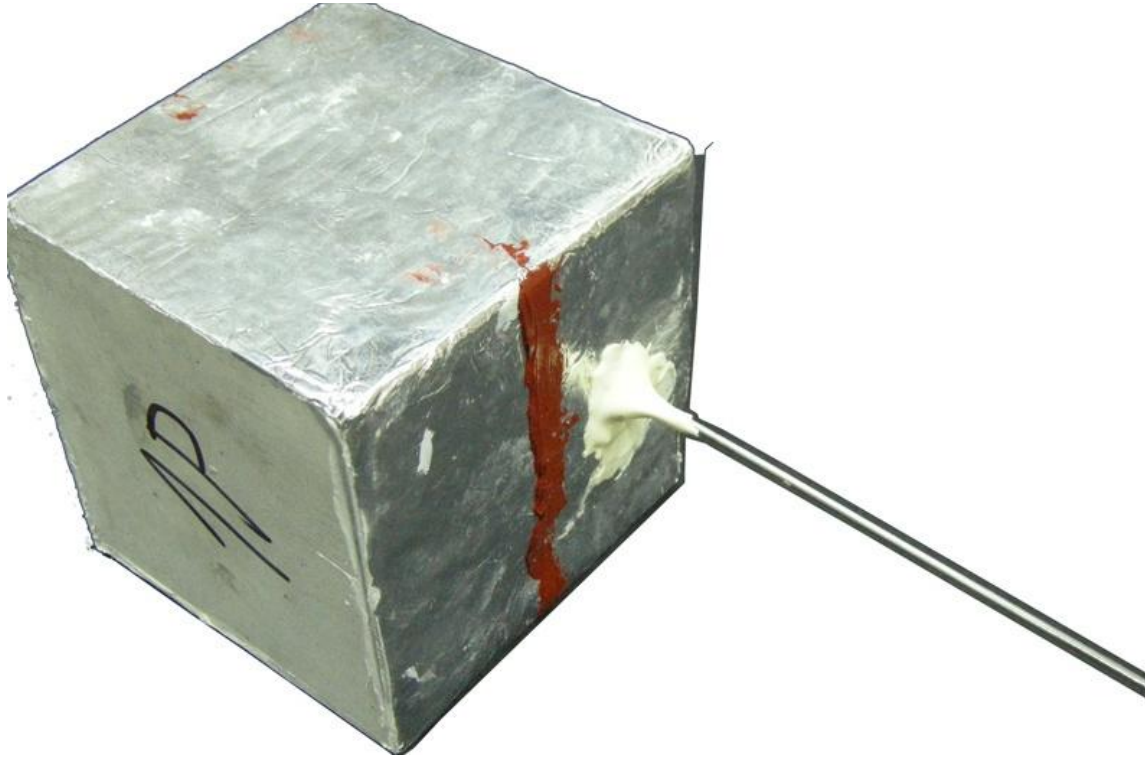

Figure 65 The sealing with cut for split test

As mentioned before, heat was imposed on the unsealed faces of concrete. The set –up was prepared by putting two radiative heaters on opposite sides. The type of radiative heater can be seen in Figure 66.

Figure 66 Radiative heater

In order to allow the pore pressure and temperature field measurements, a connector was placed at the free end of the probe. The connector and the probe must be filled with oil for proper pressure readings. Thermo-couple and the pressure sensors mounted together before running experiments. When applying the isolation, two steel strips were used to keep them still. The Figure 67 below shows the experimental set-up for heating during the test.
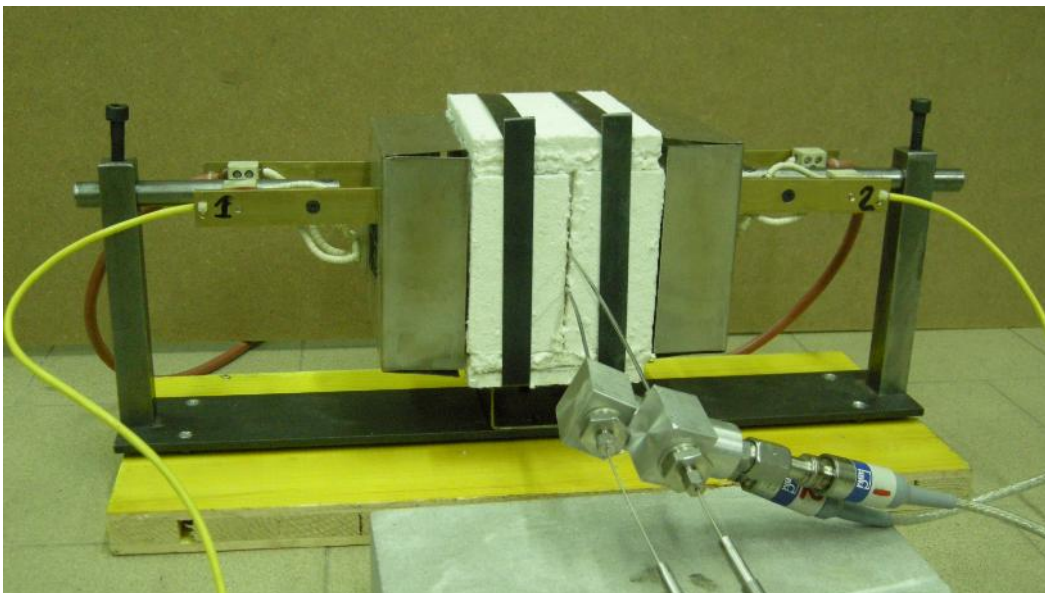

Figure 67 The heating set-up during experiment

The specimens were heated up to a target temperature (600ºC) with a determined heating rate. Three different heating rate which are 10 ºC/min, 2ºC/min and 1ºC/ min were applied. When reaching the maximum pore pressure, the cube specimen was moved to the press machine.

The data acquisition was achieved by using two software. The first one is responsible for measuring temperature and pore pressure. The data are stored up to the starting point of the split test by using this program. After moving the specimen to the press machine, the first program is stopped and the second program, responsible for split test and pore pressure measurement is run up to the failure of specimen.

4. **Results**

4.1. Introduction

The aim of this work is to evaluate the effect of pore vapor pressure on apparent tensile strength of concrete. For this purpose, several experiments were conducted; the preparation of specimens and definition of heating system are presented in Chapter 3.

In the experiments, two different kinds of concrete, namely plain and polypropylene fiber reinforced concrete were used, in order to determine also the effect of polypropylene fibers on pore pressure development inside the concrete under high temperatures.

Four heating rates were applied to heat up the specimens:

- 1°C/min,
- 2°C/min,
- 10°C/min,
- 120°C/min ($2°$C/sec).

These heating rates can be classified as very slow, slow, moderate and rapid, respectively.

As explained in previous chapters, heating rates were determined by preliminary pore pressure tests and numerical analysis. Using four different heating rates, it was expected to give a comprehensive evaluation of problem and achieve understanding of whole picture of the phenomena.

In the experiments, a total of 18 samples were tested, 12 of them were plain concrete and 6 of them were polypropylene fiber reinforced concrete. The heating rates of 2°C/min and 10°C/min were considered as primary heating rates, so 6 samples and 8 samples were tested respectively with these rates; then 2 plain concrete samples were tested for 2°C/sec and 2 plain concrete samples for 1°C/min.

As a result of these tests, time-temperature, time-pressure, temperature-pressure and pressure-tensile strength curves were obtained for two kinds of concrete with various heating rates. The results are presented in forthcoming parts of this chapter.

4.2. Test Results

4.2.1. Time-Temperature Curves

The time-temperature curves are plotted by using the data acquired during the experiments. There are four plots namely Figure 68, Figure 69, Figure 70 and Figure 71, drawn for each heating rates. In the graphs, the sample numbers were given with the sample types, which were tagged as "P" for plain concrete and "Fi" for poly-propylene fiber reinforced concrete.

It is observed that all time-temperature curves have similar trend of increase and slight plateau in between temperatures of 150°C and 200°C. The plateau occurs due to the phase transformation of intrinsic water in the concrete, from water to vapor. The steepness of plateau depends on the heating rate of the experiment. For slower heating rates, steeper plateau was obtained and vice versa. It can be argued that increasing the heating rate causes the plateau to be milder owing to the difference between Figure 68 and Figure 71 which are very slow and rapid heating rates respectively. In fact, the plateau is expected to be strictly horizontal in case of steady state flux of water and this situation is almost reached for rapid or moderate heating rate, while for very slow and slow heating rate the drying of the sample during heating became significant and the plateau is less evident.
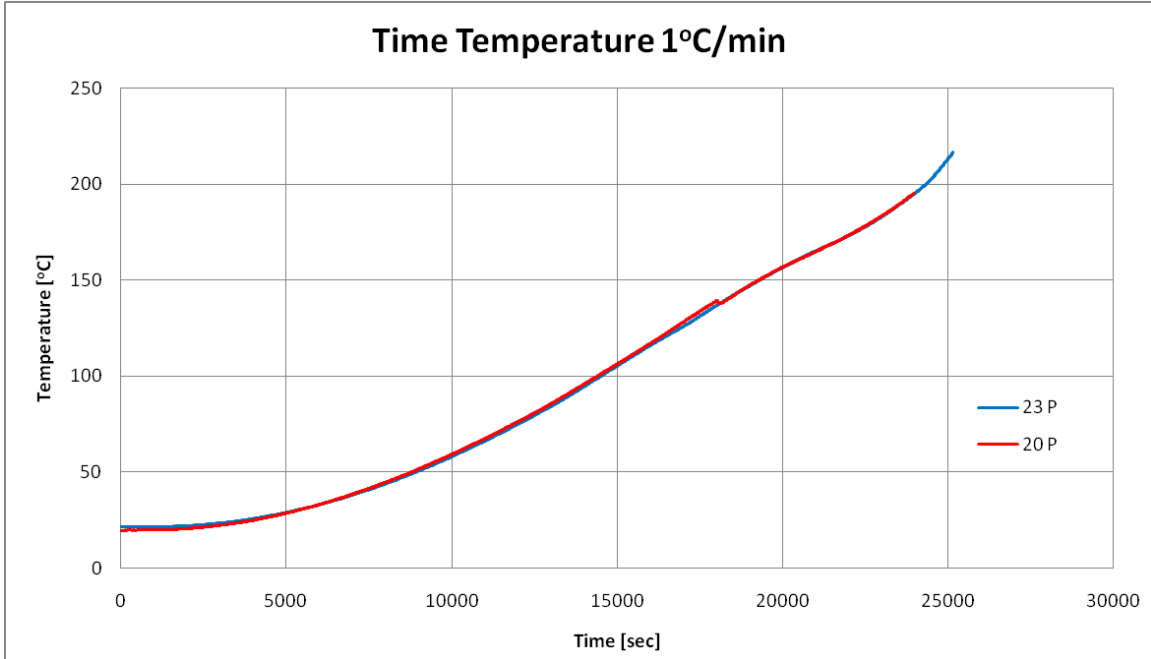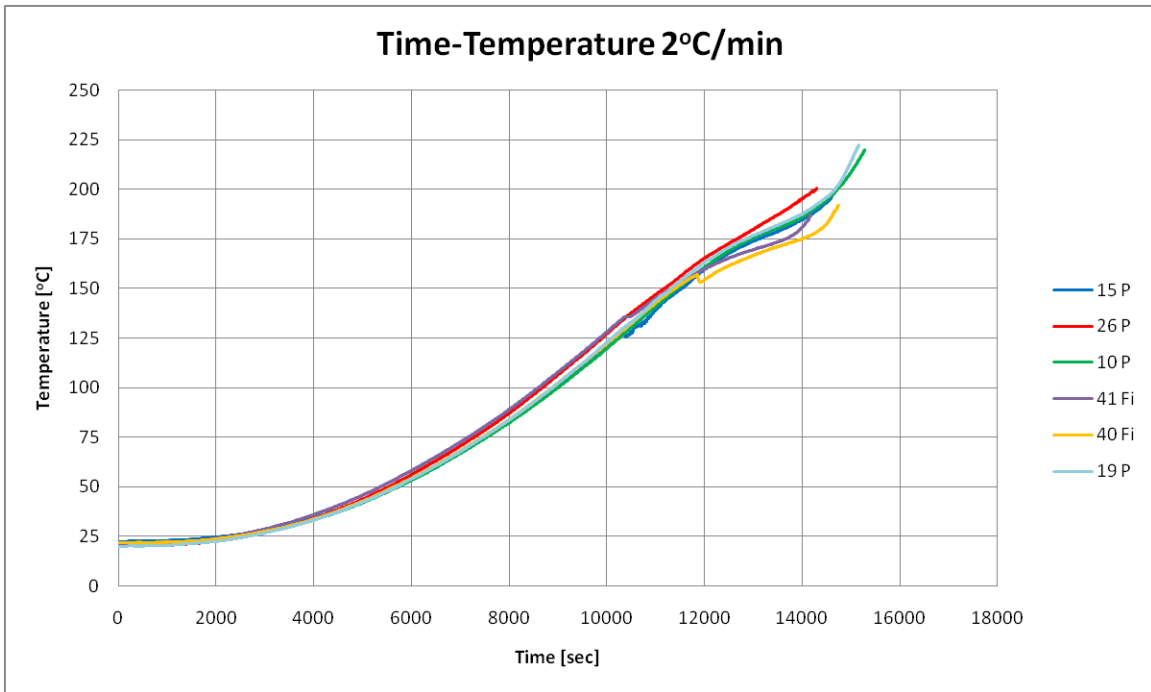
Figure 68 Time-Temperature 1°C/min

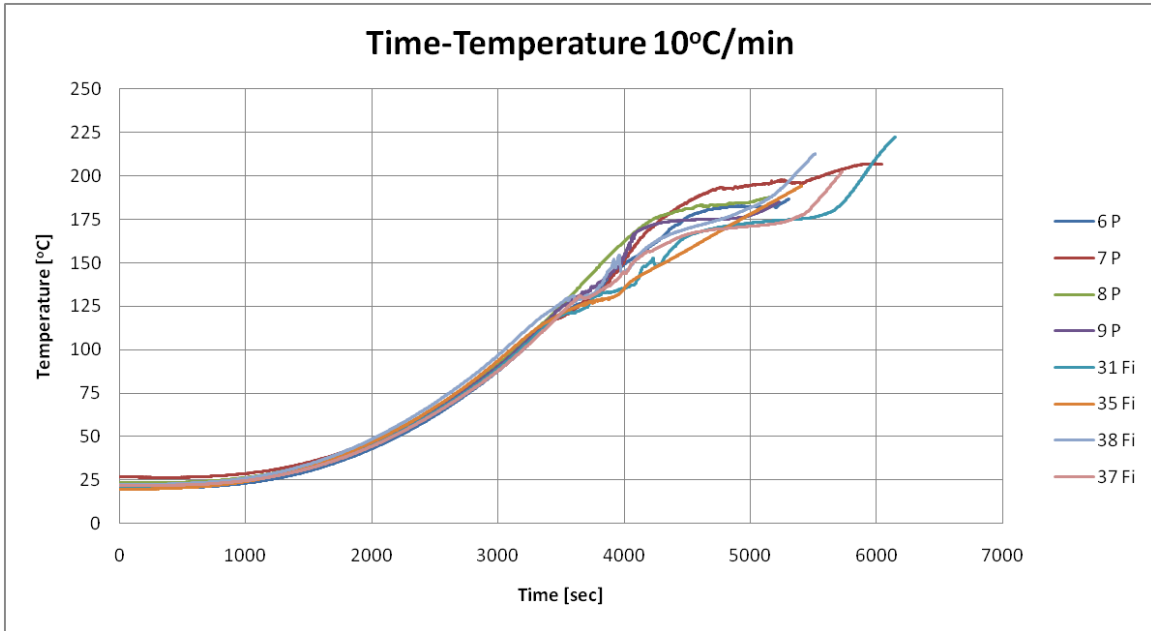
Figure 69 Time-Temperature 2°C/min
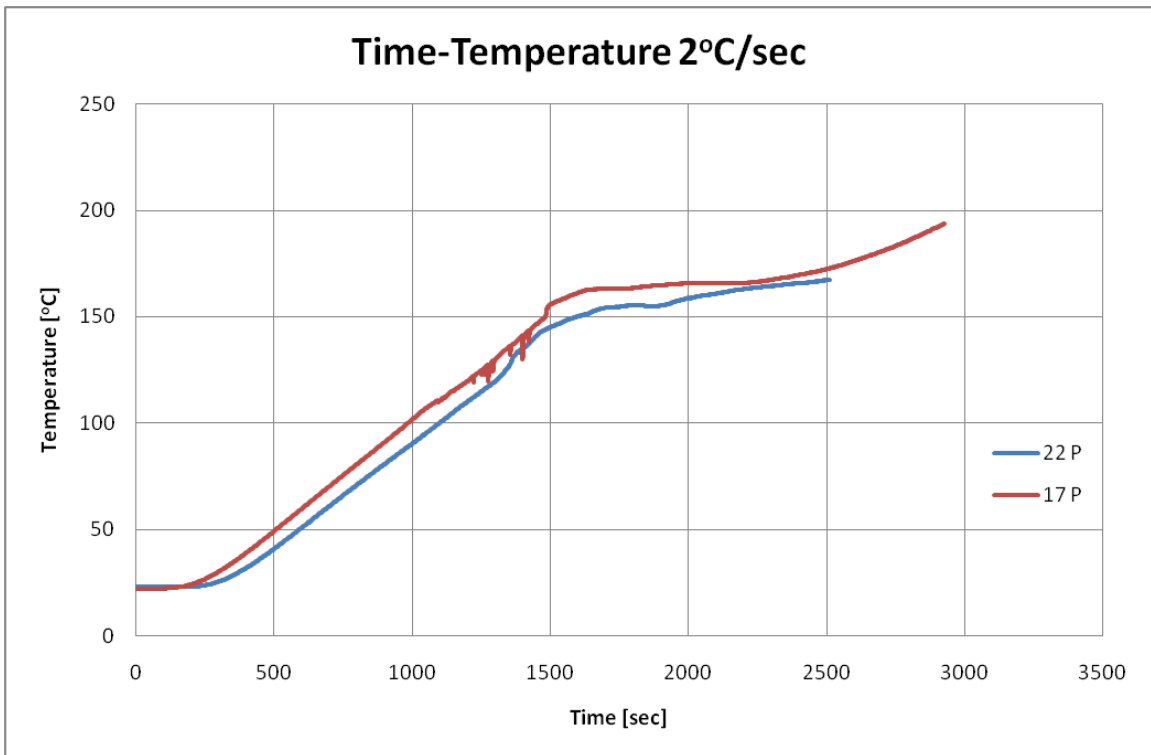
Figure 70 Time-Temperature 10°C/min

Figure 71 Time-Temperature 2°C/sec

4.2.2. Time-Pressure Curves

Time-Pressure curves were plotted by the obtained pressure data from the experiments with respect to four different heating rates and shown on Figure 72, Figure 73, Figure 74 and Figure 75.

Pressure development seems to differentiate according to the heating rate in a way that pressure trends of very slow/slow heating rate (Figure 72 and Figure 73) and moderate/rapid heating rate (Figure 74 and Figure 75) look similar to each other. The maximum pressure achieved during the experiments was 13.25 bars (1.325 MPa) which is relatively low value for pore vapor pressure; however this was expected because it is well known that normal strength (such as that used in this work) shows lower pore pressure with respect to high strength/performance concrete; hence, spalling risk is lower in normal strength concrete, and that is the reason why no spalling was experienced in the tests performed in this work. Indeed, this result confims the pore pressure values obtained by Mindeguia et al. [2].

In the work of Mindeguia et al., in fact, the pore pressure values, obtained by testing a similar type of concrete that used in this work, varies in between 2 bars and 6 bars (Figure 10) with respect to location and depth of measurement where P50 measurement point is almost the same point that the measurements had been done in this work.

Probably the higher values of pore pressure obtained in the present work with respect to Mindeguia et al. are explainable considering two aspects: 1) the sealing of the specimen that leads to a very lower loss of moisture during heating; 2) the condition of symmetry that characterized the mid section of the cubes.

In Figure 73 and Figure 74, it is obvious that the behavior of plain concrete and fiber reinforced concrete is different in the sense of pore pressure development. It seems that plain concrete samples tend to achieve higher pore pressure than the fiber reinforced concrete, whereas the trends of development are quite similar. Moreover, the pressure peaks were reached almost at the same time, in other words almost at the same temperature.

The measurements were carried out on the symmetry plane due to the fact that pressure gauges were at the mid-section and the specimens were heated from two sides

symmetrically. That means, there should be no moisture flow through the measurement point, therefore, porosity difference in between the concrete types does not affect much the results. However, the moisture flow towards the boundaries is easier in fiber reinforced concrete due to the effect of fibers inside the concrete under high temperature. It can be claimed that any leakage on the moisture sealing of specimens is more evident in the case of fiber reinforced concrete owing to abovementioned effect of fibers.
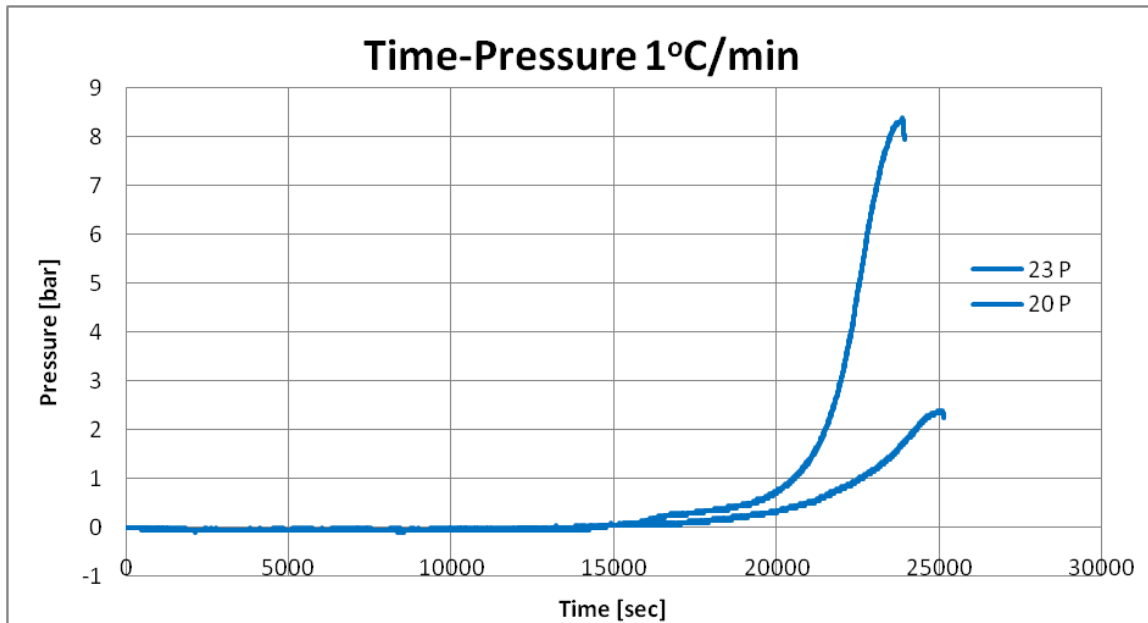

Figure 72 Time-Pressure 1°C/min
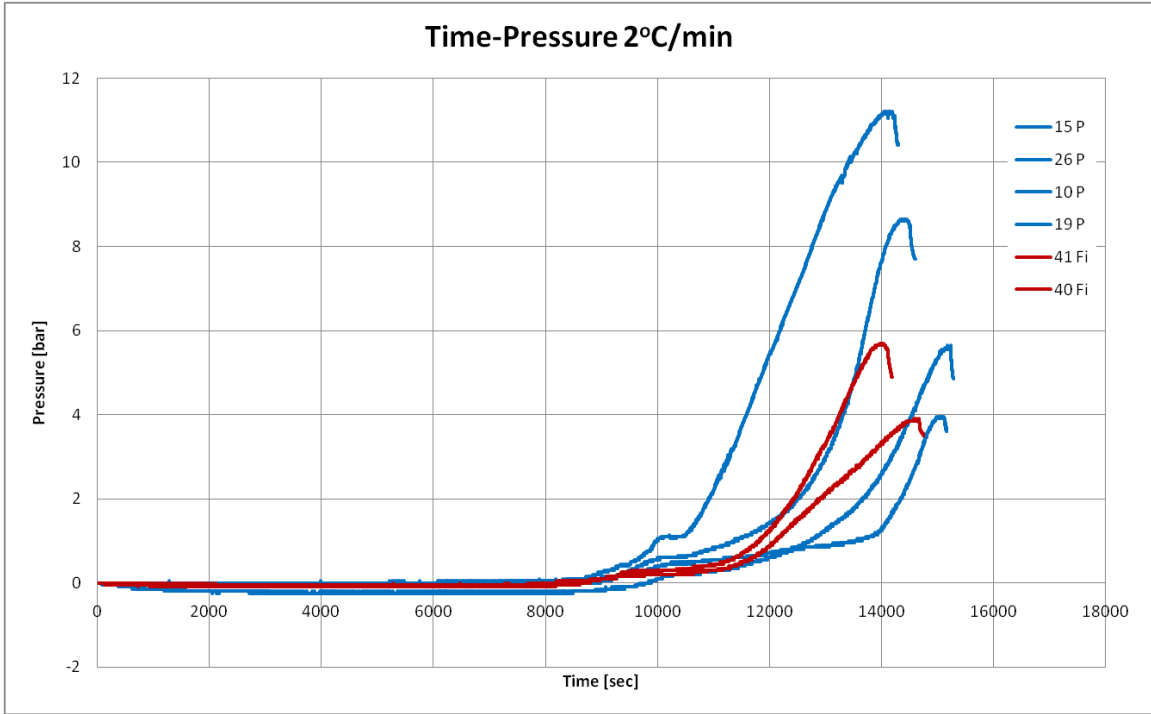
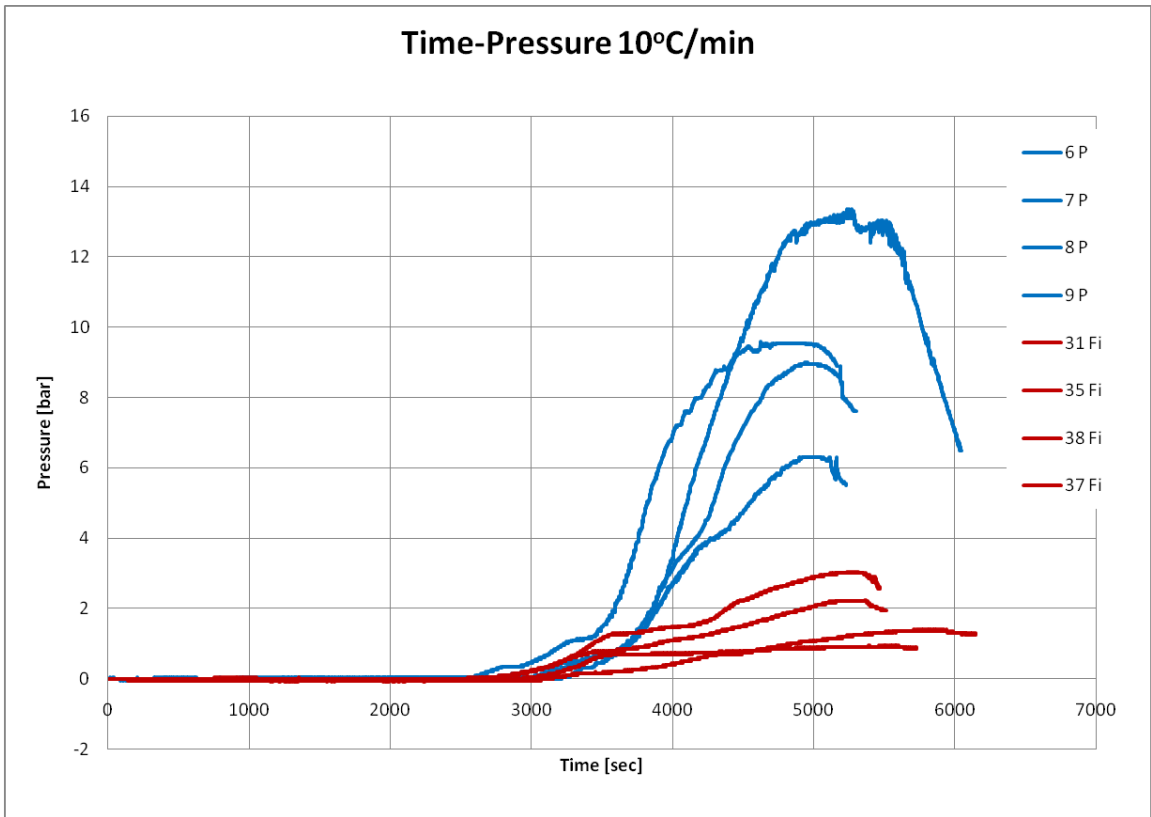Figure 73 Time-Pressure 2°C/min
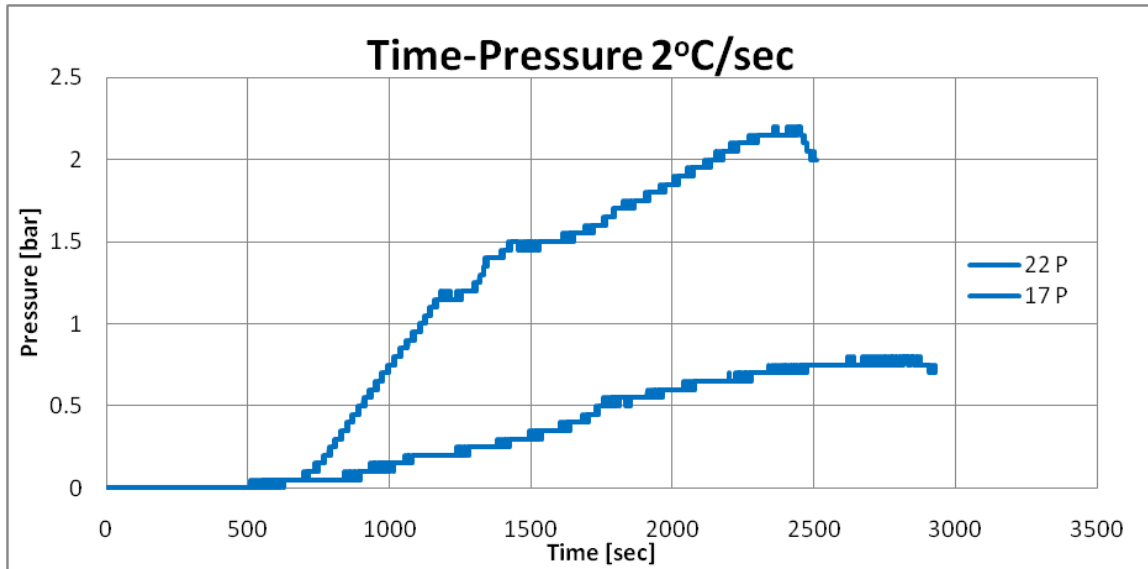

Figure 74 Time-Pressure 10°C/min

Figure 75 Time-Pressure 2°C/sec

4.2.3. Time-Pressure and Time-Temperature Curves Comparison

Pressure-Temperature curves were obtained by the combination of time-pressure and time-temperature curves. At the left hand side ordinate of graphs, temperature values [°C] are presented and at the right hand side ordinate of graphs, pressure values [bar] are presented.

In each graph, two specimens' data were plotted, of where thinner curves represent temperature variation and thicker curves represent pressure variation. The graphs demonstrate that dramatic pressure rise occurs almost at the beginning of the plateau of Time-Temperature curve and pressure peaks are achieved at the end of the plateau. Indeed, the beginning of plateau is the point at which phase transformation of water occurs. At this point intrinsic water starts to vaporize and this causes the increase in pressure.

After that water is totally transformed into vapor, plateau is left and the pressure starts to decrease.
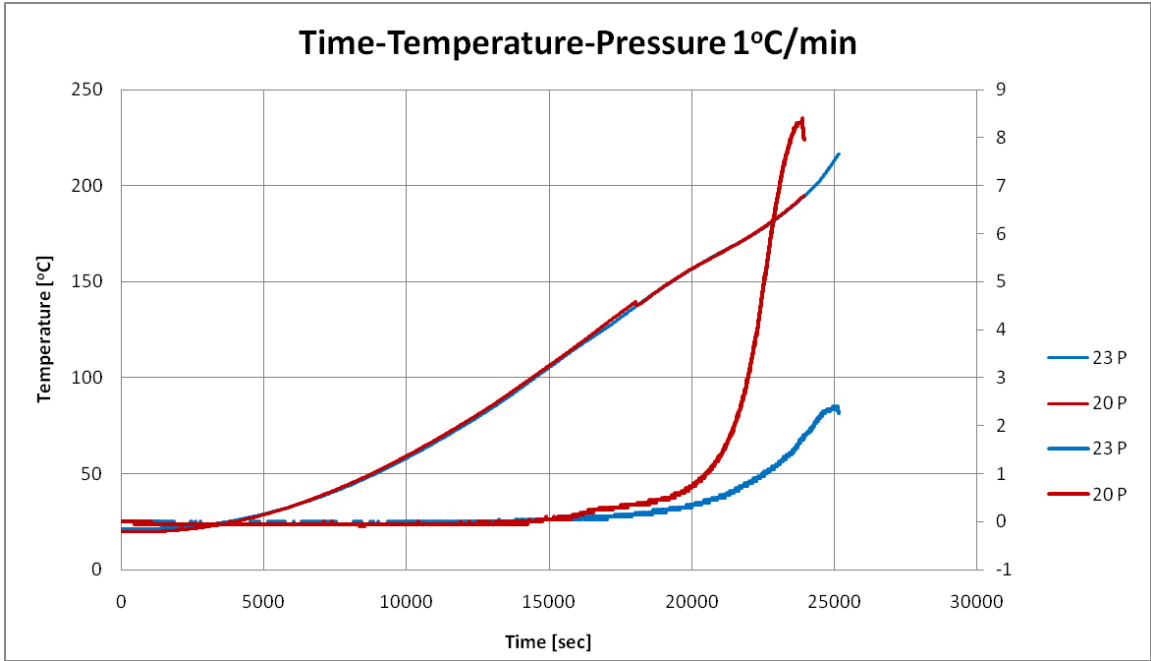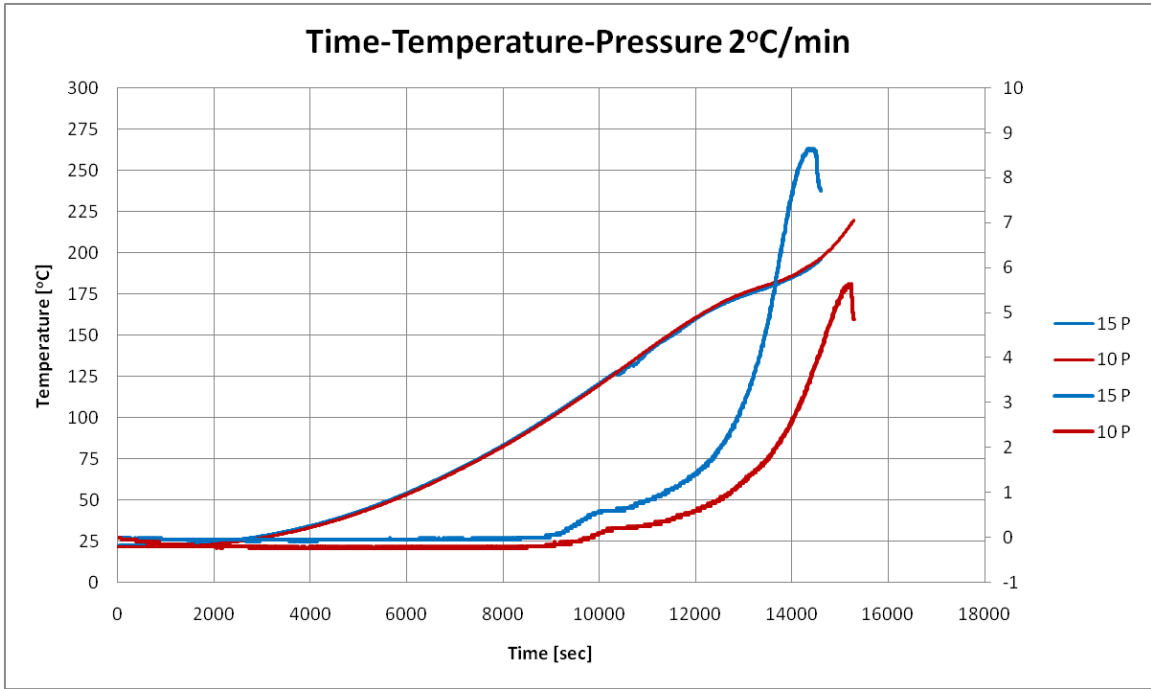
Figure 76 Time-Temperature-Pressure 1ºC/min
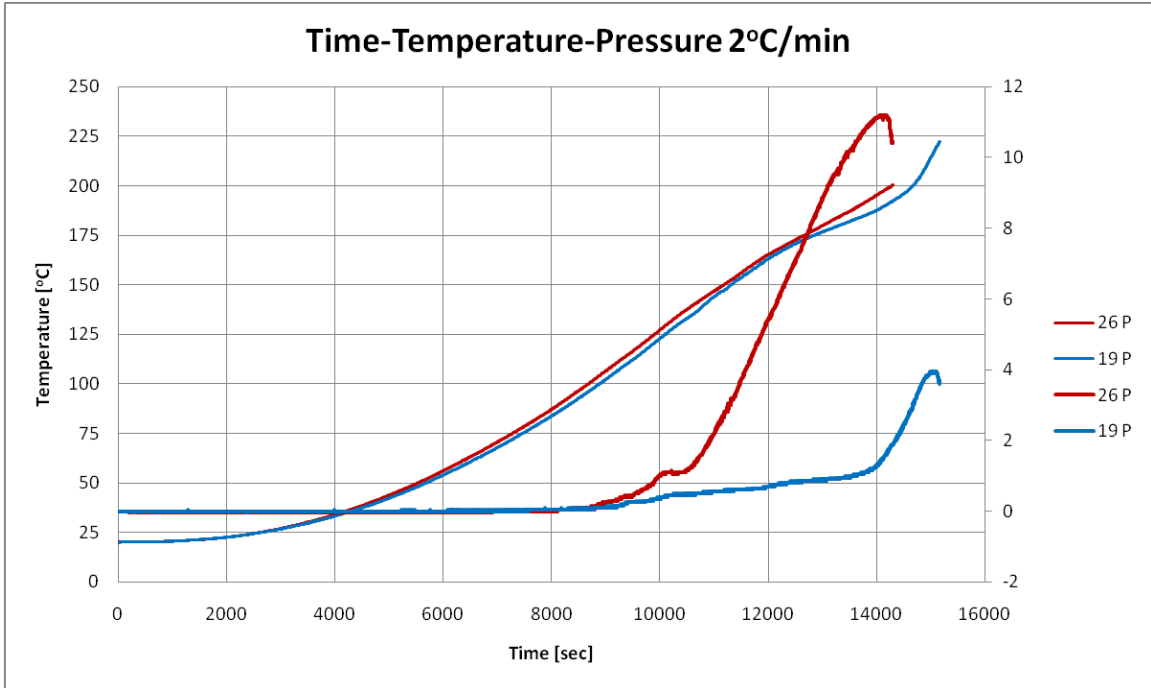

Figure 77 Time-Temperature-Pressure 2ºC/min

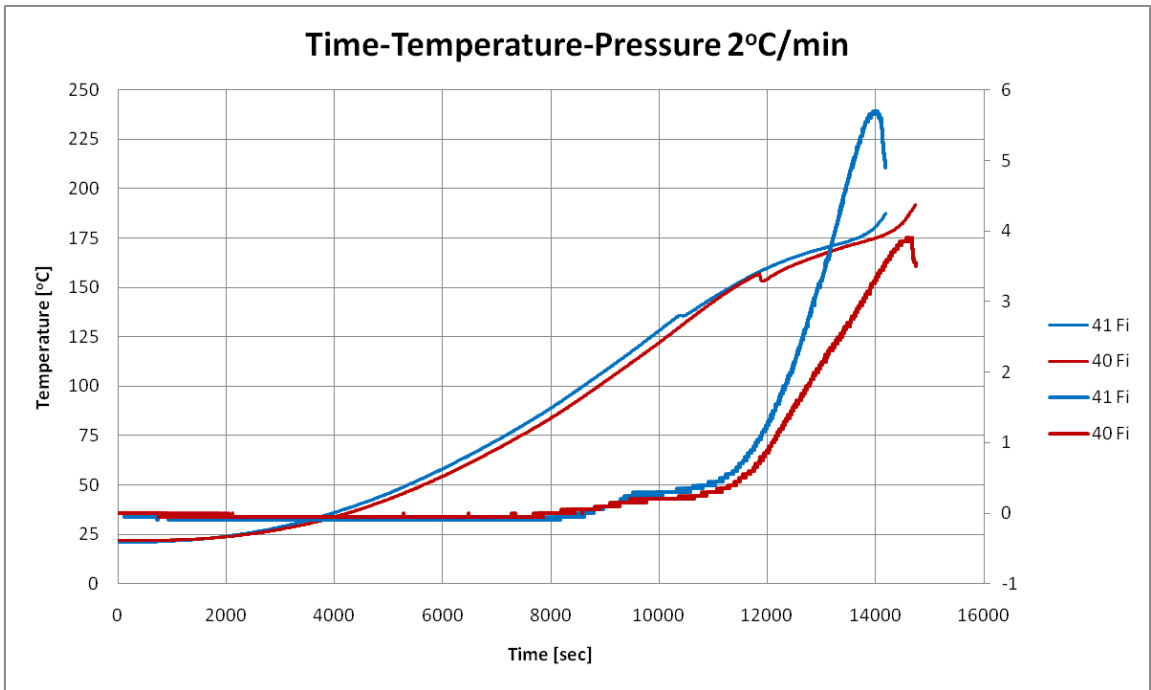Figure 78 Time-Temperature-Pressure 2°C/min
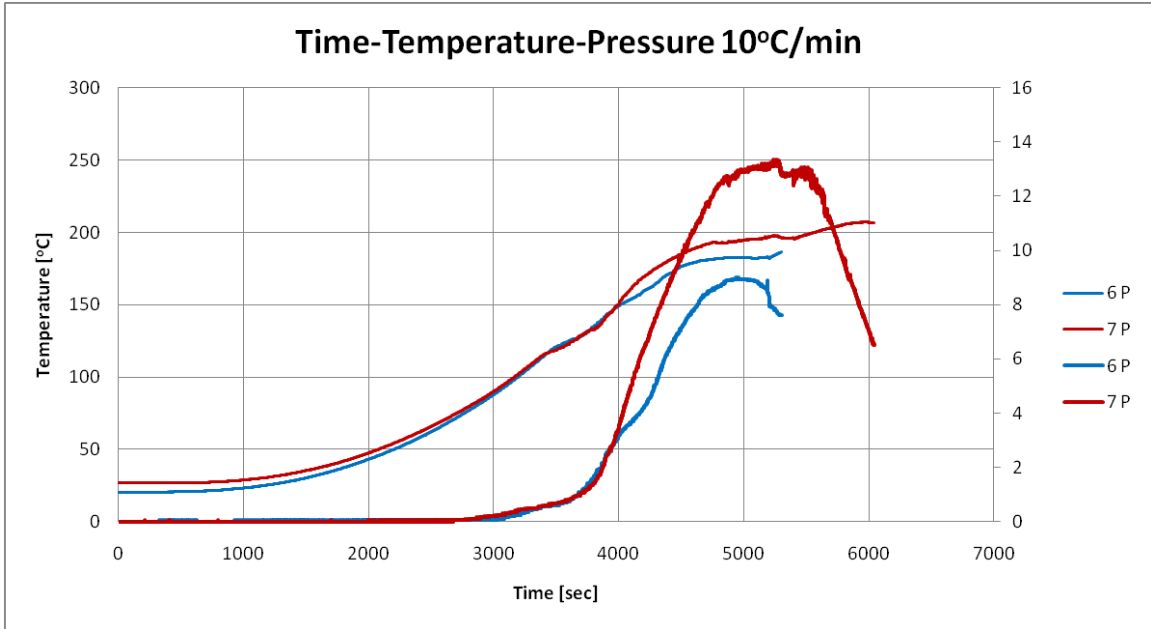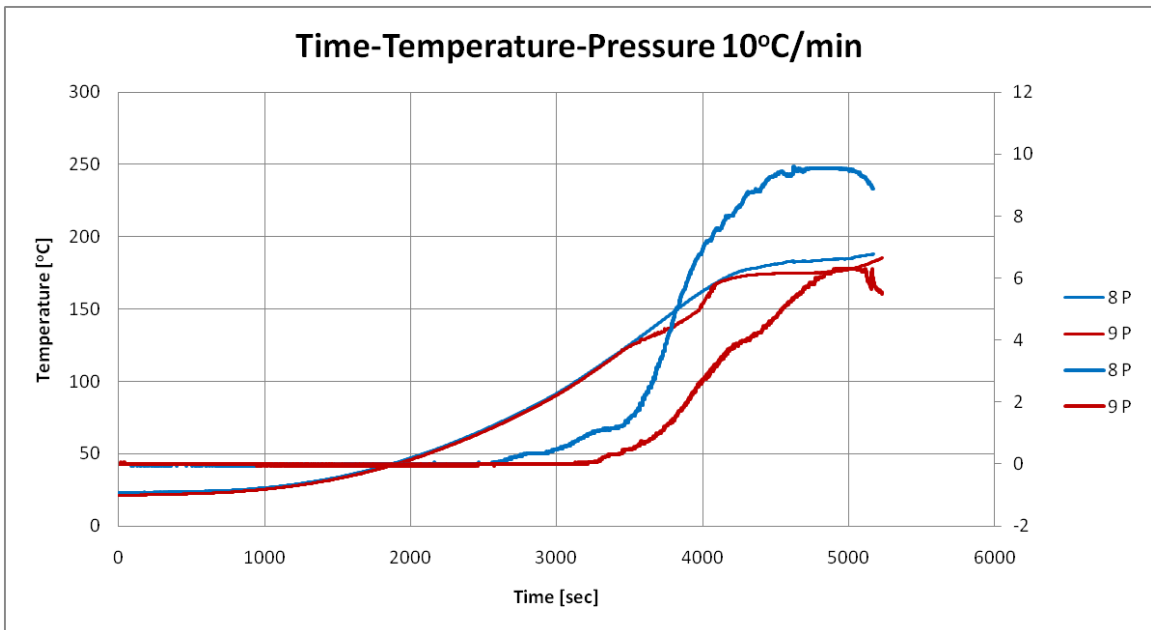

Figure 79 Time-Temperature-Pressure 2°C/min

Figure 80 Time-Temperature-Pressure 10°C/min
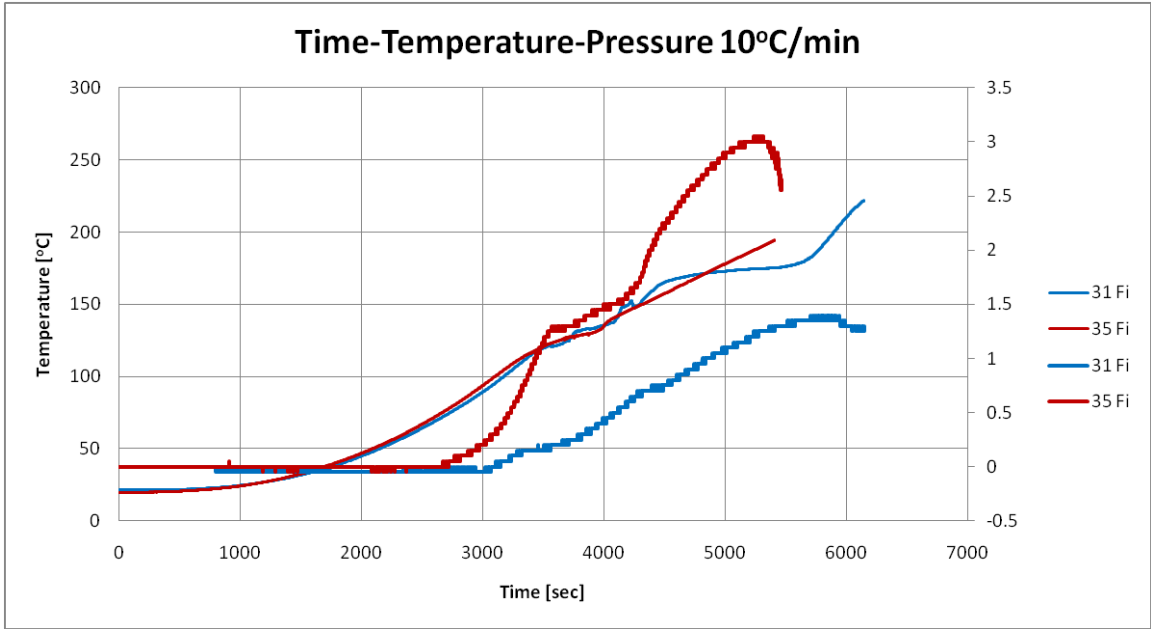

Figure 81 Time-Temperature-Pressure 10°C/min

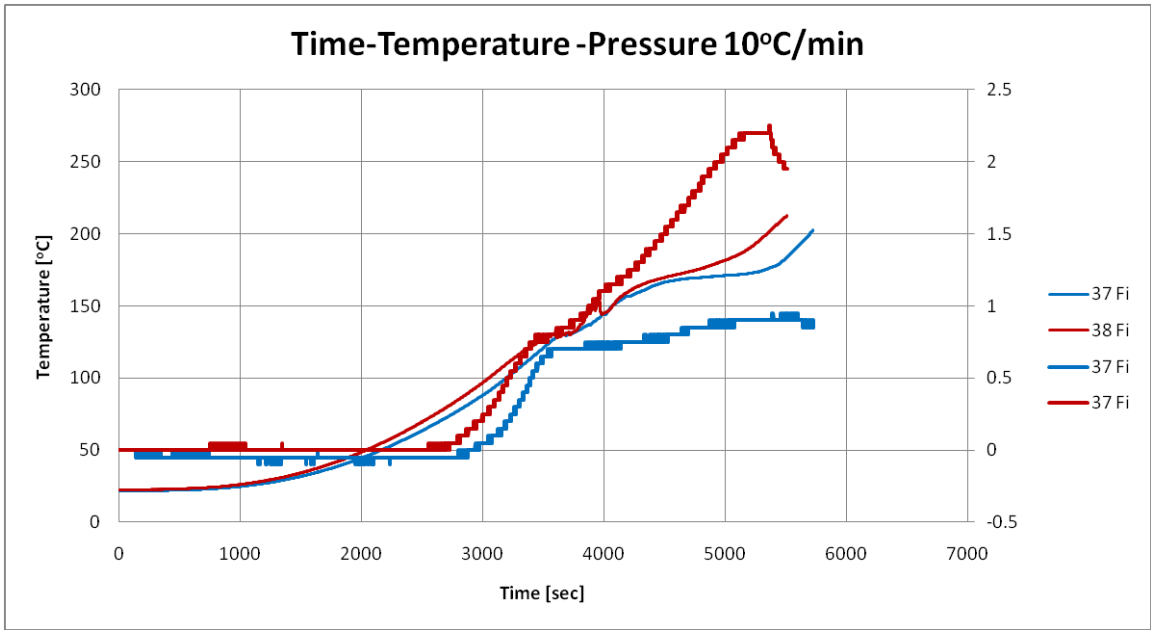Figure 82 Time-Temperature-Pressure 10°C/min

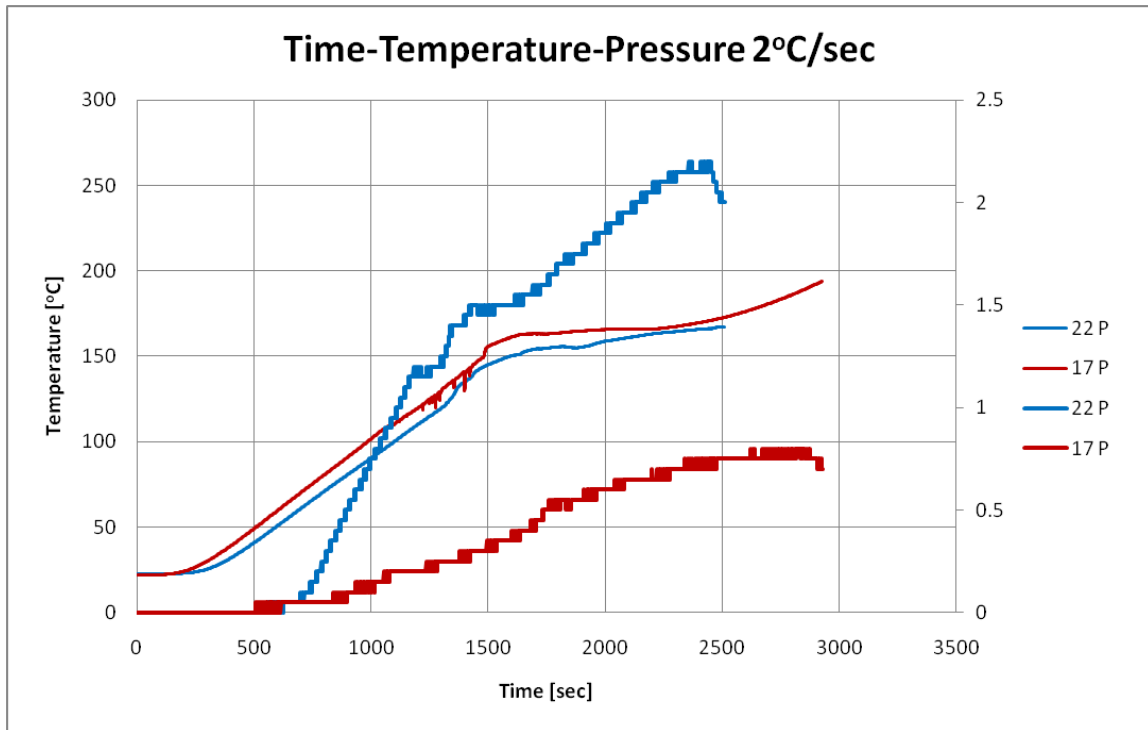Figure 83 Time-Temperature-Pressure 10°C/min

Figure 84 Time-Temperature-Pressure 2ºC/sec

4.2.4. Pressure-Temperature Curves and Saturation Curve

Temperature-Pressure graphs show that the pressure development dependent to temperature in the mid-section of the concrete. The saturation curve (P_{vs}) is introduced into these graphs; what is expected is that the saturation curve would represent a boundary condition of Pressure-Temperature relation.

Two different equations for the saturation curve were used to identify this boundary condition, which are the equations of Buck et al. and Hyland-Wexler et al. (Equation 18 and Equation 19, respectively). Theoretically, Pressure-Temperature curves cannot pass beyond the saturation curve. However, it was observed that in some experiments Pressure-Temperature curves exceed the saturation curve (i.e. Figure 87, sample 8P). Since it is theoretically impossible, vapor pressure is not responsible for this overpressure. This overpressure is often attributed to the partial pressure of the dry air that is enclosed in the porous media (Mindeguia et al.) [2].

It is obvious that there is a difference in between slow heating rates (1°C/min and 2°C/min) and fast heating rates (10°C/min and 2°C/sec). The fast heating rates cause pore pressure to ascend closer to saturation curve, whereas there are gaps formed among saturation curve and Pressure-Temperature curves in the case of slow heating rates. Indeed, it is not inconvenient to state that drying due to slow heating could be reason of delayed development of pore pressure.

In Figure 85 and Figure 88, very slow and rapid heating rates test results are plotted, which were performed only by plain concrete samples. On the other hand, Figure 86 and Figure 87 show tests that were performed by both plain and fiber reinforced concrete samples for slow and moderate heating rates.

It was observed that tests of fiber reinforced concrete specimens lead to lower pore pressure values than plain concrete counterparts. In fact, reducing fire induced pressure is one of the effects that are expected from fibers. When fiber reinforced concrete exposed to high temperature and pore pressure starts to rise, fibers tend to melt and let the pore pressure to escape, which is very beneficial to prevent spalling of concrete.

Equation 18:

$$p_{vs} = 6.1121x10^{-3} * \exp\left(\left(18.678 - \frac{T}{234.5}\right) * \left(\frac{T}{257.14 + T}\right)\right)$$

Where:

p_{vs} is in bar

T is in Celsius degree

Equation 19:

$$p_{vs} = \exp\left(-\frac{5800.22}{T + 273.16} + 1.3915 - \frac{0.04867}{T + 273.16} + 4.1765x10^{-5} * (T + 273.16)^2\right.$$
$$\left. - 1.4452x10^{-8} * (T + 273.16)^3 + 6.54597 * ln(T + 273.16)\right)x10^{-5}$$

Where:

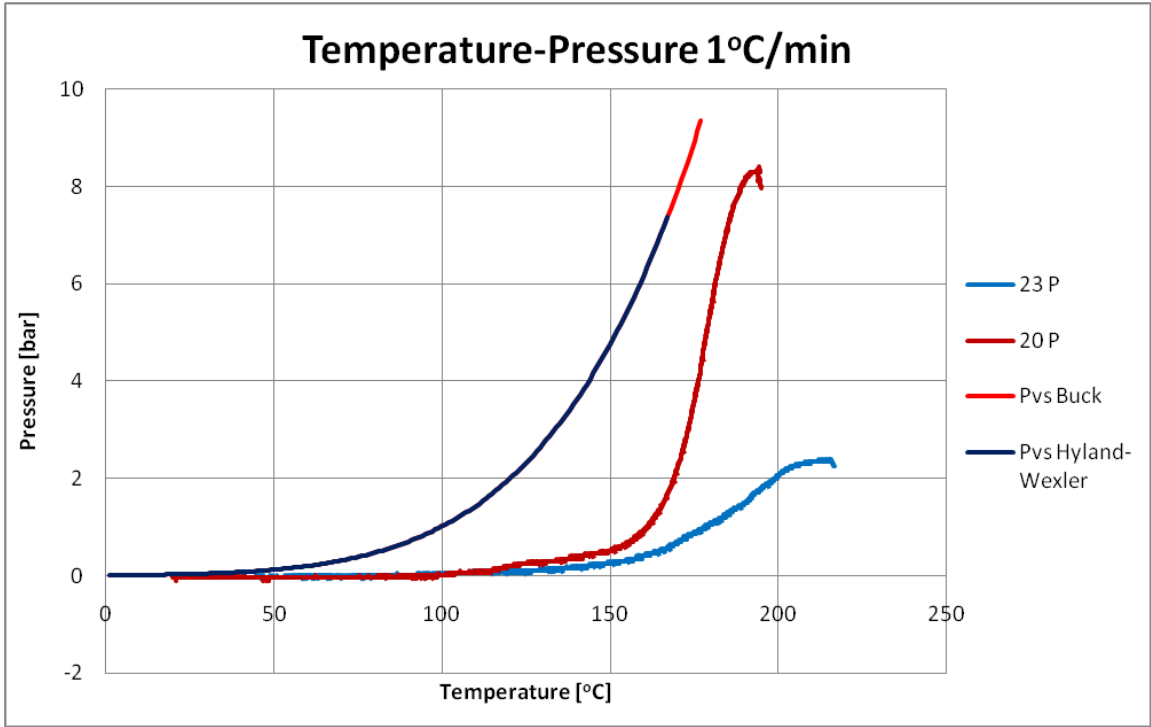p_{vs} is in bar

T is in Celsius degree
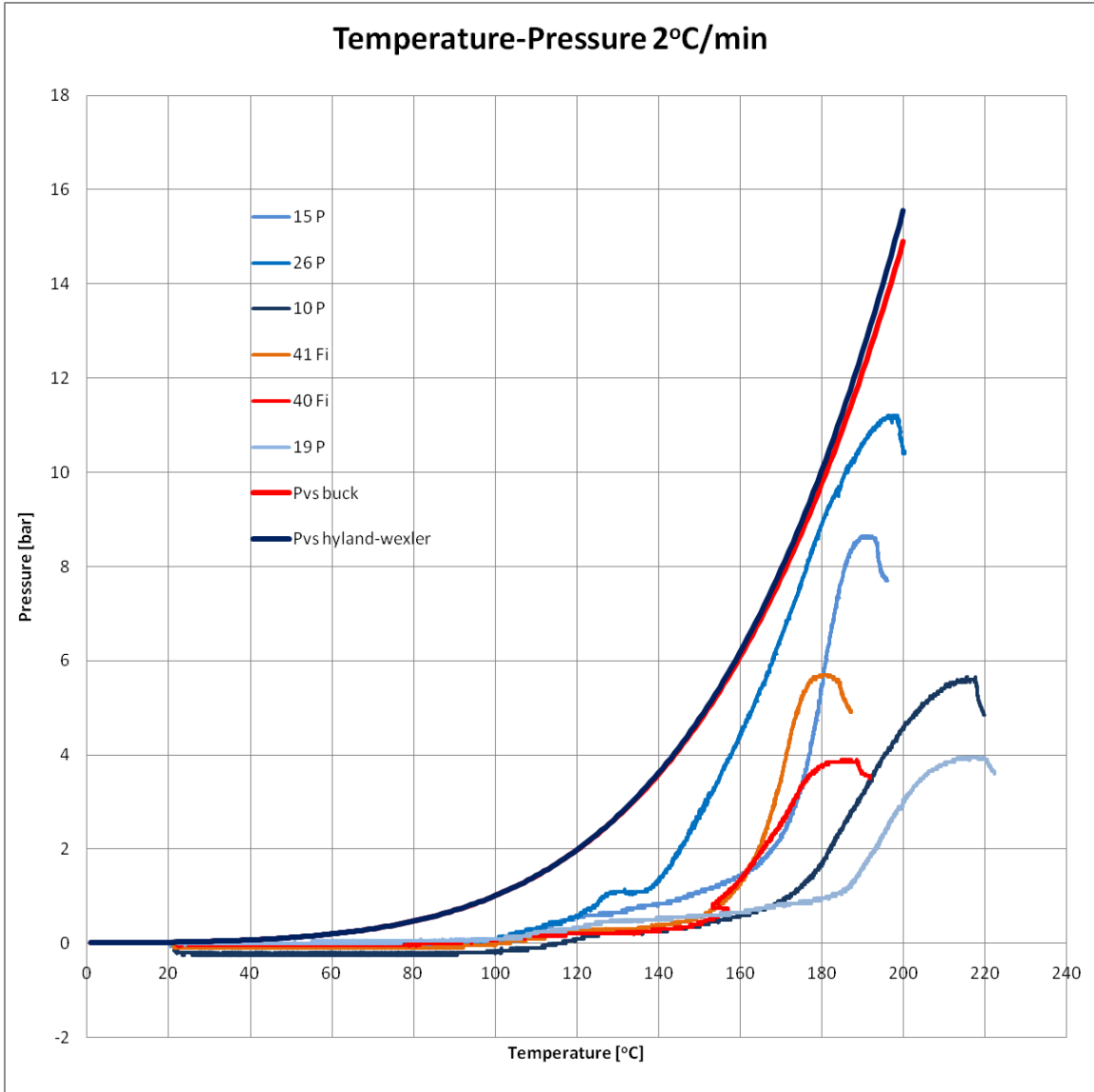
Figure 85 Temperature-Pressure 1°C/min

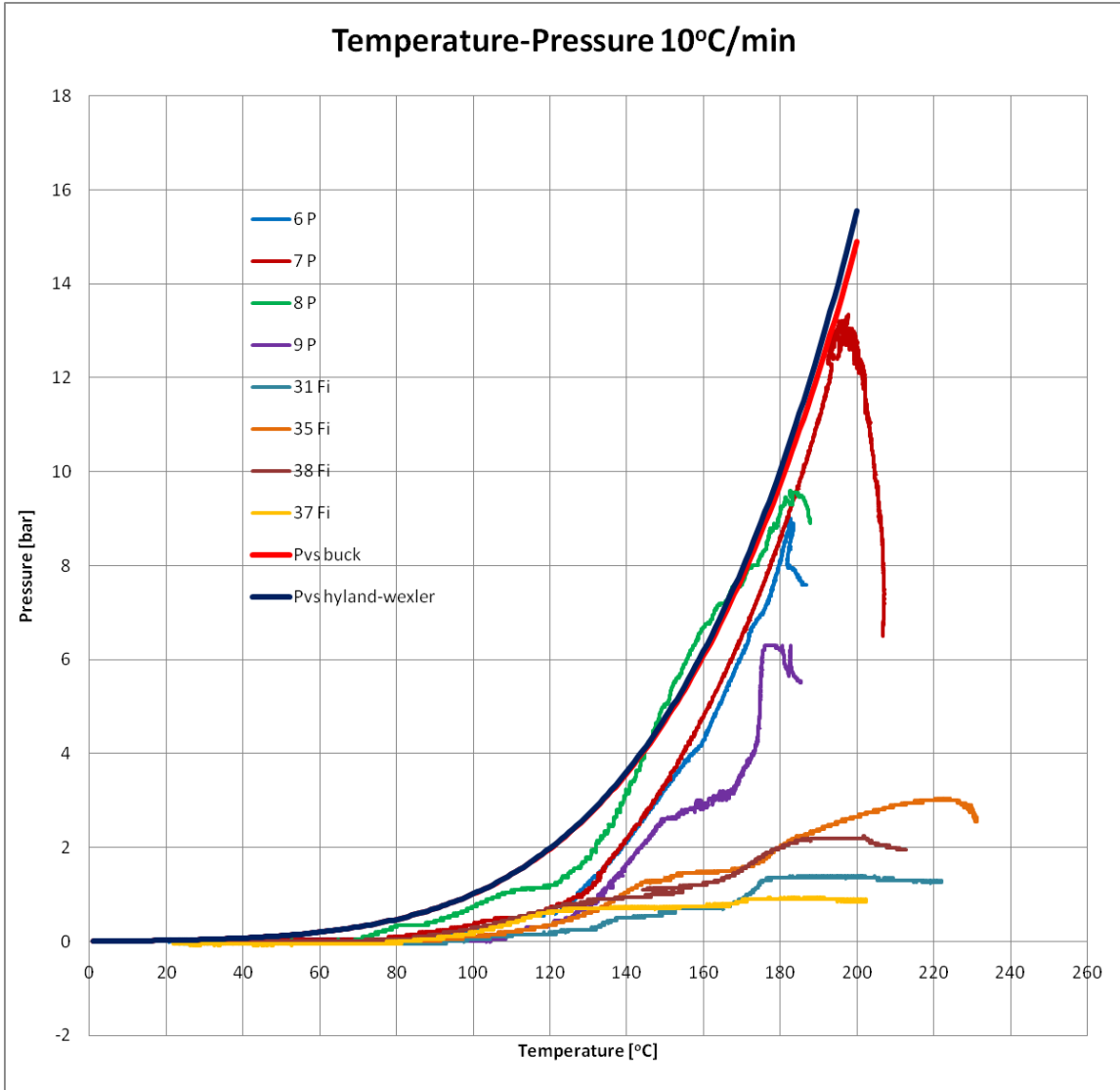Figure 86 Temperature-Pressure 2°C/min

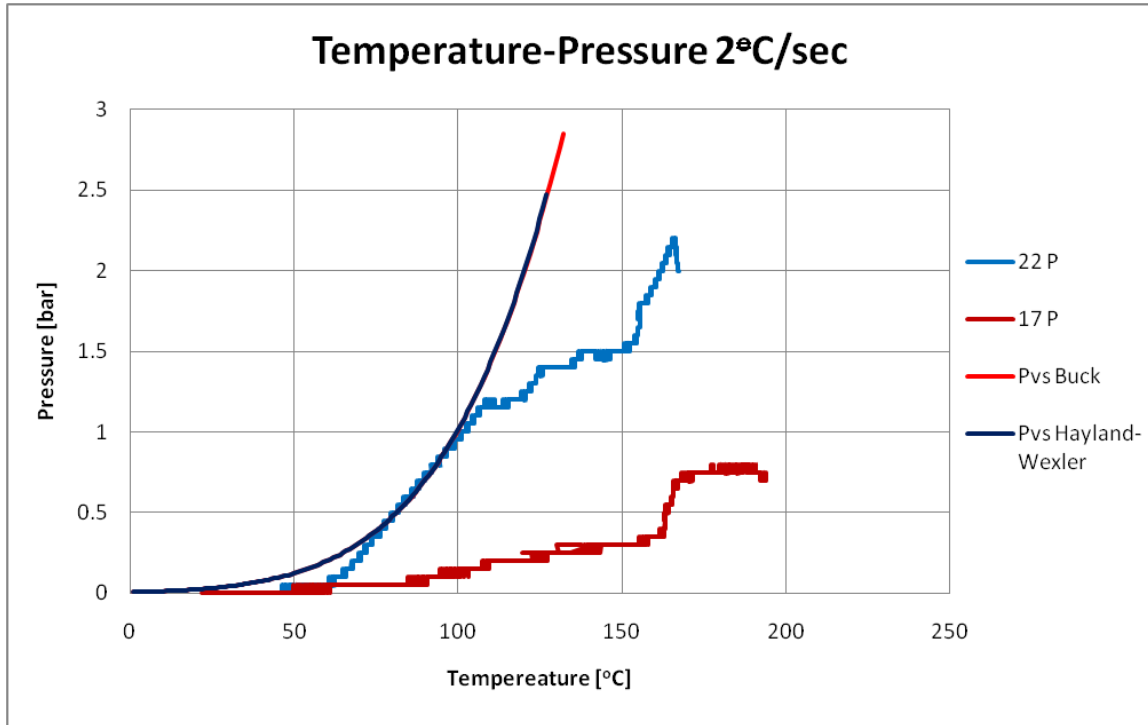Figure 87 Temperature-Pressure 10°C/min

Figure 88 Temperature-Pressure 2°C/sec

4.2.5. Pressure-Tensile Strength Graphs

The main aim of this work was to evaluate the effect of pore pressure on the apparent tensile strength of concrete. For this purpose, samples and testing set-up was prepared as it is presented in chapter 3. The proposal was to heat the sample according to desired target temperature and heating rate, and then to perform the splitting test while sample is still hot and has pore vapor pressure.

In order to evaluate the Pressure-Tensile Strength relationship better, it was thought that samples should be tested at the moment that maximum pore pressure is reached.

On Figure 89, bigger half transparent circles represents the samples dried in oven at 120°C for 16 days, whereas the other samples were unprocessed. These samples were necessary to evaluate the tensile strength at ambient temperature both in normal condition of moisture and in dried condition.

In the other figures, heated specimens are presented plain concrete is represented by blue color and fiber reinforced concrete is represented by red color. Four different heating

rates are symbolized by four geometrical shapes which are quadrilateral for 1°C/min, triangle for 2°C/min, circle for 10°C/min and square for 2°C/sec.

The relationship between pore pressure and apparent tensile strength is presented on Figure 90. It can be seen that apparent tensile strength is decreasing while pore pressure is increasing, which compromises with the expectations. It is a fact that, the data are scattered rather than being consolidated. However, Figure 89 shows that unprocessed concrete tensile strength is also dispersed in between 3 MPa and 4 MPa. Furthermore, Figure 90 includes all heating rates, which increases the dispersion of data. But it can be seen on Figure 92 that, tensile strength values measured by splitting test are scattered in a narrower bandwidth for each heating rate.

Figure 91 demonstrate the linear trend with negative slope, which is as expected due to the fact that increasing pressure causes tensile strength to decrease and vice versa. It must be highlighted that the trendline was obtained only by using the data obtained from primary heating rates, which are slow and moderate heating rate, because they represent the most populous data.

Tensile strength could be also affected by the temperature of specimen. Indeed, Eurocode [6] proposes a decrease in tensile strength of concrete exposed to elevated temperatures. This issue could make difficult to establish direct relation between pore pressure and tensile strength, due to the fact that experiments had not been performed at a specific temperature. Instead of a specific temperature, experiments were performed when maximum pore pressure achieved which may occur at different temperatures (even if the differences are not so significant)

Despite of temperature effect on tensile strength, it is argued that temperature did not affect so much the tensile strength of specimens, since maximum pressure was usually achieved in the interval of 180°C to 200°C, as shown in Figure 94. The dispersion difference is around 20°C which is enough less to think that it does not affect the tensile strength.

Effect of heating rate on apparent tensile strength of concrete is evident in the Figure 92. This figure was drawn by using the trendline slope obtained from Figure 91 (negative slope equal to arctan[−1.2529]); for each heating rate it has been considered a straight line with a slope of -1.2529 and that passes through the average point of the Pressure-

Tensile Strength points belonging to the particular heating rate considered. The lines obtained are drawn in Figure 93. These lines allow understanding what happened in the zero pressure condition, in order to comprehend also the effect of different heating rates in concrete damage, due to thermal stresses and thermal incompatibility.

The numerical analysis conducted for different heating rates and presented in chapter 3, predicted that heat induced thermal stresses significantly depend on the heating rate. It was obtained that while slower heating rates cause lower thermal stresses, more rapid heating rates induce higher thermal stresses. Figure 92 compromises the numerical analysis results, since at zero pressure; highest tensile strength corresponds to slowest heating rate and vice versa. Moreover, zero pressure tensile strength of concrete reduces while heating rate getting faster.

This reduction in tensile strength is thought to be caused by the coupled effect of thermal stresses and thermal incompatibility between aggregates and cement paste.

To be able to correlate tensile strength results of heated tests with tensile strength at ambient temperature, it was needed to run splitting tests with unheated samples. It was also desired to find out the effect of drying on tensile strength; therefore both unheated samples and samples dried in oven at 120^oC for 16 days, were tested. The results, presented in Figure 89**Error! Reference source not found.**, show that plain concrete and fiber reinforced concrete are similar from tensile strength point of view. It is clear that tensile strength of unheated samples is dispersed between 3 MPa and 4 MPa, while dried samples' is in between 2.4 MPa and 3.25 MPa. It should be stated that zero pressure tensile strength for 1^oC/min was found out to be 3.6 MPa (Figure 93) which corresponds to average of unheated samples' tensile strength. This means that even the slowest heating rate did not cause samples to dry significantly.

According to experimental results, it is possible to conclude that pore pressure is very effective on apparent tensile strength of concrete, in fact, the tensile strength decrease linearly with the pore pressure increase and this decrease is not proportional to the porosity m (usually equal to $0.1 - 0.2$, for normal concrete) but to a value close to 1.25.
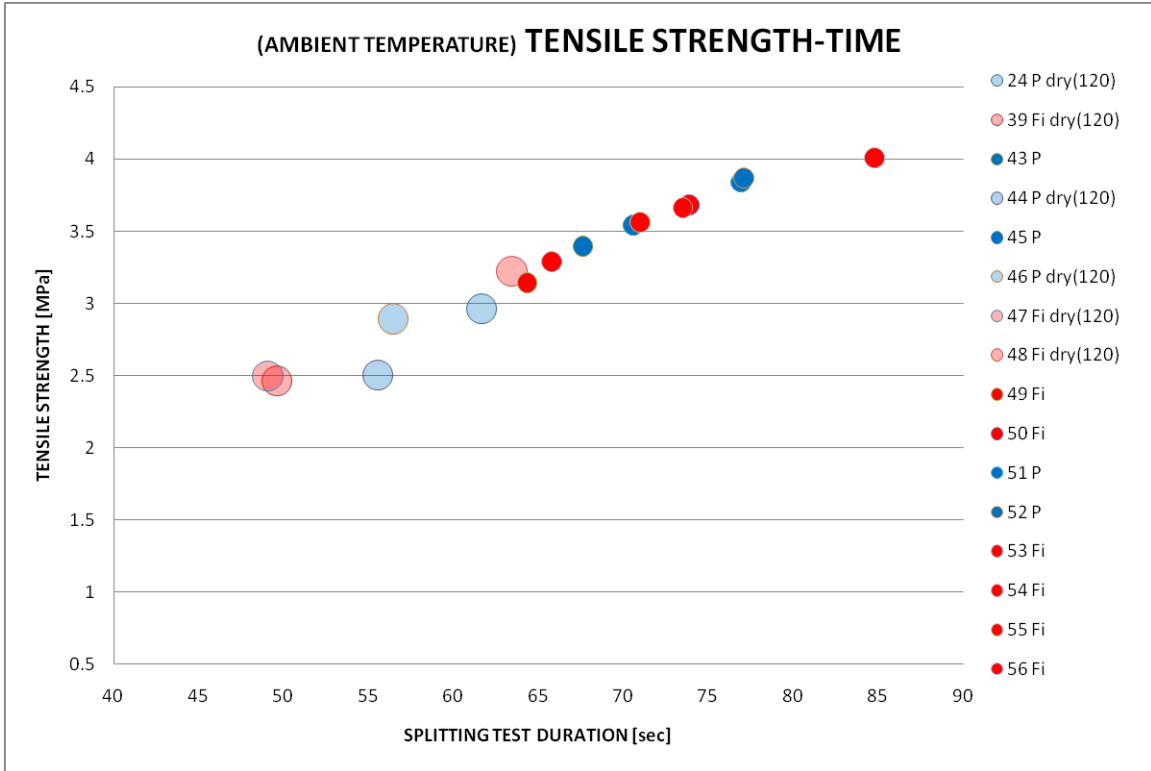
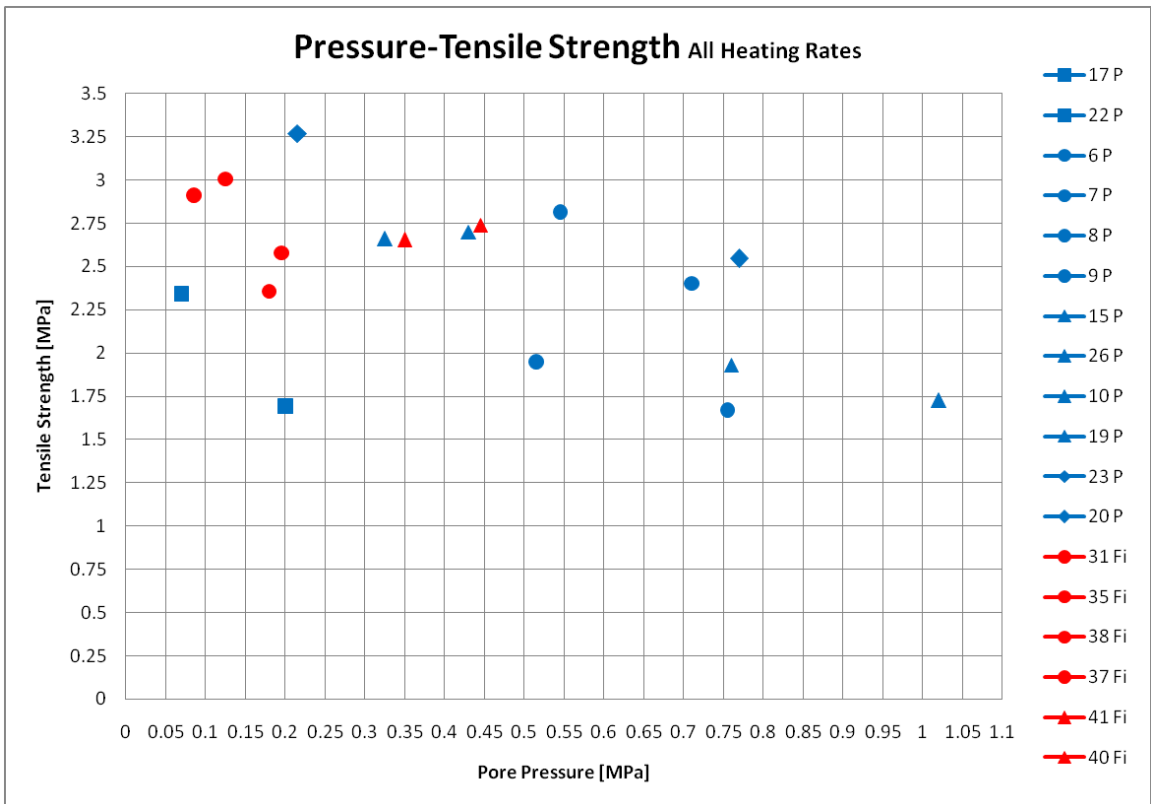Figure 89 Tensile Strength (Ambient Temperature)
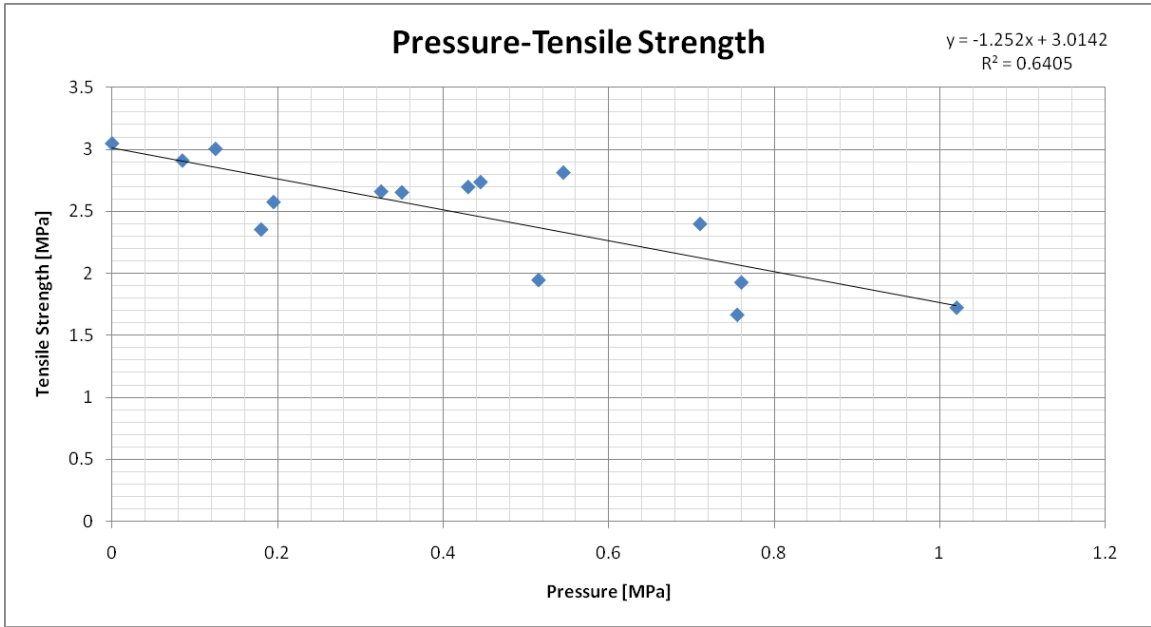

Figure 90 Pressure-Tensile Strength Relationship

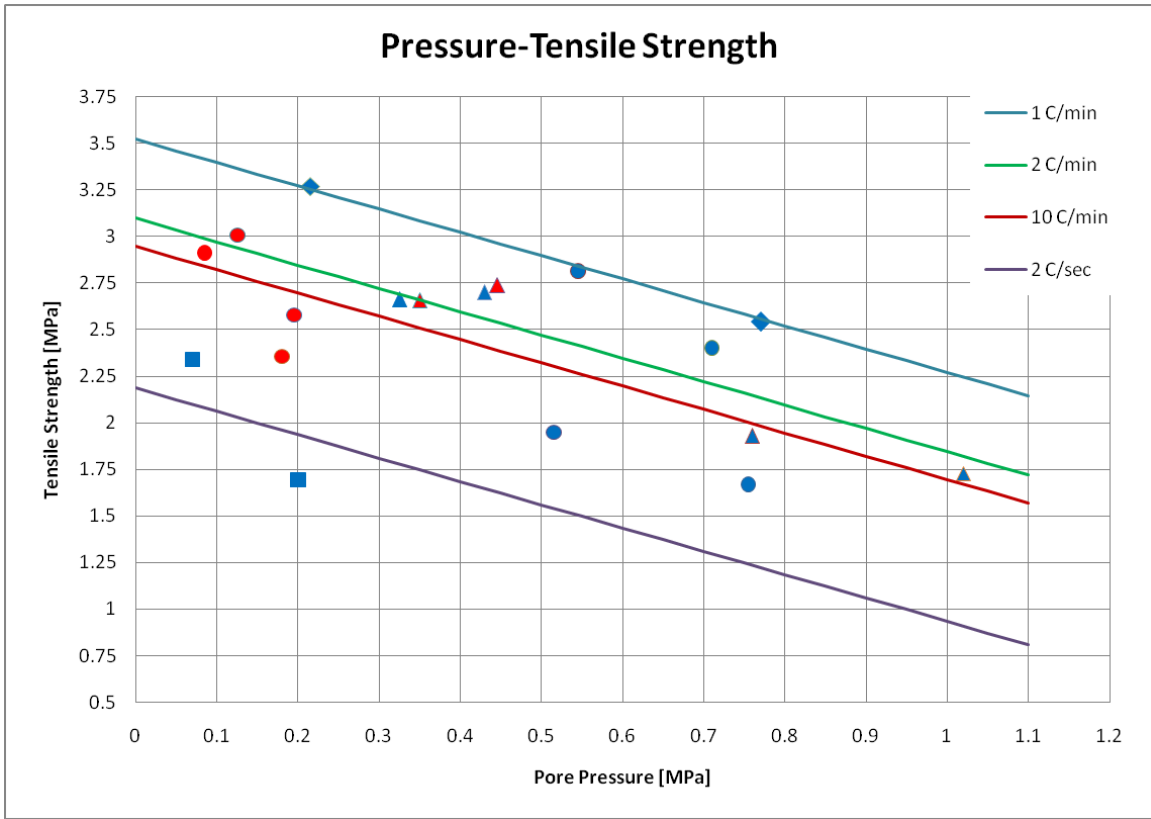Figure 91 Pressure-Tensile Strength Trendline

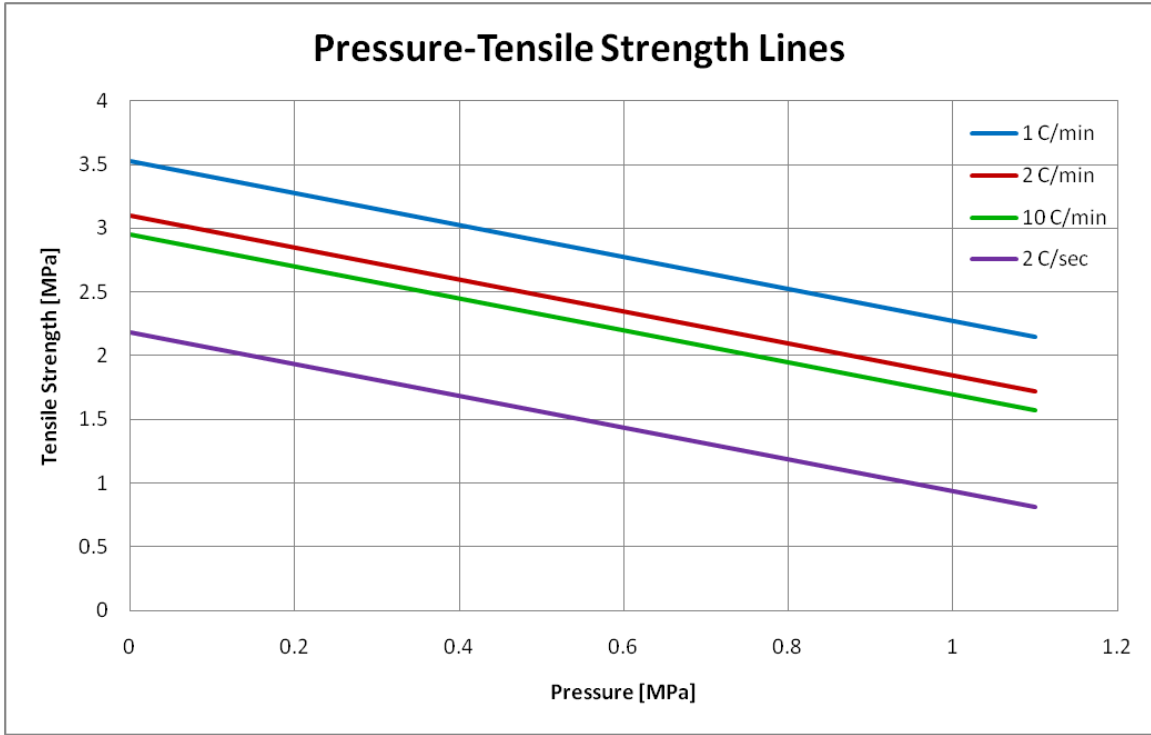Figure 92 Pressure Tensile Strength 4 Lines

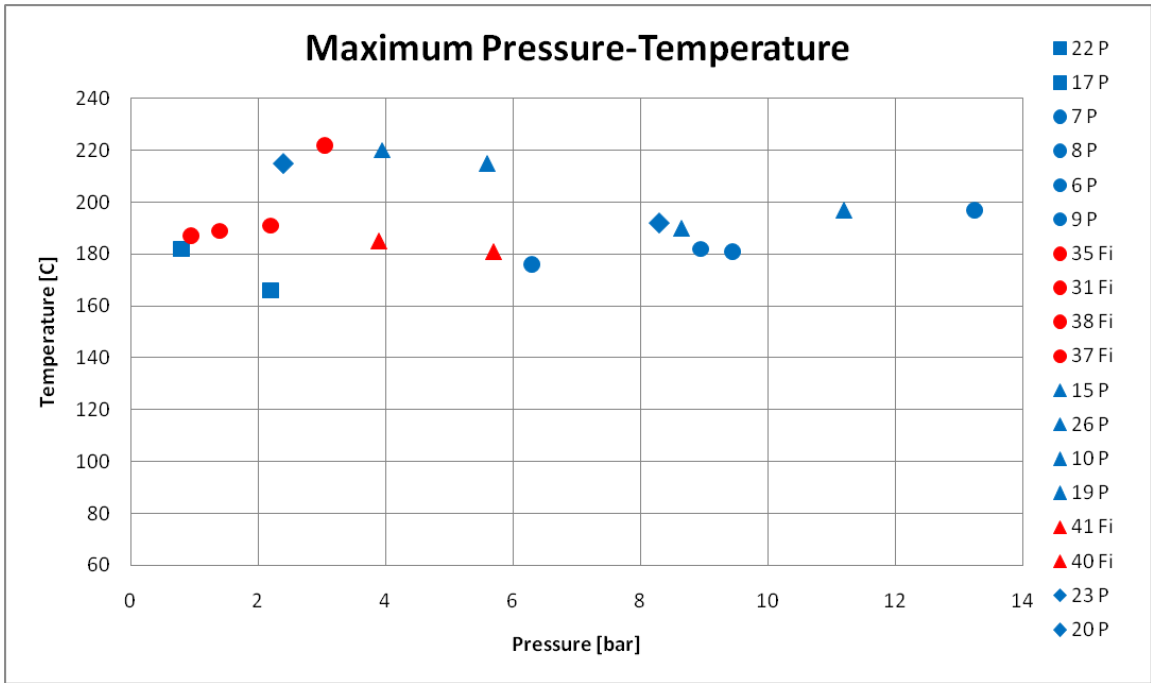Figure 93 Pressure-Tensile Strength 4 Lines

Figure 94 Maximum Pressure-Temperature Relationship

5. Analytical Models

5.1. Introduction

The effect of pore pressure on tensile strength could be described by analytical models. There are not many tentative in the literature to cast a theoretical relationship between pore pressure and decrease of the tensile strength which can be recognized in experimental tests. In most cases the approach looks similar to what is currently done in soil mechanics by defining the effective stress in a porous material. One alternative approach is based on fracture mechanics and the stability of the inherent defects of concrete. These two alternatives, namely a well known simplified model and a fracture mechanics model will be discussed and compared in the following.

Apparent tensile strength of concrete $f_{c,t}^{apparent}$ is a function of:

- The real material strength "$f_{c,t}(T)$", including the effect of thermo-physical transformation occurring at temperature "T".
- The pore pressure "P" developed in the pores.
- The effect of thermal stress "HR" due to the inhomogeneous heating of the sample along the test.

Equation 20:

$$f_{c,t}^{apparent}(P,T,HR) = f_{c,t}(T,HR) - P(HR) * K$$

5.2. Simplified Model
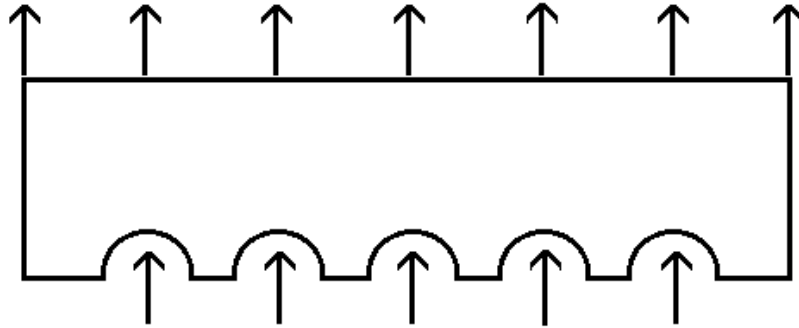
Equilibrium equation (Equation 21):

$$A_c * f_{c,t}(T, HR) = A_c * \sigma_\delta + p * A_m$$

Dividing both sides by A_c;

$$f_{c,\sigma}(T, HR) = \sigma_\delta + p * \frac{A_m}{A_c}$$

$$\frac{A_m}{A_c} = m \; (porosity)$$

$$So; \quad \sigma_\delta = f_{c,\sigma}(T, HR) - p * m$$

$$\sigma_\delta = f_{c,\sigma}^{apparent}$$

So (Equation 22):

$$f_{c,\sigma}^{apparent}(P, T, HR) = f_{c,\sigma}(T, HR) - p * m$$

This model lead to a slope k = m but in the present experimental work it was found out that k = 1.25

5.3. Fracture Mechanics Model

The tensile behavior of concrete may be interpreted as the global effect of many micro effects which reach an unstable propagation when a critical level of stress is reached. The local stress concentration around a defect is governed by the ratio between stress intensity factor (K_I) and stress (σ). K_I is a function of the boundary conditions which depends on how the material is loaded. That is, K_I is proportional to the stress. The defects propagate when K_I reaches a critical value K_{Ic} which is a property of the material (K_{Ic} =f(Modulus of elasticity, Fracture energy)).

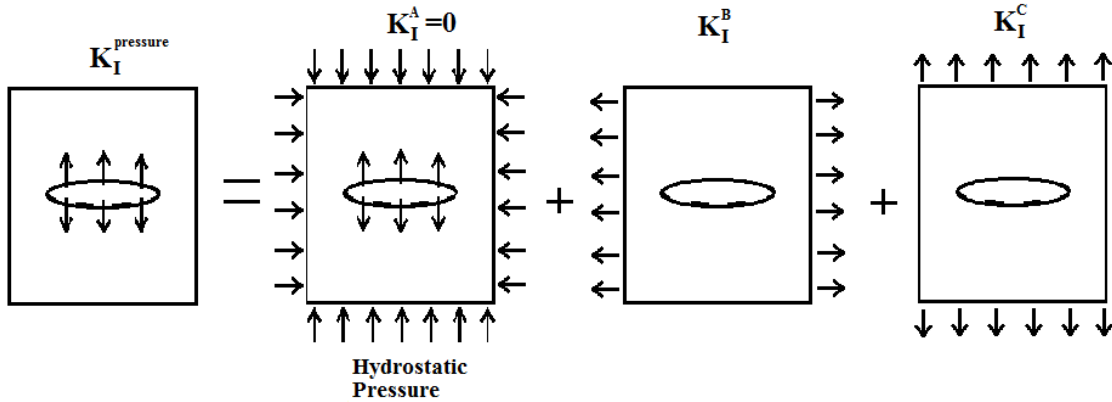In this model, an infinitesimal square part of concrete is considered with only one defect inside (Figure 96).

Figure 96 Fracture Mechanics Model

Figure 96 demonstrates that pore pressure can be identified by summation of hydrostatic pressure $K_I{}^A = 0$, external tensile stress in longitudinal direction and tensile stress in transverse direction. According to elastic theory, hydrostatic pressure has no effect, and biaxial tensile loading tests prove that tensile strength in one direction is almost independent of the tensile strength in other direction (Figure 97). In other words, $K_I^{pressure}$ is equal to K_I^C and $K_I^B = \alpha * K_I^C$ where α has a small value (around 0.1-0.2) (Equation 23). Therefore, it can be stated that Figure 96 is equivalent of the representation shown in Figure 98. The result of Equation 23 compromises with the test results which K_I value was determined to be 1.25.

Equation 23:

$$K_I^{pressure} = K_I^C + K_I^B$$

$$K_I^B = \alpha * K_I^C$$
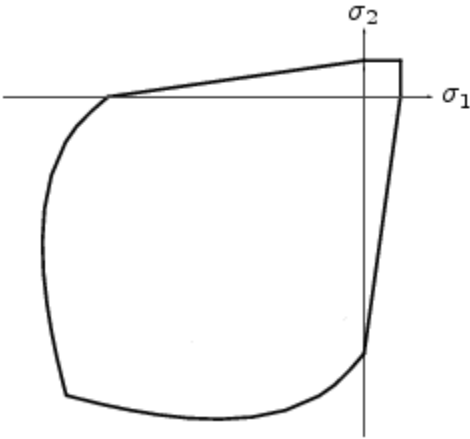
$$K_I^{pressure} = (1 + \alpha) * K_I^C$$

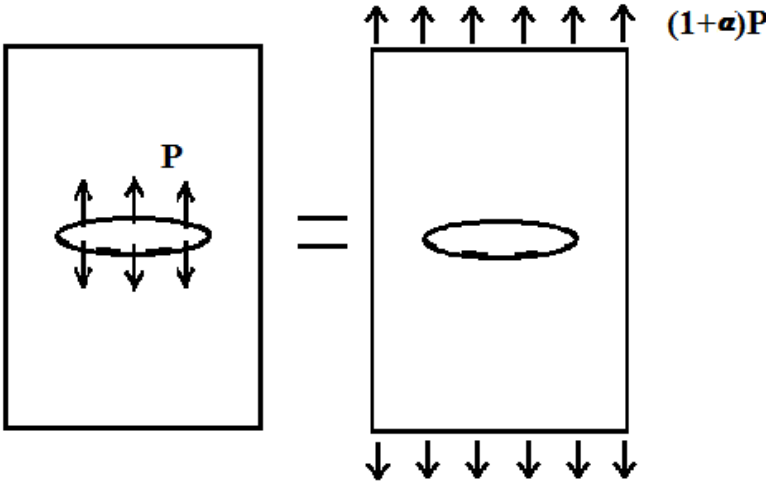Figure 97 Concrete Biaxial Loading Diagram

Figure 98 Equivalent External Load for Pore Pressure

6. **Conclusions**

In this work, it was studied to evaluate the relationship between pore vapor pressure and apparent tensile strength of concrete. Establishing this relationship is a complex issue due to the fact that there are many aspects of the problem. Tensile strength of concrete under high temperature is affected by not only pore pressure, but also magnitude of temperature, heating rate, duration of heating etc.

Concrete itself is not a regular material which makes its comprehensive understanding quite difficult. In order to tackle the problem a simple test method was developed. A series of tests under different conditions were performed so to be able to separate different factors affecting the results.

The heating rate was a crucial issue for tensile strength evaluation, since thermal stresses induced in the concrete have a significant influence. Therefore, numerical analyses were performed for the same heating rates adopted in the tests, namely very slow, slow, moderate and rapid. The results showed that significantly high heating rates may influence the results, whereas, slow heating causes negligible effect.

As in any transient phenomena, the concrete members, a first slow rise of temperature is followed by a faster heating. Nonetheless, the influence of water vaporization can be recognized in the form of 2 plateaus which tends to disappear when concrete drying tends to prevail.

The experiments showed that pore pressure formation in concrete is directly related with the heating rate which affects it both in magnitude and evaluation in time. However, in all tests, it was observed that rapid increase pressure occurs in range of the temperature plateau and reaches the peak at the end of the plateau.

Temperature at the mid-section of specimen was found out to be important for the development of pore pressure due to the fact that heat is needed for vaporization. Generally, pore pressure started rise significantly around 150$^{\text{o}}$C and reached peak around 200$^{\text{o}}$C. Theoretically, the temperature-pressure curves cannot exceed saturation curve, but in some experiments they did. It is argued that dry air inside the concrete could possibly cause encroach of saturation curve. On the contrary, it was observed that slower heating rates cause formation of a gap in between saturation curve and temperature-pressure

curves, whereas, in case of faster heating rates, pressure increased closer to the saturation curve. It could be due to the fact that drying of samples becomes significant during slow heating.

The relationship between pressure and tensile strength was tried to be evaluated by various tests conducted by applying four heating rates.

The tests proved that pore pressure significantly affects the apparent tensile strength of concrete. As it was expected, the tensile strength of concrete reduces while pore pressure increases. It should be kept in mind that both pore pressure and tensile strength depend on heating rate and temperature, which makes difficult to assess this relationship.

However, according to experimental results, it is possible to conclude that pore pressure is very effective on apparent tensile strength of concrete, in fact, the tensile strength decrease linearly with the pore pressure increase and this decrease is not proportional to the porosity m (usually equal to $0.1 - 0.2$, for normal concrete) but to a value close to 1.25. This relation has been explained with the Fracture Mechanics Model, defined in the paragraph 5.3.

One of the aims of this work was to evaluate the effects of poly-propylene fibers inside concrete. It is found out that fibers deeply affect the response of concrete at elevated temperatures. Fiber reinforced concrete samples showed lower pore pressure values than plain concrete samples, which is very beneficial to prevent spalling. Moreover, splitting tests showed that fibers do not cause any reduction in tensile strength.

7. References

1. Jaleta, Abera Mamo. " Acoustic Methods for the Assessment of Fire Damage in Concrete Structures." M.Sc. Thesis. Politecnico di Milano, 2011.

2. Mindeguia, Jean-Christophe, Pierre Pimienta, Albert Noumowé, and Mulumba Kanema. "Temperature, Pore Pressure and Mass Variation of Concrete Subjected to High Temperature — Experimental and Numerical Discussion on Spalling Risk." *Cement and Concrete Research* 40.3 (2010): 477-87. Web. <http://ees.elsevier.com/CEMCON/default.asp>

3. Kalifa, Pierre, Grégoire Chéné, and Christophe Gallé. "High-temperature Behaviour of HPC with Polypropylene Fibres from Spalling to Microstructure." *Cement and Concrete Research* 40 (2001): 1487-499. *Pergamon*

4. Khoury, Alexander Gabriel. "Effect of fire on concrete and concrete structures." *Prog. Struct. Engng. Mater.* 2 (2000): 429-447.

5. Dal Pont, S., A. Dupas, A. Ehrlacher, and H. Colina. "An Experimental Relationship between Complete Liquid Saturation and Violent Damage in Concrete Submitted to High Temperature." *Magazine of Concrete Research* 57.8 (2005): 455-61. Web.

6. Eurocode 2: Design of concrete structures, Part 1: General rules-Structural fire design. EN 1992.

7. Rocco, C., G.V. Guinea, J. Planas, and M. Elices. "Review of the Splitting-test Standards from a Fracture Mechanics Point of View." *Cement and Concrete Research* 31 (2001): 73-82. *Pergamon*.

8. Lin, Zhuhai, and Laurence Wood. "Concrete Uniaxial Tensile Strength and Cylinder Splitting Test." *Journal of Structural Engineering* 129.5 (2003): 692-98.

9. British Standards: Testing hardened concrete, Part 6: Tensile splitting strength of test specimens. BS EN 12390-6:2000.

10. Dwaikat, M.D., and V.K.R. Kodur. "Hydrothermal Model for Predicting Fire-induced Spalling in Concrete Structural Systems." *Fire Safety Journal* 44 (2009): 425-34. *www.elsevier.com/locate/firesaf*. Web.

11. Zeiml, Matthias. "Concrete Subjected to Fire Loading – from Experimental Investigation of Spalling and Mass-Transport Properties to Structural Safety Assessment of Tunnel Linings Under Fire" Ph.D. Thesis. Institut für Mechanik der Werkstoffe und Strukturen, 2008.